# MAGNETIC RESONANCE STUDIES OF SOME MOLYBDENUM(V) COMPLEXES

Thesis for the Degree of M. S. MICHIGAN STATE UNIVERSITY LAURAINE ANITA DALTON 1967

H= 7068079

#### **ABSTRACT**

### MAGNETIC RESONANCE STUDIES OF SOME MOLYBDENUM(V) COMPLEXES

### by Lauraine Anita Dalton

A detailed study of the magnetic properties of a number of paramagnetic Mo(V) complexes has been conducted.

Ligand hyperfine interaction as well as hyperfine interaction from the Mo(V) nucleus has been observed for some fluoride, chloride, bromide, iodide, thiocyanate, and phosphorus-containing complexes. A careful study of the dependence of the hyperfine interaction upon the orientation of the external magnetic field with respect to the molecular axis of the Mo(V) complexes has permitted an evaluation of the relative importance of Fermi contact and electron-nuclear dipolar hyperfine interactions in these complexes. These observations have permitted a reexamination of molecular orbital theory for these complexes.

Electron relaxation studies indicate that anisotropic and spin-rotational relaxation mechanisms are the dominant relaxation mechanisms in dilute solutions of Mo(V) complexes. In concentrated solutions electron-electron spin exchange is found to be the linewidth determining mechanism.

An analysis of the anisotropic rotational relaxation mechanism has permitted the determination of the signs of the components of the hyperfine interaction tensors for molybdenum(V), fluorine, chlorine, and nitrogen hyperfine interactions. The isotropic and anisotropic components of the molybdenum hyperfine interaction tensor are positive. The isotropic part of the fluorine,

chlorine, and nitrogen superhyperfine interaction tensors is positive while the anisotropic components are negative.

Detailed nuclear spin relaxation studies were carried out: They were interpreted in terms of nuclear relaxation through the modulation of electron-nuclear and Fermi contact hyperfine interactions. Measurements of nuclear relaxation times at high concentrations of paramagnetic ions indicated that the rate of nuclear relaxation is determined by electron-electron spin exchange. Such interaction was taken into account theoretically and an expression predicting the appropriate relaxation behavior in the high concentration region was derived.

The nuclear relaxation studies have also provided insight into the detailed nature of some of the Mo(V) complexes in solution.

# MAGNETIC RESONANCE STUDIES OF SOME MOLYBDENUM(V) COMPLEXES

bу

### Lauraine Anita Dalton

## A THESIS

Submitted to

Michigan State University
in partial fulfillment of the requirements
for the degree of

MASTER OF SCIENCE

Department of Chemistry

1967

747079 12-20-67

To my father,
Mr. Alvin W. Nehmer

### ACKNOWLEDGMENTS

The author wishes to express her sincere appreciation to Professor C. H. Brubaker, Jr. for his continued interest, counsel, and encouragement during the course of this investigation.

# TABLE OF CONTENTS

INTRODUCTION	1
HISTORICAL	3
THEORETICAL	13
I. Theory of Magnetic Resonance	13
II. Magnetic Relaxation	24
III. Theory of Nuclear Magnetic Relaxation in	
Paramagnetic Complexes	26
IV. Paramagnetic Relaxation in Inorganic Complexes	39
EXPERIMENTAL	46
I. Preparation of Samples	46
II. Solvent Purification	51
III. Crystal Preparation	51
IV. Reference Standards	52
V. Preparation of Samples for EPR	53
VI. Instrumental	53
VII. Computer Programs	55
RESULTS	57
I. Molybdenyl Halide Complexes	57
II. Mixed Halide Complexes	90
III. Mo(V) Complexes Containing Phosphorus	90
IV. Mo(V) Complexes Containing Nitrogen	108
V. Mo(V) Complexes with Ligands Containing Sulfur	119

## TABLE OF CONTENTS - Continued

VI. Nuclear Relaxation Results	127
VII. Electronic Relaxation Results	129
VIII. ENDOR Measurements	137
CONCLUSIONS	138
I. Haloöxomolybdate(V) Complexes	138
II. Mo(V) Complexes with Ligands Containing Phosphorus	142
III. Mo(V) Complexes with Ligands Containing Nitrogen	144
IV. Mo(V) Complexes with Ligands Containing Sulfur	144
V. Zeeman and Metal Hyperfine Interactions	145
VI. Analysis of the Electron Paramagnetic Resonance Linewidths	145
VII. Analysis of the Nuclear Relaxation Results	153
REFERENCES	165

## LIST OF TABLES

TABLE		page
I.	Magnetic Tensor Elements for Molybdate Complexes	5
II.	Values of <g> for Mixed Complexes of Mo(V).</g>	11
III.	Coefficients in the Kivelson Expression for Linewidth	40
IV.	Coefficients of $m_{\overline{I}}$ in the Linewidth Expression of	
	Dye and Dalton	42
ν.	Theoretical Expressions for Spin-Lattice Relaxation	45
VI.	Magnetic Tensor Elements of Mo(V) Complexes	65
VII.	Elements of the Ligand Superhyperfine Interaction Tensor	68
VIII.	Equilibrium Constants and Magnetic Tensors for Mixed	
	Complexes	93
IX.	Contact Frequency Shifts for Some Mo(V) Complexes	130
х.	Electronic Relaxation Times	136
XI.	Spin Densities in Ligand Orbitals	140
XII.	Exchange Polarization and Distortion Expressions for	
	Molybdates	146
XIII.	Values of $\tau_{c}$ Calculated from Electron and Nuclear Relaxation	
	Studies	157

## LIST OF FIGURES

Figure		page
1	The Energy Level Diagram for the Interaction of a Paramagnetic Electron with Four Equivalent Fluorines in the Presence of a Static Magnetic Field	15
2	The Interaction of a Paramagnetic Electron with the Four Equatorial Ligands for Two Orientations of the External	
	Magnetic Field with respect to the Axis of Highest Symmetry	19
3	EPR Spectra of [MoOF <sub>5</sub> ] <sup>2-</sup>	59
4	EPR Spectrum of [MoOBr <sub>5</sub> ] <sup>2</sup> - in a Frozen Acid Glass at 77°K	62
5	EPR Spectra of a Single Crystal of $(NH_4)_2[MoOCl_5]$ in $(NH_4)_2[InCl_5\cdot H_2O]$	74
6	The Variation of the Chlorine Superhyperfine Interaction as a Function of the Orientation of the External Magnetic Field with respect to the Quantization Axes of the Chlorine	
	Superhyperfine Tensor	78
7	EPR Spectra of Polycrystalline $(NH_4)_2[MoOCl_5]$ in $(NH_4)_2[InCl_5 \cdot H_20]$ at 77°K	80
8	EPR Spectra of Polycrystalline $(NH_4)_2[MoOBr_5]$ and $K_2[MoOF_5]$ in Diamagnetic Hosts	87
9	EPR Spectra of a Single Crystal of K <sub>2</sub> [MoOF <sub>5</sub> ] in K <sub>3</sub> TlF <sub>6</sub> ·2H <sub>2</sub> O at 77°K	91
10	EPR Spectra of a Complex Formed by Adding (NH <sub>4</sub> ) <sub>2</sub> [MoOCl <sub>5</sub> ] to H <sub>3</sub> PO <sub>4</sub>	95
11	EPR Spectra of Complexes Containing (EtO) PO as a Ligand	98

# LIST OF FIGURES - Continued

12	EPR Spectra of Complexes Containing (EtO) 2PSS as a Ligand	103
13	Nitrogen Superhyperfine Interaction in Mo(V) Complexes	
	Containing Thiocyanate as a Ligand	109
14	Solution and Frozen Glass EPR Spectra of [MoO(NCS) <sub>5</sub> ] <sup>2-</sup>	112
15	EPR Spectra of a Complex Containing Dimethylglyoxime as a	
	Ligand	116
16	EPR Spectra of Complexes Containing Pyridine as a Ligand	120
17	EPR Spectra of Mo <sub>2</sub> O <sub>3</sub> (SO <sub>4</sub> ) <sub>2</sub>	123
18	EPR Spectra of Chlorine Superhyperfine Interaction in	
	MoOC1SO <sub>4</sub>	128
19	The Nuclear Spin-Lattice $T_{1N}$ and Nuclear Spin-Spin $T_{2N}$ Relaxation Times as a Function of Paramagnetic Ion	
	Concentration and Radiofrequency Field	131
20	Electronic and Nuclear Relaxation Times as a Function of	
	Acidity of the Solution for [MoOCl <sub>5</sub> ] <sup>2-</sup> in a Mixture of	
	HCl and DCl	134
21	Electron Spin-Spin Relaxation Time, T <sub>2e</sub> , and Exchange	
	Contribution to the Transverse Proton Relaxation $_{S}^{T}_{2,ex,H}$	
	as a Function of the Mo(V) Concentration	159

#### INTRODUCTION

Considerable interest has been aroused in the electronic structure and kinetic processes of molybdenum(V) complexes. Electron paramagnetic resonance (EPR) studies led workers to conclude that the unpaired electron was essentially a d electron with little spin polarization or hyperfine interaction with the ligand nuclei. Chemical equilibria were first recognized in the  $[MoOCl_5]^2$ -system. This complex was shown to form paramagnetic and diamagnetic dimers in solutions of low acidity, while the  $[MoOBr_5]^2$ - system is less well understood. More recent studies on the molybdenyl system,  $[MoOX_5]^2$ -, where X may be F-, Cl-, Br-, or  $HSO_4$ -, have shown ligand substitution equilibria to be operative and as indicating the presence of appreciable electron density on ligand orbitals. A,8,10,11,12

However, the previous work has left several unresolved problems, such as the nature of the hyperfine interaction, nature of chemical equilibria, relative stability of ligands, the rates of ligand exchange and relation of the exchange rate to the stability of the ligand in the complex, the extent of solvent association within the inner coordination sphere, and the importance of the molybdenum-oxygen double bond in determining the kinetics of substitutional and electronic or nuclear processes.

Dialkoxotetrachloromolybdates, originally synthesized by Funk, et al.  $^{13}$ , have recently been studied in detail by optical, infrared, and EPR techniques.  $^{14}$  These spectroscopic measurements have led to interpretation of the structure of the  $[Mo(OR)_2Cl_4]^-$  (R =  $CH_3$ ,  $C_2H_5$ ) complex as characterized by  $C_{4y}$  symmetry, and

have shown the axial field to be comparable to the field in molybdenyl complexes.

In this investigation, a number of complementary magnetic resonance techniques have been employed in an effort to extend the present knowledge of the structure of Mo(V) complexes and the dynamic processes in solution. Dialkoxomolybdate(V) as well as molybdenyl complexes have been studied by nuclear spin echo, electron spin echo, and NMR as well as EPR spectroscopy in an effort to obtain a more precise estimate of the magnitude of the axial field gradient in these complexes.

In addition, the development of a systematic means of detecting ligand hyperfine interaction has been sought and it is shown that the basis of such systematization lies in understanding relaxation processes. Studies in vanadyl and copper(II) complexes indicate that these relaxation processes are general and may serve as a guide to the observation of ligand hyperfine interaction.

#### HISTORICAL

Several methods for the preparation of molybdenyl pentahalide complexes have been recorded. James and Wardlaw 18 prepared (NH,) [MoOC1] by electrolytic reduction of a hydrochloric acid solution of molybdenum trioxide, followed by addition of NH<sub>4</sub>Cl to the concentrated Mo(V) solution. The bromide salts were prepared by an analogous method by Angell, James, and Wardlaw 19, who found salts of the type  $[MoOBr_{\varsigma}]^{2-}$  to be more air-sensitive than the corresponding chloride salts. The air-sensitivity of (NH<sub>A</sub>)<sub>2</sub>[MoOBr<sub>5</sub>] was also noted by Allen and Neumann who prepared this complex by dissolution of ammonium paramolybdate in fuming hydrobromic acid, evaporation of solvent, and recrystallization from hydrobromic acid. Allen et al.  $^{20}$  recently prepared salts of the type M(I)<sub>2</sub>[MoOX<sub>5</sub>], where M(I) = a univalent cation and  $X = Cl^{-}$  or  $Br^{-}$ , by separate dissolution of molybdenum pentachloride and the appropriate metal halide or amine hydrohalide in concentrated HCl or HBr followed by admixture of the solutions so that the M(I): Mo ratio was 2:1. Saturation of the resulting solution at 0°C with the corresponding hydrohalide gas caused the precipitation of the molybdenyl halide salts, which were filtered under nitrogen, washed with ether containing 10% thionyl chloride, rinsed with dry ether, and stored in vacuo. Comparable methods employed for preparation of Mo(V) complexes include the reduction of Mo(VI) in K2MoO4 to Mo(V) with hydrazine in hydrochloric acid solution and subsequent precipitation of Mo(V) hydroxide. This MoO(OH), precipitate was washed with  $\mathrm{NH_4OH}$  and then dissolved in either concentrated HCl or HBr with formation of molybdenyl pentahalide species in solution; this method is also applicable to the production of molybdenyl fluoride<sup>8,12</sup> and thiocyanate<sup>11</sup> complexes in solution.

Abraham et al.  $^{21}$  prepared  $[\text{MoOCl}_5]^{2-}$  in solution by reducing a concentrated hydrochloric acid solution of molybdenum trioxide with excess Zn or Hg and characterized the resulting molybdenyl chloride anion in solution by EPR. A solution of the molybdenyl thiocyanate was prepared by addition of NH<sub>4</sub>SCN and a solution of SnCl<sub>2</sub> in concentrated HCl to a solution of MoO<sub>3</sub> in HCl.  $^{21}$ 

The electron paramagnetic resonance of the molybdenyl chloride species was investigated as an aqueous solution of  $(NH_4)_2[MoOCl_5]$  by Garif'yanov and Fedotov<sup>22</sup> at 77°K and 295°K. At 77°K a wide asymmetric line from the even molybdenum isotopes ( $^{92}Mo$ ,  $^{94}Mo$ ,  $^{96}Mo$ ,  $^{98}Mo$ ,  $^{100}Mo$ ; nuclear spin quantum number I = 0) was superimposed upon a frozen glass pattern arising from interaction of the odd isotopes ( $^{95}Mo$  and  $^{97}Mo$ ; I = 5/2) with the applied magnetic field. At room temperature the line from the even isotopes of molybdenum is symmetric and centrally superimposed upon the isotropic hyperfine lines arising from the odd Mo isotopes. The magnetic tensors for molybdenyl complexes are summarized in Table I.

Garif'yanov and Fedotov reported dissolution of  $(NH_4)_2[MoOCl_5]$  in water; however, spectrophotometric studies of  $[MoOCl_5]^{2-}$  in varied concentrations of HCl by Haight<sup>5</sup> indicated that the  $[MoOCl_5]^{2-}$  species was monomeric only in concentrated acid solutions (10M to 12M) and dimerization predominates at acid concentrations lower than 6M HCl. Sacconi and Cini<sup>23</sup> have reported that addition water to concentrated HCl solutions of Mo(V) results in reduced magnetic susceptibility. Hare, Bernal, and  $Gray^2$  observed an EPR spectrum of  $(NH_4)_2[MooCl_5]$  in 10-12M HCl solution identical to that reported by the Russian workers, <sup>22</sup> and also observed the intensity of this spectrum to decrease markedly as the HCl concentration was reduced from 10M to 4M, and at HCl concentrations below 2M the paramagnetic species disappeared entirely. These workers concluded that the

TABLE I: Magnetic Tensor Elements for Molybdate Complexes.

	;; 66 >	<u></u>	<b></b>	ख ख ४	Aa	Ва	Ref.
	1.950 ±0.002	1.972 ±0.004	1.942 ±0.005	47.1 ±0.7	74.6 ±0.9	30.8 ±3.6	21
	1.947 ±0.002	1.96	1.938 ±0.005	52.7	81.4	44.3	22
	1.947			≃45.4 <sup>b</sup>			2
	1.947	1.970	1.936 <sup>c</sup>	47.0	75.0	33°	10
	1.950	1.970	1.934	47.0			4
	1.949 ±0.003			45.5 ±1.8			∞
	1.950						25
$(NH_4)_2[MoOC1_5]$ in $(NH_4)_2[InC1_5\cdot H_2^0]$	1.9477 <sup>d</sup>	1.9732	1.9400	46.6 <sup>d</sup>	74.7	32.6	ı
	1.994	2.092	1.944			36.3	4
	1.994 ±0.003			40.0 ±1.9			6
	1.994 ±0.003						œ

TABLE I, continued.

Complex	<b>⇔</b> 0	₩ —	₩	ଷ ୯ ୯	A a	Ва	Ref.
$[MOOBr_5]^{2}$	1.994 ±0.003						25
$[MoOBr_5]^{2-e}$	1.993	2.090	1.945 <sup>c</sup>	41.7	0.99	30.°	10
$(QuinH)_2[MoOBr_5]$		2.018	1.946				4
$[MoOF_S]^{2-f}$	1.910						œ
$[MOO(HSO_4)_5]^{2-}$	1.921						25
[MoO(NCS) <sub>5</sub> ] <sup>2- g</sup>	1.940 ±0.003			44.4 ±3			11
[MoO(SCN) <sub>5</sub> ] <sup>2-</sup>	1.938 ±0.002	1.932 ±0.002	1.944 ±0.005	44.0 ±0.4	68.5 ±0.5	33.6 ±0.9	21
	1.935 ±0.002	1.928 ±0.005	1.944 ±0.005	45.0 ±2.7	68.3 ±4.5	34.4 ±4.5	29
X <sub>5</sub> Mo-S-PS(OC <sub>2</sub> H <sub>5</sub> ) <sub>2</sub>	1.970 <sup>d</sup>	2.001 ±0.002	1.955 ±0.002	40.5 ±1.8	59.8 ±1.9	26.5 ±1.8	30
C <sub>5</sub> H <sub>6</sub> N[Mo(OCH <sub>3</sub> ) <sub>2</sub> Cl <sub>4</sub> ] in N,N-dimethylformamide	1.9453 ±0.0008 ide	1.9673 ±0.0002	1.934 ±0.002	46.93 ±0.08	75.1 ±0.1	33.0 ±0.3	14

TABLE I, continued.

 $^{a}$ In units of cm $^{-1}$  x  $^{10}$ 

In units of cm  $^{-}$  x 10  $^{\rm b}$  (a) listed as approximately 50 gauss by authors.

<sup>C</sup>Calculated from isotropic and parallel values.

dCalculated from parallel and perpendicular values.

 $^{e}_{Br} = 35.9 \text{ cm}^{-1} \text{ x } 10^{-4}$ 

 $f_{a>F} = 11.1 \pm 0.9 \text{ cm}^{-1} \times 10^{-4}$ 

 $R_{\text{ca}} = 1.8 \text{ cm}^{-1} \times 10^{-4}$   $R_{\text{ca}} = 40.5 \pm 1.8 \text{ cm}^{-1} \times 10^{-4}$   $R_{\text{p}} = 35.6 \pm 1.8 \text{ cm}^{-1} \times 10^{-4}$  $R_{\text{p}} = 36.4 \pm 1.8 \text{ cm}^{-1} \times 10^{-4}$  monomer  $[MoOCl_5]^{2-}$  exists in solutions 10M to 12M in HCl, that this monomer is in equilibrium with a paramagnetic dimer in the HCl concentration range 4M to 10M, and that only a diamagnetic dimer is present in solutions less than 2M in HCl.

Later EPR investigations of the  $[MoOCl_5]^{2-}$  system included the study by DeArmond et al. on a single crystal of  $(NH_4)[MoOCl_5]$  substituted into the diamagnetic host  $(NH_4)_2[InCl_5 \cdot H_2O]$  (prepared by the method of Wentworth and Piper at both X-band (9.3 Gc) and K-band (35.5 Gc).

The corresponding pentabromomolybdenyl system has been investigated in the spectroscopic studies of Allen and Neumann<sup>6</sup> and the EPR studies of Kon and Sharpless<sup>10</sup> and Dowsing and Gibson<sup>4</sup>, as well as the EPR investigations of mixed pentahalomolybdenyl complexes.<sup>8,9</sup> It may be noted that the EPR study of Dowsing and Gibson,<sup>4</sup> contrary to the work of Allen and Neumann,<sup>6</sup> presented evidence that monomeric [MoOBr<sub>5</sub>]<sup>2-</sup> was present in concentrated hydrobromic acid solutions.

In this work<sup>4</sup> as well as in the study of dimerization by Hare  $\underline{\text{et al.}^2}$ , the measurement of "absolute" concentrations of the species in equilibrium in the acid solution was based upon the relative EPR signal intensities. Detailed measurements of susceptibility recorded in the literature<sup>26-28</sup> have permitted the estimate that the smallest limit of error for measurement of susceptibility of a single EPR line having a shape identical to the shape of the reference standard line is  $\pm 10\%$ , while in cases of merger of hyperfine lines the limits of error were found to be a minimum of  $\pm 25\%$ . In this light the reported accuracy ( $\pm 10\%$ ) of the measurements of Dowsing and Gibson is unreasonably small.

Kon and Sharpless<sup>10</sup> observed an anomalous fine structure in the perpendicular band of the EPR spectrum of  $[MoOBr_5]^{2-}$  enriched with <sup>98</sup>Mo in HBr at 77°K, which they showed to be due to the Br<sup>-</sup> ligand by comparison of the spectrum with <sup>98</sup>Mo to the spectrum taken with naturally occurring molybdenum. The conclusion of this study was interpretation of the symmetry of  $[MoOBr_5]^{2-}$  as  $C_{4v}$ . The

hyperfine structure was considered to arise from interaction of the unpaired electron in the Mo  $d_{xy}$  orbital with the p orbitals of the in-plane bromide ligands in the form of  $\pi$  bonding.

Fine structure due to ligand hyperfine interaction was also observed for  $[\text{MoOF}_5]^{2-}$  in concentrated HF by Van Kemenade et al. Since the nuclear spin of the  $^{19}$ F ligand is 1/2 (I = 3/2 for both  $^{79}$ Br and  $^{81}$ Br) and the nuclear moment of F is comparable to that of Br, the ligand hyperfine lines on the perpendicular band were of comparable amplitude, but fewer in number than in the  $[\text{MoOF}_5]^{2-}$  spectrum and consequently the  $[\text{MoOF}_5]^{2-}$  spectrum was easier to analyze.

A study of mixed fluoride-bromide and fluoride-chloride molybdenyl complexes by Ryabchikov, et al. 8 has shown that as the ratio [HF]/[HX] where X = Cl or Br is increased, new lines characteristic of fluorine ligand hyperfine interaction appear. The signal obtained from both  $[MoOCl_5]^{2-}$  and  $[MoOBr_5]^{2-}$  by these workers consisted of a single central line due to the even molybdenum isotopes flanked by the hyperfine structure due to the odd molybdenum isotopes. As the concentration of HF was increased, a doublet characteristic of interaction of the Mo(V) unpaired electron with the  $^{19}$ F nucleus also increased in intensity. In the series of mixed complexes with varied [HF]/[HX] ratios the intensity of the EPR lines of both chloride and bromide complexes decreased when the temperature was lowered, while lines due to the fluoride complex increased in intensity as the temperature was decreased. The structure in the central Mo line in concentrated HF consists of several overlapping lines due to the F ligand hyperfine interaction, the spectrum being in agreement with that observed by Van Kemenade, et al. Ligand superhyperfine splittings are indicated in Table I.

In general, the studies of mixed molybdenyl halide and bisulfate complexes have shown  $^{8,9,25}$  that the g values of the mixed complexes follow a regular incremental pattern as j decreases and i increases in anions of the form  $[\text{MoOX}_{j-i}Y_i]^{3-(j+i)}$  from the initial conditions j=5, i=0 to j=0, i=5. From an analysis of the relative

intensity of each line of differing g value representing an intermediate complex, the amount of each of the intermediate complexes was calculated as a function of [HX] and [HY], where  $X = Cl^-$ ,  $Y = Br^-(Ref. 9)$ ,  $X = F^-$ ,  $Y = Cl^-$ ,  $Br^-(Ref. 8)$  and  $X = Cl^-$ ,  $Y = Br^-$ ,  $X = HSO_4^-$ ,  $Y = Cl^-$ ,  $Br^-(Ref. 25)$ . From these data, summarized in Table II, calculation of the equilibrium constant for the substitution reaction

$$[MoOX_{j}]^{3-j} + iY^{-} \rightarrow [MoOX_{j-i}Y_{i}]^{3-(j+i)} + iX^{-}$$

was possible. 9 However, care must be exercised in interpretation of EPR spectra since the lines from the individual mixed complexes overlap sufficiently so that the relative intensity (and thus the measure of concentration of each species) of each line could not be determined with more accuracy than an order of magnitude.

In addition to the work on pentahalomolybdenyl anions, studies on the pseudohalide thiocyanate system have been reported.  $^{10,11,21,29}$  Abraham et al.  $^{21}$  as well as Kon and Sharpless  $^{10}$  and Garif'yanov et al.  $^{29}$  report magnetic tensors (Table I) and describe the Mo(V) thiocyanate complex as being characterized by the axially symmetric spin Hamiltonian. Since no ligand splittings were observed in this complex, it was formulated as  $[\text{MoO(SCN)}_5]^{2-}$  by Garif'yanov et al.  $^{29}$  Ryabchikov et al.  $^{11}$  however, were able to observe  $^{14}$ N (I = 1) splittings when thiocyanate samples were prepared in 2M perchloric acid media, and thus formulated the complex as the isothiocyanate:  $[\text{MoO(NCS)}_5]^{2-}$ .

The diethyldithiophosphoric acid complex of Mo(V) yields an EPR spectrum consisting of a central line due to the even Mo isotopes flanked by six hyperfine lines of lower intensity due to the odd Mo isotopes; each of these seven lines is further split into two components by the  $^{31}$ P (I = 1/2) nucleus.  $^{30}$  The composition of the complex, formulated by these workers as  $X_5$ Mo-S-PS(OC<sub>2</sub>H<sub>5</sub>)<sub>2</sub> where X is a solvent molecule, has been interpreted as indicative of  $^{31}$ P contact interaction with Mo(V) through the sulfur atom.

TABLE II: Values of  $\langle g \rangle$  for Mixed Complexes of Mo(V).

Ligands	$[Mo0\chi_{\rm S}]^{2-}$	[Mo0x <sub>4</sub> Y] <sup>2-</sup>	$[MO0X_3Y_2]^{2}$	$[\text{MoOX}_4\text{Y}]^{2}$ $[\text{MoOX}_3\text{Y}_2]^{2}$ $[\text{MoOX}_2\text{Y}_3]^{2}$ $[\text{MoOXY}_4]^{2}$ $[\text{MoOY}_5]^{2}$ Ref.	[MoOXY <sub>4</sub> ] <sup>2-</sup>	[MoOY <sub>5</sub> ] <sup>2-</sup>	Ref.
$X = F^{-}$ $Y = C1^{-}$	1.910		1.917	1.929	1,939	1.950	∞
X = F _ Y = Br _	1.910		1,930	1.954	1.974	1.994	∞
X = C1 Y = Br	1.949	1,969	1.970	1.983		1.994	6
$X = HSO_4^-$ $Y = C1^-$	1.921		1.928	1.935	1.943	1.950	25
$X = HSO_4^{-}$ $Y = Br^{-4}$	1.921		1.943	1.966	1.980	1.994	25

Although considerable work has been done on molybdenyl systems, relatively little has been done on alkoxomolybdates. Originally prepared by Funk et al.  $^{13}$ , McClung et al.  $^{14}$  have made a thorough study of trans-dialkoxotetrachloromolybdates(V). The EPR, optical spectra, and infrared spectral measurements have led to an interpretation of the symmetry of these complexes as  $C_{4v}$ . Failure to locate the charge-transfer band as well as uncertainty in the molybdenum spin-orbit coupling constant have prevented the detailed structural analysis (in terms of molecular orbital coefficients) of these complexes. This paper suggested the further use of EPR spectroscopy for study of the equilibria of these complexes in solution.

#### THEORETICAL

- I. Theory of Magnetic Resonance.
  - A. General Theory.

The general theory of EPR and NMR is discussed in depth in a number of excellent texts  $^{31-40}$  and will not be reviewed here.

- B. Transition Probabilities and Shape of Absorption Patterns.
  - Calculation of Zeeman and Hyperfine Interaction Tensors from EPR Spectra.

Since hyperfine splittings of over 100 gauss were obtained for some samples, it was decided that the most appropriate means of calculating isotropic hyperfine interaction and g values was to employ the mothod first proposed by Breit and Rabi<sup>41</sup> which will be reviewed briefly.

The isotropic part of the Hamiltonian of an atom in an external magnetic field H is given by

$$H = 2\Delta W/(I + \frac{1}{2})\vec{I} \cdot \vec{J} + g_{I}\mu_{O}\vec{J} \cdot \vec{H} + g_{I}\mu_{O}\vec{I} \cdot \vec{H}$$

where  $\Delta W$  is the zero-field hyperfine splitting,  $\vec{I}$  is the nuclear spin, I its magnitude, and  $\vec{J}$  is the electronic spin, and J its magnitude. For Mo(V) complexes,  $J=\frac{1}{2}$ . In zero field the levels  $F=I+\frac{1}{2}$  and  $F=I-\frac{1}{2}$  are separated by  $\Delta W$ . In the presence of a field, the levels split and the resulting energy levels for a state of given  $m_F=m_J+m_I$  are given by the modified Breit-Rabi equation  $^{42}$ 

$$W(H, m_J, m_I) = -[\Delta W/2(2I+1)] + g_I \mu_o H m_F \pm (\Delta W/2) \{1 + 4 m_F \chi/(2I+1) + \chi^2\}^{\frac{1}{2}}$$

where  $\chi = (g_J - g_I) \mu_O H/\Delta W$ ,  $m_J$  is the electronic spin quantum number, and  $m_I$  is the nuclear spin quantum number. At high field, the microwave resonance transition will occur between states for which  $m_I = 0$ ,  $m_J = \pm 1$ . The microwave radiation at frequency  $\nu$  will thus be absorbed at the 2I+1 magnetic field values,  $H_i$ , which satisfy the equations

$$hv = W(H_i, m_J^{-1}, m_T) - W(H_i, m_J^{-1}, m_T)$$

or

$$hv = g_{I}^{\mu} {}_{0}^{H} {}_{1} + \frac{\Delta W}{2} \left[ \left( \chi_{i}^{2} + \frac{2(2m_{I}+1)}{2I+1} \chi_{i} + 1 \right)^{\frac{1}{2}} + \left( \chi_{i}^{2} + \frac{2(2m_{I}-1)}{2I+1} \chi_{i} + 1 \right)^{\frac{1}{2}} \right]$$

2. Calculation of Hyperfine Interaction Tensors from ENDOR Spectra.

Because of the incomplete nature of the electron-nuclear double resonance (ENDOR) studies on the A values arising from interactions of the paramagnetic electron with the fluorine nuclei in the complex  $[\text{MoOF}_5]^{2-}$  will be reported. This complex possesses  $C_{4v}$  symmetry with four equivalent equatorial fluorine nuclei; hence the ENDOR spectra can be described by the following spin Hamiltonian:

$$\hat{H} = \gamma_{e} \vec{h}_{o} \cdot \vec{S} - \sum_{i=1}^{4} \gamma_{F_{i}} \vec{h}_{o} \cdot \vec{I}_{i} + \sum_{i=1}^{4} (T_{F_{i}})_{i} \vec{S} \cdot \vec{I}_{i} - \gamma_{F} \vec{h}_{o} \cdot \vec{I} + T_{F_{i}} \vec{S} \cdot \vec{I}$$

where  $\vec{S}$  = electron spin operator

 $\vec{I}$  = nuclear spin operator

 $\vec{H}_{O}$  = external magnetic field

T = superhyperfine interaction tensor for equatorial fluorines

 $T_{\parallel \parallel}$  = superhyperfine interaction tensor for axial fluorines. The Hamiltonian and accompanying energy level diagram for the four equivalent equatorial fluorines is shown in Figure 1. The ENDOR transitions occur at frequencies corresponding to the following equations

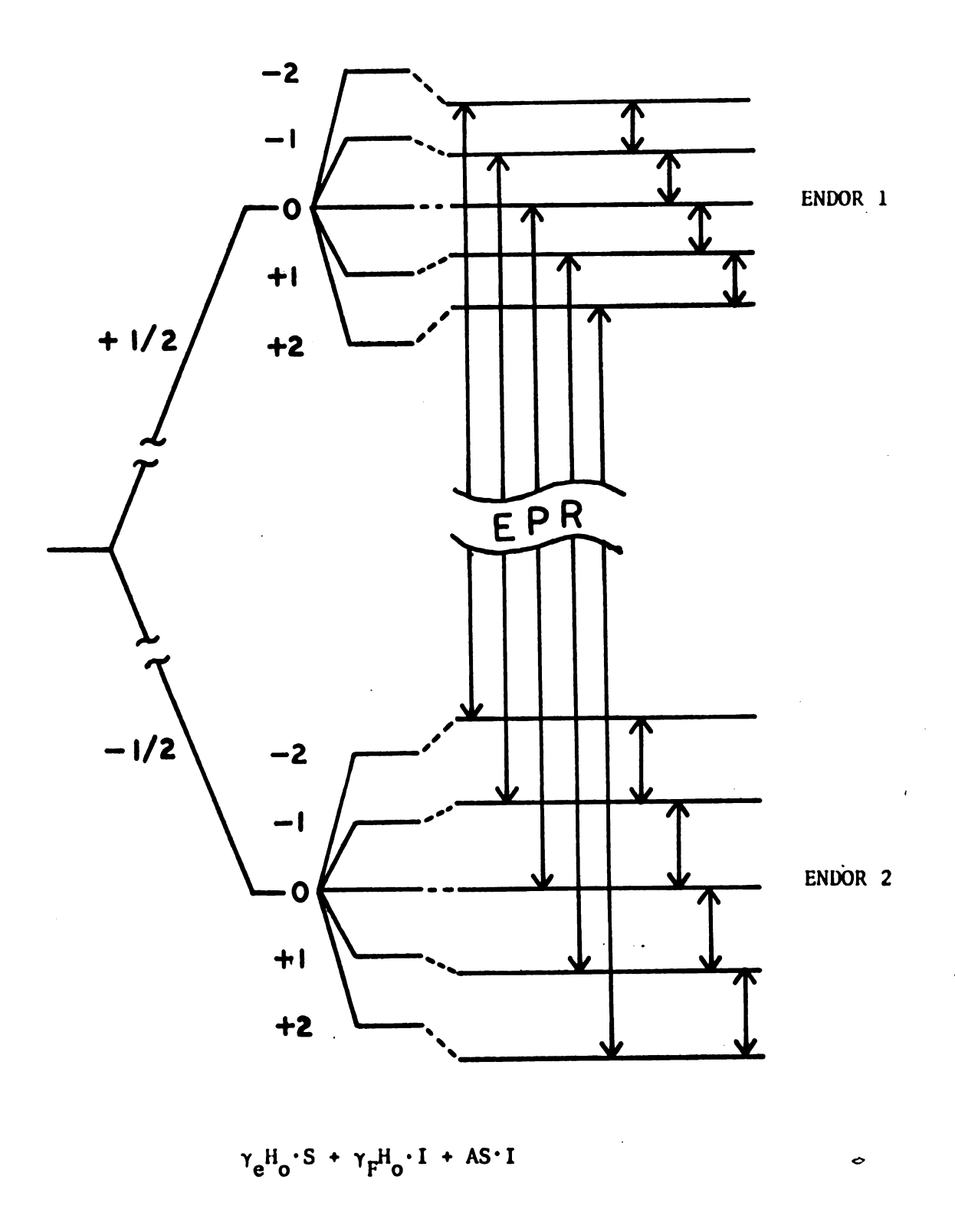


Figure 1. Energy level diagram for an electron coupled to four equivalent equatorial fluorine nuclei in a static magnetic field.

$$v_{\text{ENDOR}}^{\pm} = (T_{\text{F}}/2) + v_{\text{F}}$$

and

$$v_{\text{ENDOR}}^{\pm} = (T_{\text{F}}/2) \pm v_{\text{F}}$$

where  $v_F = \gamma_F H_o / 2\pi$ .

3. Contact Versus Dipolar Hyperfine Interaction in Electron Paramagnetic Resonance Spectra.

In the previous studies of Mo(V) complexes, in which ligand superhyperfine structure has been observed,  $^{8,10,11,12,30}$  the electron-nuclear interaction has been interpreted as contact hyperfine interaction acting through equatorial (in-plane)  $\pi$  bonding. This interpretation neglects completely the possibility of a contribution to the hyperfine interaction arising from through-space (dipole-dipole) electron-nuclear interaction.

As will be discussed subsequently, a consideration of both types of interaction is necessary to account for the nuclear spin echo results. Moreover, certain of the electron spin resonance spectra which have been recorded are difficult to interpret in terms of Fermi or contact interaction alone.

It may be pointed out that the lack of consideration of dipole-dipole hyperfine interaction in the spectra of inorganic complexes appears to stem from the fact that molecular orbital theory reserves no place for dipole-dipole interaction rather than because careful experimental examination has shown such contributions to be absent: Indeed, this interaction has been well documented and has been shown to be the major source of electron-nuclear interaction in organic radicals.

In view of the range of magnetic resonance techniques employed in this investigation, it is advantageous to consider these two types of interaction in sufficient detail to ascertain how contributions from each type would be expected to affect the electron resonance spectra.

 $\operatorname{Abragam}^{35}$  gives the formula for the interaction energy of two point-dipoles as

$$E_{d} = \frac{\overrightarrow{\mu}_{1} \cdot \overrightarrow{\mu}_{2}}{\mathbf{r}^{3}} - \frac{(3\overrightarrow{\mu}_{1} \cdot \overrightarrow{\mathbf{r}}_{12})(\overrightarrow{\mu}_{2} \cdot \overrightarrow{\mathbf{r}}_{12})}{\mathbf{r}^{3}}$$

where  $\vec{\mu}_1$  and  $\vec{\mu}_2$  are the two interacting dipoles, r is the midpoint-distance between the dipoles, and  $\vec{r}_{12}$  is the unit vector along r.

If it is assumed that one dipole is a paramagnetic electron and the other is a nuclear dipole, the equation can be rewritten in slightly different form, introducing the electronic dipole field  $H_{\rm ed}$ 

$$E_{ed} = -\overset{\rightarrow}{\mu}_{N}\overset{\rightarrow}{H}_{ed} = -\overset{\rightarrow}{\mu}_{N} - \frac{\overset{\rightarrow}{\mu}_{e}}{r^{3}} + 3\overset{\rightarrow}{r}_{eN} \frac{\overset{\rightarrow}{\mu}_{e}\overset{\rightarrow}{r}_{eN}}{r^{3}}$$

For parallel spins the equation reduces to  $\frac{\mu_e \mu_N}{r^3}(1 - 3\cos^2\theta)$  where  $\theta$  is the angle between  $r_{eN}$  and  $\mu_e$ . The dipole field  $H_{ed}$  changes from  $\frac{2\mu_e}{r^3}$  at  $\theta = 0$  to  $\frac{-\mu_e}{r^3}$ 

at  $\theta$  =  $\pi/2$ , since it is perpendicular to  $\mu_e$  at  $\theta$  = 54°44'. It will also be noted that the dipole interaction is proportional to the inverse cube of the distance r.

The contribution to the hyperfine interaction arising from Fermi contact  $density^{35,44}$  may be written as

$$E_{c} = \frac{8\pi}{3} (\overset{\rightarrow}{\mu}_{1} \cdot \overset{\rightarrow}{\mu}_{2}) \left| \psi(\mathbf{r}) \right|^{2} = \frac{8\pi}{3} \gamma_{S} \gamma_{I} \kappa^{2} (\overset{\rightarrow}{S} \cdot \overset{\rightarrow}{I}) \left| \psi(\mathbf{r}_{L}) \right|^{2}$$

where  $|\psi(\mathbf{r}_L)|$  is the value of the electronic wavefunction at the ligand nucleus and the other symbols have their usual meanings. The state of lowest energy is the one with the magnetic moments antiparallel. Visualization of this contact effect may be facilitated by introduction of a "contact field"  $H_{\mathbf{fc}}$  at the site of each ligand nucleus with a direction antiparallel to the magnetic moment of the interaction electron spin.

It is to be noted that the functional dependence of  $\psi(r)$  upon r probably is exponential and hence Fermi contact hyperfine interaction will be expected to decrease with increasing electron-nuclear distance much faster than dipole-dipole interaction. The Fermi contact hyperfine interaction is isotropic.

An analysis of the hyperfine structure for a typical Mo(V) ion in particular orientations with respect to the external field will next be considered. It will be assumed that the complex is a tetragonally distorted octahedron ( $C_{4V}$  symmetry) with four ligands on the corners of a square and the Mo(V) ion in the center of the square with the two ligands above and below this square inequivalent with respect to the equatorial ligands. For simplicity the electron and nuclear dipoles will first be considered as point dipoles. The field generated by a paramagnetic electron is about three orders of magnitude larger than the field generated by a ligand nucleus. For this reason it will be assumed that the electronic magnetic moment is polarized along the external magnetic field while the ligand nuclear moment is directed along the vectoral sum of the external field, electronic dipolar field, and Fermi contact field.

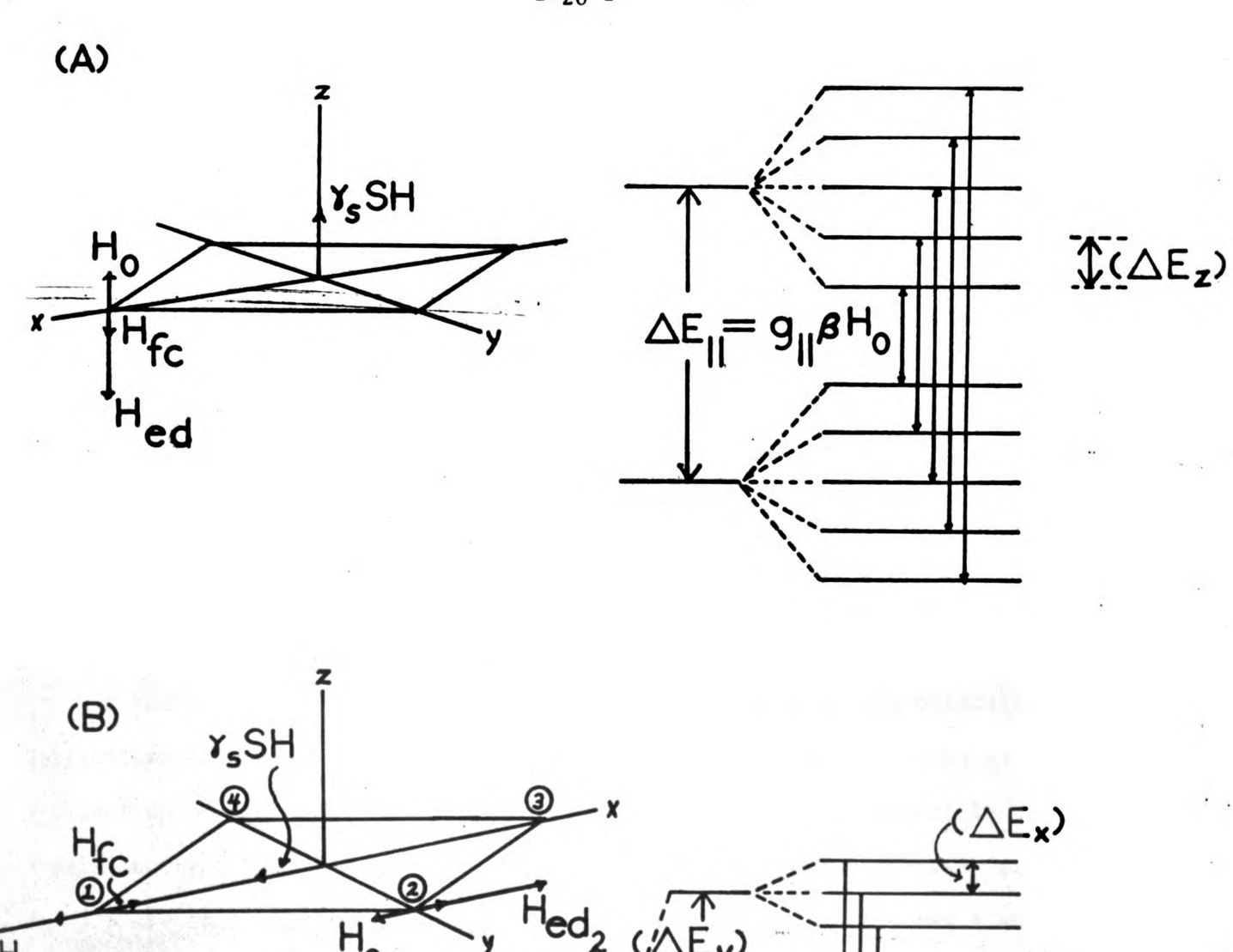
First the case where the external field is parallel to the z-axis of the molecule will be considered. The four ligands in the xy plane are all equivalent with respect to the external field (see Figure 2). The total energy of the complex may be written as

$$E = -\stackrel{\rightarrow}{\mu}_{e} \cdot \stackrel{\rightarrow}{H}_{ext} - \stackrel{\rightarrow}{\stackrel{\rightarrow}{\lim}}_{I} \stackrel{\rightarrow}{\iota} \stackrel{\rightarrow}{H}_{ext} - \stackrel{\rightarrow}{\stackrel{\rightarrow}{\lim}}_{I} \cdot (\stackrel{\rightarrow}{H}_{fc} + \stackrel{\rightarrow}{H}_{ed}).$$

In this particular case all vectors are parallel to the z-axis and  $\vec{\mu}_e$  as well as  $\vec{\mu}_T$  are quantized along that direction:

Figure 2. The Interaction of a Paramagnetic Electron with the Four Equatorial Ligands for two Orientations of the External Magnetic Field with respect to the Axis of Highest Symmetry of the Complex.

- (A) The external field parallel to the axis of highest symmetry.
- (B) The external field directed along one pair of molybdenum-equatorial ligand bond.



 $\Delta \dot{E}_{\perp} = g_{\perp} B H_{0}$ 

$$\mu_{ez} = \gamma_{e} \text{Km}_{S}$$

$$\mu_{Tz} = \gamma_{T} \kappa m_{T}$$

The case where I = 1/2 as occurs with fluorine nuclei, shown in Figure 2, will next be considered. The total quantum number  $M_I = \sum_{I} m_{Ii}$  can assume the values 0,  $\pm 1$ ,  $\pm 2$ . Each electronic spin level is split into five sublevels, the splittings being determined by the magnitudes of the external field interaction, the dipole interaction, and the contact interaction. Taking into account the selection rules  $\Delta m_I = 0$ ,  $\Delta m_S = \pm 1$ , this situation leads to five resonances with relative intensities 1:4:6:4:1. The transition energies are given by  $g_{\parallel} \beta H_{\rm ext} - 2 M_I \gamma_I \hbar (|H_{\rm ed}| + |H_{\rm fc}|)$  (see Figure 2).

If the external field is perpendicular to the z-axis of the molecule, application of the external field in the xy plane may be either in an x- or y-direction on the one hand, or  $H_{\text{ext}}$  may be rotated 45° with respect to the x-axis on the other. An inspection of Figure 2a shows that ligands at sites 1 and 3 are in equivalent environments, but the environment at sites 1 and 3 differs from the environment at sites 2 and 4. For a point dipole on the metal site  $H_{\text{ed}_1} = -2H_{\text{ed}_2}$ . If  $M_1 = m_{11} + m_{13}$  and  $M_2 = m_{12} + m_{14}$  then  $M_{1,2} = 0$ ,  $\pm 1$  for I = 1/2, as is the case for fluorine. Each level of the triplet of one pair is split again into a triplet by the other pair of ligands and as many as 9 resonances may be expected. It is easily seen that the resulting ligand superhyperfine structure is symmetrical around  $g_{\perp}$ . It will be noted, however, that the nine signals are not spaced at equidistant intervals. The transition energies  $\Delta(M_1, M_2)$  between levels of specified  $M_1$  and  $M_2$  are given in Figure 2b.

When the external field is applied at an angle 45° to the x-axis, higher symmetry results: the dipole fields on the four ligand sites are of equal

magnitude and different directions. All angles between the three types of fileds,  $\vec{H}_{ext}$ ,  $\vec{H}_{fc}$ , and  $\vec{H}_{ed}$ , at the sites are also equal. The four ligand sites are thus equivalent, resulting in five equidistant resonance lines. The magnitudes of the splittings depend upon the angle between  $\vec{H}_{ext}$  and  $\vec{H}_{ed45}$ , the local dipole field applicable in this case.

In the point dipole approximation it is clear that the contribution to the superhyperfine interaction arising from dipole-dipole interaction is expected to depend strongly upon the angle betweeen the z-axis of the complex and the external magnetic field. In a frozen glass where all orientations are equally probable a rather complex superhyperfine structure is expected to be observed if the contribution to the superhyperfine interaction arising from dipole-dipole interactions is appreciable. The shape of this spectrum can be calculated by use of the computer program of Lefebvre. 45 In solution the superhyperfine structure is expected to be unresolvable because of the averaging of the large number of spectral types corresponding to the different orientations. Since the Fermi contact interaction is isotropic, all orientations will, for I = 1/2nuclei, give the same five line pattern with relative intensities 1:4:6:4:1. Thus, if the hyperfine interaction is determined by Fermi contact interaction alone, the superhyperfine pattern in solution is expected to be identical to that in the solid, if relaxation effects in the different states are neglected. This seems to provide a simple criterion for distinguishing between the two types of hyperfine interactions. It may be noted that this criterion has been used for years by workers studying organic radicals.

However, the validity of the point dipole approximation must also be considered. Clearly, one should be able to approximate the ligand nuclei as point dipoles to a very high degree of accuracy, but if the paramagnetic electron is

in a d<sub>xy</sub> orbital, it would be highly doubtful that such an approximation is justified for the electronic dipole. For this reason the symmetry of the "electron cloud" must be taken into account.

With the field along the z-axis of the complex the ligand nuclear dipoles are influenced by the same electronic dipolar field as in the point dipole approximation. On the contrary, when the external field is applied in the xy plane along the Mo-L<sub>1</sub> bond there is a substantial deviation from point dipole behavior. Although the exact values will depend on the true shape of the ground state wavefunction, the dipolar fields at ligands L<sub>1</sub> and L<sub>2</sub> will be given approximately by  $|H_{ed_1}| \approx 1.7 |H_{ed}|$  and  $|H_{ed_2}| \approx 0.7 |H_{ed}|$ . When the external magnetic field is applied in the xy plane at an angle 45° from the x-axis, the electron moment  $\gamma_e hS/\sqrt{2}$ . At site 1 the x-component gives a field  $(2^{-\frac{1}{2}})H_{ed_1}$  in the x direction and the y-component gives a field  $(2^{-\frac{1}{2}})H_{ed_2}$  in the negative y direction. Combining these and using the above estimates for  $H_{ed_1}$  and  $H_{ed_2}$ , a dipole field of the order of 1.25  $|H_{ed}|$  with an angle of about 20° with the x-axis is obtained. Because of the equivalence of the ligands L<sub>1</sub>, L<sub>2</sub>, L<sub>3</sub>, and L<sub>4</sub>, their local dipole fields are of equal magnitudes; their directions follow from those to be obtained for the point dipole case,

The direction of quantization of  $\vec{\mu}_I$  is obtained by combining  $\vec{H}_d$  with  $\vec{H}_c$  and  $\vec{H}_{ext}$ . Therefore, in the general expression of the energy,  $\vec{\mu}_I$  is no longer parallel to either  $\vec{H}_d$  or  $\vec{H}_{ext}$ .

Now the contact hyperfine interaction is considered in greater detail than previously discussed. For a pure  $d_{xy}$  orbital the ligands are located on nodes of this function. However, spin-orbit coupling will cause a small amount of  $d_{x^2-y^2}$  to be mixed in, thus producing a small, but non-zero, value of  $|\psi(\mathbf{r_L})|^2$ 

at the ligand site. Hence if appreciable contact hyperfine interaction is observed, it is expected to arise from  $\pi$  bonding of a fluorine p orbital with the Mo  $d_{xy}$  orbital. For such bonding it would not be unreasonable to expect the overlap integral to be 0.05 to 0.10. Further speculation could be made if further assumptions about the bonding were also to be made, but the essential result of this discussion is that the distinctions between contact and dipole-dipole hyperfine interaction remain even if the distribution of the electronic charge cloud over the molecule is taken into account.

#### II. Magnetic Relaxation.

At the outset of this discussion it should be noted that two largely independent mathematical formalisms exist for treating relaxation phenomena in magnetic spin systems.

The first derives from statistical thermodynamics and is structured around the concept of spin temperature. This method assumes that the spins are capable of transferring energy among themselves much more effectively or quickly than from themselves to the lattice, and thus the spins can be described as being in equilibrium. The system can then be described by the distribution functions (e.g., Maxwell-Boltzmann, Fermi-Dirac) of equilibrium statistical thermodynamics. Since the concept of thermalization or temperature broadening of the distribution of particles over the available energy levels is central to the method of equilibrium statistical thermodynamics, it is clear that spin temperature will be a convenient parameter for characterizing the particular distribution under consideration.

Experimental systems having longitudinal or spin-lattice relaxation times of greater than a few milliseconds are capable of being described in terms of

the spin temperature. The concept can be employed conveniently by using the phenomenological approach by Bloch. 46

The second method of calculating relaxation times is that of the density matrix method of Redfield. This method complements the spin-temperature method since it is most effective for the case where the rate determining relaxation process is the transfer of energy from one spin to another rather than to the lattice. Processes where the rate of transfer of energy from the spin system to the lattice is fast and hence which are most effectively treated by the density matrix method include systems undergoing chemical exchange, rapid Brownian movement, translational diffusion, rapid molecular vibrations or rearrangements, or motional narrowing. 48-50

The mathematical operation of the density matrix method involves the solution of differential equations of motions characteristic of the particular system under consideration by using the formalism of matrix algebra. The particular restriction to physical systems where the rate of energy transfer from the spins to the lattice is faster than the rate of energy transfer among the spins themselves arises from the mathematical approximation  $\omega \tau_c << 1$  where  $\omega$  is the precession frequency of the given spin system under consideration and  $\tau_c$  is a correlation time characteristic of the rate of transfer of energy from the spin system to the lattice or the dynamic lattice process which causes this transfer.

The question of deciding which method to use in a given experimental situation always exists. Experimentally there are two solutions to this problem. One is to measure the lattice times by the saturation or spin echo methods. The spin-lattice relaxation time can be used as a criterion; times of a microsecond or less indicate that the density matrix method is preferable while times of greater than a millisecond dictate that the spin temperature

method should be employed. (In reality the popularity of the density matrix method arises from its mathematical convenience and similarity to perturbation theory in quantum mechanics and has resulted in its application to cases (solids, frozen glasses, and crystals) where the relaxation time may be on the order of seconds and where the above criterion certainly would not predict its applicability. The good agreement obtained between theory and experiment in these cases is somewhat puzzling.) A second method of determining the desirability of the respective theoretical methods is to perform an analysis of the shape of the particular absorption under consideration. The density matrix method predicts Lorentzian shape while the spin temperature method may result in either Gaussian or Lorentzian line shapes.

Since the details of the two mathematical methods have been adequately reviewed 33,35-38,51,52 elsewhere it will not be done here.

#### III. Theory of Nuclear Magnetic Relaxation in Paramagnetic Complexes.

The influence of paramagnetic electrons of a substance on nuclear resonance manifests itself in the decrease in the longitudinal,  $T_1$ , and transverse,  $T_2$ , relaxation times of the nuclear magnetization  $\vec{M}$ , and also in the shift  $\delta$  of the nuclear resonance frequency  $\omega_I$ . These effects are due to the action of the magnetic field of the paramagnetic atoms on the nuclear moments. This action varies in time as the result of free precession, electron spin relaxation processes, exchange, and thermal motions. In a number of theoretical papers  $^{48,53-64}$  these effects were studied in substances with a low concentration of paramagnetic ions and without taking the interaction between these electrons into account. A consequence of this approximation was the derivation of the theory of additivity of effects of paramagnetic ions on the relaxation times  $T_1$  and  $T_2$ :  $T_1$  and  $T_2$  are proportional to the reciprocal of the concentration

of paramagnetic ions,  $N_S$ . Experiments carried out at low concentrations of paramagnetic materials have confirmed this conclusion.

At high concentrations of paramagnetic ions exchange interactions can arise between the ions which result in exchange of electron spin orientations and give rise to changes in the internal fields simultaneous with changes due to precession, electron spin relaxation and thermal motion. As a result, the internal fields must average out to a greater degree than in the absence of exchange, and are manifest in a decrease in the effectiveness of the influence on the relaxation times  $T_1$  and  $T_2$  by additional paramagnetic atoms newly added to the substance. Under these conditions the relation  $T_1^{-1}$ ,  $T_2^{-1}$  a  $N_S$  must break down.

In the subsequent paragraphs an attempt is made to develop a theory of the shape and of the width  $(T_2^{-1})$  of the resonance line due to nuclei in paramagnetic media, taking into account the exchange interactions between the paramagnetic ions, which are in turn modulated by the thermal motion in the system. In the limit of dilute solutions (i.e., the absence of electron exchange) these equations reduce to those developed by other workers.  $^{48,53-64}$  This development is important for three reasons. First, it permits an analysis of relaxation data at all concentrations from which one may obtain spin echoes (or free precession tails) or reasonably wide NMR lines. Second, it facilitates a better understanding of the approximation of non-interaction electron spins made in the earlier calculations,  $^{48,53-64}$  and finally, the result permits a better correlation of nuclear relaxation data with electron relaxation data. The calculations were carried out utilizing the method of Kubo and Tomita.  $^{65,66}$ 

According to Kubo and Tomita<sup>65</sup> the half-width  $\Delta\omega_{\chi}=1/T_2$  of a magnetic resonance line and the spin-lattice relaxation time  $T_1$  are determined by the

formulas

$$(T_2)^{-1} = \sum_{\beta} \sigma_{1\beta}^2 \tau_{1\beta}^2$$
,  $(T_1)^{-1} = \sum_{\beta} \sigma_{0\beta}^2 \tau_{0\beta}^2$  (1)

$$\tau_{\alpha\beta}' = \operatorname{Re} \int_{0}^{\infty} e^{i\omega\beta\tau} f_{\alpha\beta}(\tau) d\tau \tag{2}$$

$$h^2 \sigma_{\alpha\beta}^2 f_{\alpha\beta}(\tau) = \langle \{ [\hat{I}_{\alpha}, \hat{H}_{\beta}(\tau)] [\hat{H}_{\beta}', \hat{I}_{-\alpha}] \} \rangle / \langle |\hat{I}_{\alpha}|^2 \rangle$$
(3)

$$f_{\alpha\beta}(0) = 1; \{AB\} = (1/2)(AB + BA)$$

$$\hat{I}_{o} = \hat{I}_{z}, \hat{I}_{\pm 1} = \hat{I}_{x}^{\pm} i \hat{I}_{y}$$
 (4)

where the notation is standard density matrix notation. 65,66

Formulas (1) through (4) are valid for  $(E_{\ell} - E_{k}) \ll kT$  and  $\sigma\tau_{c} \ll 1$ .  $E_{\ell}$  and  $E_{k}$  are the energies of the magnetic sublevels of the particles;  $\tau_{c}$  is a parameter having the meaning of a correlation time of the perturbation  $\hat{H}'(\tau)$ . The indicated inequalities are almost always fulfilled for liquids. The angular brackets in Eq. (3) signify averages over the spin and lattice variable with the density matrix of the system.

Next the autocorrelation function for the nuclear magnetization in a system which contains  $N_{\rm I}$  identical magnetic nuclei and  $N_{\rm S}$  paramagnetic ions per unit volume will be considered.

The shape of the absorption line,  $I(\omega)$ , is given by the Fourier transform of the autocorrelation function G(t) of the component of the magnetic moment parallel to the direction (x) of the variable (radiofrequency) magnetic field:  $^{65}$ 

$$I(\omega) = (1/2\pi) \int_{0}^{\infty} G(t) e^{-i\omega t} dt$$
 (5)

$$G(t) = \langle \{M_{v}(t)M_{v}(0)\} \rangle$$
 (6)

The angle brackets in Eq. (6) denote averaging of the symmetrized product  $\{M_X(t)M_X(0)\}$  by use of the density matrix  $\rho$ . Since the gaps between the magnetic sublevels are small (N $\omega$  << kT), it can be assumed that

$$\rho = 1/\{(2I+1)^{(N_I)}\}\{(2S+1)^{(N_S)}\}$$
(7a)

so that

$$M_{\mathbf{Y}}(t) = \exp(it\hat{H}/\hbar)M_{\mathbf{Y}}\exp(-it\hat{H}/\hbar)$$
 (7b)

where  $\hat{H}$  is the total Hamiltonian for the system without the variable radio-frequency field which in the case under consideration includes the Zeeman energies

$$\hat{H}_{z}^{I} = \gamma_{I} \hat{H}_{o} \sum_{k} \hat{I}_{k}^{z} = g_{I} \beta_{N} \hat{H}_{o} \sum_{k} \hat{I}_{k}^{z}$$

$$(7c)$$

$$\hat{H}_{z}^{S} = \gamma_{S} H_{o} \sum_{\ell} \hat{S}_{\ell}^{z} = g \beta H_{o} \sum_{\ell} \hat{S}_{\ell}^{z}$$
(7d)

of the nuclear and electronic moments in a constant magnetic field  $\vec{H}_0$  ( $\vec{H}_0$  || z), the energy of interaction of nuclear and electronic moments,

$$\hat{H}_{IS} = \gamma_{I} \gamma_{S} \sum_{k>\ell} r_{k\ell}^{-3} [\hat{I}_{k} \hat{S}_{\ell} - 3r_{k\ell}^{-3} (\hat{I}_{k} \dot{r}_{k\ell}) (\hat{S}_{\ell} \dot{r}_{k\ell})] + \kappa \sum_{k>\ell} A_{k\ell} \hat{I}_{k} \hat{S}_{\ell}$$
(7e)

where the first term represents the through-space or dipolar spin-spin interaction and the second term represents the scalar coupling or Fermi contact hyperfine interaction, the energy of the exchange interaction of electron spins among themselves,

$$\hat{H}_{e} = \tilde{h} \sum_{i>j} J_{ij}(r_{ij}) \hat{S}_{i} \hat{S}_{j} , \qquad (7f)$$

the kinetic energy of the system  $\hat{H}_K$  and the energy  $\hat{H}_{SK}$  of interaction of the electron spin system with  $\hat{H}_b$ .

The Hamiltonian  $\hat{H}$  may be separated into three parts:

$$\hat{H}_{1} = \hat{H}_{z}^{I}; \hat{H}_{2} + \hat{H}_{z}^{S} + \hat{H}_{SK} + \hat{H}_{K} + \hat{H}_{e}; \hat{H}^{I} = \hat{H}_{IS}$$
(8)

where  $\hat{H}'$  is to be considered the perturbation. These Hamiltonians  $(\hat{H}_1, \ \hat{H}_2, \ \hat{H}')$  satisfy the commutation relations  $^{49,50}$ 

$$[\hat{H}_1, \hat{H}_2] = [\hat{H}_2, \hat{M}_x] = 0$$
 (9)

Upon substitution of the solution of the Heisenberg equation into (6)

$$ih\hat{M}_{x} = [\hat{M}_{x}(t), \hat{H}_{1} + \hat{H}_{2} + \hat{H}^{\pm}]$$
 (10)

the first terms of the series  $G(t) = G_n(t)$  are obtained

$$G_0(t) = (1/6)N_I\gamma_I^2I(I+1)[e^{(i\omega_It)} + ...]$$
 (11)

$$G_1(t) = 0 (12)$$

$$G_{2}(t) = (-1/6)N_{I}\gamma_{I}^{2}I(I+1)\left[e^{(i\omega_{I}t)} \times \sum_{\gamma} \sigma_{\gamma}^{2} \int_{0}^{4} d\tau (t-\tau)e^{(i\omega_{\gamma}\tau)} f_{\gamma}(\tau) + ...\right]$$

$$(13)$$

where

$$\sigma_{\gamma}^{2} = \tilde{h}^{(-2)} < |[\hat{M}_{+}^{(0)}, \hat{H}_{\gamma}^{\prime}(0)]|^{2} > / < |M_{+}^{(0)}|^{2}>,$$

$$M_{\pm}^{(0)} = \gamma_{I_{k}} \sum_{k} (I_{k}^{x} \pm i I_{k}^{y}), \qquad (14)$$

$$f_{\gamma}(\tau) = \hat{N} < [\hat{M}_{X}^{(0)}, \hat{H}_{\gamma}^{\dagger}(\tau)] [\hat{H}_{\gamma}^{\dagger}, \hat{M}_{-}^{(0)}] >,$$
 (15)

$$H'(\tau) = \sum_{\gamma} e^{(i\omega_{\gamma}\tau)} \hat{H}'(\tau) = \sum_{\gamma} e^{(i\omega_{\gamma}\tau)} \exp(i\tau \hat{H}_{2}/\hbar) \hat{H}'_{\gamma} \exp(-i\tau \hat{H}_{2}/\hbar).$$
 (16)

Here  $\sigma_{\gamma}^{\ 2}$  is the contribution to the second moment of the resonance line (in frequency units) due to  $\hat{H}'_{\gamma}$  (the contributions of the individual terms in the perturbation  $\hat{H}_{1S}$  to the second moment are additive);  $f_{\gamma}(\tau)$  is the correlation function for the quantities  $\hat{H}'_{\gamma}(\tau)$  which vary in time under the influence of  $\hat{H}_{2}$  (modulation of the perturbation by "motion").  $\hat{N}$  is a formal operator defined by the relation

$$NA(t) = A(t)/A(0).$$

It is to be noted that  $G_0(t)$  describes the unperturbed motion of the nuclear magnetization—the free precession.

In order to obtain  $f_{\gamma}(\tau)$  of the form (15) one must evaluate

$$\hat{H}_{\gamma}^{\prime}(\tau) = \exp[i\hbar^{-1}\tau(\hat{H}_{z}^{S} + \hat{H}_{SK} + \hat{H}_{K} + \hat{H}_{e})] \times \hat{H}_{\gamma}^{\prime}\exp[-i\hbar^{-1}\tau(\hat{H}_{z}^{S} + \hat{H}_{SK} + \hat{H}_{K} + \hat{H}_{e})]$$
(17)

The electronic Zeeman Hamiltonian,  $\hat{H}_z^S$ , in (17) yields time factors of the form  $\exp(i\beta\omega_S\tau)$ ,  $\beta=0$ ,  $\pm 1$ .  $\hat{H}_{SK}$  describes relaxation processes for the components of the electron spin, so that  $f_{\gamma}(\tau)$  is equivalent to

$$\hat{N} < \hat{S}_{\beta}(\tau) \hat{S}_{-\beta}(0) > = \exp(-|\tau|/T_{\beta})$$

$$T_{\beta} = \{ T_{1}, \beta = 0 \}$$

$$T_{\beta} = \{ T_{2}, \beta = \pm 1 \}$$
(18)

Further, it is assumed that the time variation of the exchange energy

$$\hat{H}_{e}(\tau) = \exp(i\tau \hat{H}_{K}/K)\hat{H}_{e}\exp(-i\tau \hat{H}_{K}/K)$$

under the influence of thermal motion in the system  $\hat{H}_{K}$  is characterized by the correlation time  $\tau_{e}$ :

$$\hat{N} < \hat{H}_{e}(\tau) \hat{H}_{e}(0) > = \exp(-|\tau|/\tau_{e})$$
 (19)

Considering the limiting condition

$$<|\hat{H}_{e}|^{2}> << <|H_{K}|^{2}>$$

(17) may be expanded into a series in powers of  $\hat{H}_e$ . The effect of  $\hat{H}_e$  on the correlation function for the perturbation is manifest in the term in the expansion quadratic in  $\hat{H}_e$  (the term linear in  $\hat{H}_e$  gives zero upon averaging).

Taking into account the properties of  $\hat{H}_{\gamma}^{\prime}(\tau)$  and  $f_{\gamma}(\tau)$ , the result of calculation is

$$<|[\hat{M}_{+}^{(0)}, \hat{H}_{Y}^{'}(0)]|^{2}>f_{Y}(\tau) = \sum_{\beta} \sum_{\alpha=1,2}^{\prime} e^{(i\beta\omega} S^{\tau)} <|[\hat{M}_{+}^{(0)}, \hat{H}_{Y\beta,\alpha}^{IS}(0)]|^{2}>f_{Y\beta,\alpha}(\tau)$$

$$\times (1 - \omega_{eY\beta,\alpha}^{2} F(\tau)) \exp(-|\tau|/T_{\beta}), \qquad (20)$$

$$f_{\gamma\beta,1}(\tau) = \hat{N} \sum_{k>\ell} \langle \exp(i\hbar^{-1}\tau \hat{H}_{K}) \underline{\Phi}_{k\ell}^{\gamma\beta} \times \exp(-i\hbar^{-1}\tau \hat{H}_{K}) \underline{\Phi}_{k\ell}^{-\gamma,-\beta} \rangle,$$

$$= \hat{N} \sum_{k>\ell} \langle \underline{\Phi}_{k\ell}^{\gamma\beta}(\tau) \underline{\Phi}_{k\ell}^{-\gamma,-\beta}(0) \rangle,$$
(21)

$$f_{\gamma\beta,2}(\tau) = \hat{N} \sum_{k,\ell} \langle \exp(i\hbar^{-1}\tau \hat{H}_{K}) A_{k\ell}^{\gamma\beta}(\mathbf{r}_{k\ell}) \times \exp(-\hbar^{-1}\tau \hat{H}_{K}) A_{k\ell}^{-\gamma,-\beta}(\mathbf{r}_{k\ell}) \rangle$$

$$= \hat{N} \sum_{k,\ell} \langle A_{k\ell}^{\gamma\beta}(\tau) A_{k\ell}^{-\gamma,-\beta}(0) \rangle;$$

$$F(\tau) = \int_0^{\tau} (\tau - \tau') d\tau' \exp(-|\tau|/\tau_e), \qquad (22)$$

$$\omega_{e\gamma\beta,\alpha}^{2} = \langle |[\hat{H}_{e}, [\hat{M}_{+}^{(0)}, \hat{H}_{\gamma\beta,\alpha}^{IS}]]|^{2} \rangle / \kappa^{2} \times \langle |[\hat{M}_{+}^{(0)}, \hat{H}_{\gamma\beta,\alpha}^{IS}]|^{2} \rangle$$
(23)

Here  $H_{1\beta,\alpha}^{IS}$  are the terms in the expansion of the energy of interaction between nuclear and electron spins in terms of the Zeeman frequencies of nuclear and electron spins

$$\hat{H}' = \hat{H}_{IS} = \sum_{\gamma,\beta} (\hat{H}_{\gamma\beta,1}^{IS} + \hat{H}_{\gamma\beta,2}^{IS})$$

$$= \sum_{\gamma,\beta} \left[ \sum_{k>\ell} \{k\ell\}_{\gamma\beta,1} \Phi_{k\ell}^{\gamma\beta} + \sum_{k,\ell} \{k\ell\}_{\gamma\beta,2} A_{k\ell}^{\gamma\beta} \right]$$

The subscript  $\alpha$  distinguishes quantities which refer to the dipole ( $\alpha$  = 1) and the hyperfine ( $\alpha$  = 2) interactions. The shape of the resonance line is of concern out to distances from the center of the line of the order of its width. Information with respect to this part of the line will be obtained if the integration in (13) is carried out up to t =  $T_2^0$ , where  $T_2^0$  is the transverse relaxation time of the nuclei in the absence of motion. It can be shown that  $F(\tau) = \tau^2/2$  for  $T_2^0 << \tau_e$  and  $F(\tau) = |\tau|\tau_e$  for  $T_2^0 >> \tau_e$ . Then following the procedure of Ref. 65 and denoting  $\omega_{e\gamma\beta,\alpha}^2 = \omega_e^2$ , one can write

$$1 - \omega_{e\gamma\beta,\alpha}^{2} F(\tau) \simeq \exp[-\omega_{e}^{2} F(\tau)]$$

$$= \begin{cases} \exp(-\tau^{2} \omega_{e}^{2}/2), & T_{2}^{0} << \tau_{e} \\ \exp(-|\tau|\tau_{e}^{2} \omega_{e}^{2}), & T_{2}^{0} >> \tau_{e} \end{cases}$$
(24a)

The quantity  $\omega_{e\gamma\beta}^{\ 2}$  (23) has the meaning and the dimensions of the square of the exchange frequency.

For the correlation function (21) of the coordinate part of the perturbation  $\hat{H}^{IS}_{\gamma\beta,1}$  which varies under the influence of the classical thermal motion of  $\hat{H}_{K}$  one can take  $^{48}$ 

$$f_{\gamma\beta,1}(\tau) = \exp(-|\tau|/\tau_1) \tag{25a}$$

With respect to the hyperfine interaction energy two cases must be distinguished.

If one intends to consider the interaction of the electron and nuclear spins

belonging to different particles moving independently, then one can set

$$f_{\gamma\beta,2}(\tau) = \exp(-|\tau|/\tau_2),$$
 (25b)

where  $\tau_2$  represents the lifetime of the diamagnetic particle in the solvate shell of the paramagnetic ion. Obviously in a solid  $\tau_2^{-1} = 0$ , but if the isotropic interaction of the nuclear moment of the ion with its own electron is considered (the anisotropic part is customarily not very great and its effect is negligible), then  $\tau_2^{-1} = 0$ , and

$$f_{\gamma\beta,2} = 1 \tag{25c}$$

since this interaction is not modulated by thermal motion.

Upon substitution of (21) into (13) and employing the relationships (24) and (25) one obtains for  $G_0(t) + G_2(t)$  the expression (omitting a constant factor)

$$e^{(i\omega_{\mathbf{I}}\mathbf{t})} \left(1 - \sum_{\alpha=1,2} \sum_{\gamma,\beta} \sigma_{\gamma\beta,\alpha}^{2} \int_{0}^{\mathbf{t}} d\tau (\mathbf{t}-\tau) \exp[i(\gamma\omega_{\mathbf{I}} + \beta\omega_{\mathbf{S}})\tau] \right)$$

$$\times \exp[-|\tau|\tau_{\alpha}^{-1} - |\tau|T_{\beta}^{-1} - \omega_{\mathbf{e}}^{2}F(\tau)] + \dots$$
(26)

which can be approximately represented in the form

$$\exp \left[i\omega_{\mathbf{I}}\mathbf{t} - \sum_{\alpha=1,2} \sum_{\gamma,\beta} \sigma_{\gamma\beta,\alpha}^{2} \int_{0}^{t} d\tau (\mathbf{t}-\tau) \exp[i(\gamma\omega_{\mathbf{I}} + \beta\omega_{\mathbf{S}})\tau]\right] \times \exp[-|\tau|\tau_{\alpha}^{-1} - |\tau|T_{\beta}^{-1} - \omega_{\mathbf{e}}^{2}F(\tau)] + \dots$$
(27)

The next consideration is the calculation of the line shape for two limiting cases--fast motion (liquids) and slow motion (viscous liquids, solids)--of the system.

A. Fast thermal motion: 
$$T_2^0 > \tau_e$$

In order to find the line shape  $I(\omega)$  near its maximum one should (in the case  $T_2^{\ o} >> \tau_e$ ) evaluate the Fourier transform of the autocorrelation function (27) making use of (24b). A Lorentz line of half-width  $\Delta\omega_{\frac{1}{2}}$  and with its center at the frequency  $^{67}$   $\omega_{\frac{1}{4}}$  +  $\delta$  is obtained:

$$\Delta\omega_{\frac{1}{2}} = S(S+1)\sigma_{IS}^{2} \left[ (1/3)R_{01} + (1/2)(R_{11}^{-1}/[R_{11}^{-2} + \omega_{S}^{2}]) + (1/4)(R_{01}^{-1}/[R_{01}^{-2} + \omega_{I}^{2}]) \right]$$

$$+ (1/2)(R_{11}^{-1}/[R_{11}^{-2} + (\omega_{S} + \omega_{I})^{2}]) + (1/12)(R_{11}^{-1}/[R_{11}^{-2} + (\omega_{I} - \omega_{S})^{2}])$$

$$+ (1/3)[S(S+1)] < A^{2} > \left[ R_{02} + R_{12}^{-1}/[R_{12}^{-2} + (\omega_{I} - \omega_{S})^{2}] \right]$$

$$-\delta = S(S+1)\sigma_{IS}^{2} \left[ (1/2)(\omega_{I}/R_{01}^{-2} + \omega_{I}^{2}) + (1/2)([\omega_{I} + \omega_{S}]/[R_{11}^{-2} + (\omega_{I} + \omega_{S})^{2}]) \right]$$

$$+ (1/12)([\omega_{I} - \omega_{S}]/[R_{11}^{-2} + (\omega_{I} - \omega_{S})^{2}])$$

$$+ S(S+1) < A^{2} > ([\omega_{I} - \omega_{S}]/[R_{12}^{-2} + (\omega_{I} - \omega_{S})^{2}])$$

$$R_{0,\alpha}^{-1} = \tau_{\alpha}^{-1} + T_{1}^{-1} + \tau_{e}\omega_{e}^{2} ; R_{1,\alpha}^{-1} = \tau_{\alpha}^{-1} + T_{2}^{-1} + \tau_{e}\omega_{e}^{2}$$

$$(30)$$

A brief discussion of formulas (28) - (30) follows. First, it follows from the definition of  $R_{0,\alpha}^{-1}$ ,  $R_{1,\alpha}^{-1}$  in (30) that the half-width and the shift of

the resonance line due to nuclear spins are determined by the velocities of thermal motion, by the electron relaxation or by the electron exchange motion depending on which process proceeds at the greatest rate:  $\tau_{\alpha}^{-1}$ ,  $T_{\beta}^{-1}$ , or  $\tau_{e}\omega_{e}^{2}$ . For paramagnetic ions of the type  $Cu^{2+}$ ,  $VO^{2+}$ , etc.,  $T_{1}^{-1}$ ,  $T_{2}^{-1} \simeq 10^{8} \text{ sec}^{-1}$ ; for other paramagnetic ions (Ti<sup>3+</sup>, Fe<sup>2+</sup>, Co<sup>2+</sup> from the iron group and the rare earth ions) the relaxation times are very short, and apparently, one can estimate  $T_{1}^{-1} > 10^{10} \text{ sec}^{-1}$ .

In nonviscous liquids  $\tau_1^{-1} \simeq 10^{11}~\text{sec}^{-1}$ . One can suppose that the values of  $\tau_e^{-1}$  will be somewhat greater than the values  $\tau_1^{-1}$  in view of the greater sensitivity of the exchange energy to the variations in the distances between the paramagnetic ions. For rough calculations one can assume that  $\tau_e^{-1} \simeq \tau_1^{-1}$ . The lifetime of a particle in the solvate shell of the ion,  $\tau_2$ , as a rule will be greater than the relaxation times  $T_1$  and  $T_2$  and the effect of thermal motion on the hyperfine interaction will become unobservable. Moreover, in concentrated solutions,  $\sigma_{\rm IS}^2 >> < A^2 >$ , since the internal field amount to approximately  $10^3$  to  $10^4$  gauss, while  $|A| \simeq 10$  to  $10^2$  gauss. In concentrated solutions  $\omega_e$  can attain values of  $10^{10}$  to  $10^{11}$  sec<sup>-1</sup>.

These estimates show that very different situations can be realized in practice. One case of interest occurs when the dominant terms in  $R_{\beta}^{-1}$  are the terms  $\omega_e^2 \tau_e^2 + \tau_\alpha^{-1}$ . It is realized in solutions of relatively high concentrations of paramagnetic particles with not too short relaxation times  $T_1$ ,  $T_2$ . Then

$$R_{\beta,\gamma} = \tau_{\alpha}/(1 + \tau_{\alpha}\tau_{e}\omega_{e}^{2})$$

and for  $R_{\beta,\alpha}^{-1} >> \omega_I$ ,  $\omega_S$  the following expression is obtained from (28) for the half-width

$$\Delta\omega_{\frac{1}{2}} = (20/12)S(S+1)\sigma_{1S}^{2}\tau_{1}/(1 + \tau_{1}\tau_{e}\omega_{e}^{2}) + (2/3)S(S+1)\langle A^{2}\rangle\tau_{2}/(1 + \tau_{2}\tau_{e}\omega_{e}^{2})$$
(31a)

For large values of  $\omega_e^2$  one obtains by neglecting in the denominators of expression (31a) unity in comparison to  $\tau_\alpha \tau_e \omega_e^2$ 

$$\Delta\omega_{1/2} = S(S+1)[(20/12)\sigma_{1S}^2 + (2/3)\langle A^2 \rangle]/\tau_e\omega_e^2$$
 (31b)

Since  $\sigma_{\rm IS}^2$ ,  $\omega_{\rm e}^2$ ,  ${<}{\rm A}^2{>} \simeq {\rm N}_{\rm S}$  (the hyperfine interaction with an electron spin belonging to a different ion is under consideration), then it follows from (31a) that in this range the dependence of  $\Delta\omega_{\rm L}$  on concentration will be due to the variations in  $\tau_{\rm e}$  which increases as the concentration is increased; therefore,  $\Delta\omega_{\rm L}$  will decrease. Further, in accordance with (28), the line width will gradually diminish as the external field increases. In weak fields  $(R_{\beta,\alpha}^2\omega_{\rm S}^2<<1)$  the observed width is given by (31a). In strong fields  $(R_{\beta,\alpha}^2\omega_{\rm S}^2>>1$ , but  $R_{\beta,\alpha}^2\omega_{\rm I}^2<<1)$  the following expression is obtained

$$\Delta\omega_{\frac{1}{2}} = (7/12)S(S+1)\sigma_{IS}^{2}R_{\beta,1} + (1/3)S(S+1) < A^{2} > R_{\beta,2}$$
 (31c)

In the absence of exchange (low concentration of paramagnetic ions), (28) together with (30) become similar to the well known formulas of Bloembergen<sup>57</sup> and of Conger and Selwood.<sup>68</sup>

Of some interest are the investigations of the line shift - $\delta$  (formula (29) gives the shift in units of rad/sec). As can be seen from (29), - $\delta$  passes through a maximum (as the external field is varied) at  $\omega_{\rm I} = R_{01}^{-1}$  and  $\omega_{\rm S} + \omega_{\rm I} = R_{11}^{-1}$ . At the same time the shift diminishes as the velocity of the motion  $R_{\beta,\alpha}^{-1}$  increases.

B Slow thermal motion:  $T_2^{o} \ll \tau_e$ 

The condition  $T_2^0 << \tau_e$ ,  $\tau_1$ ,  $\tau_2$  corresponds to a slow modulation of the exchange, hyperfine and dipole interactions with the thermal motion. The

nature of the phenomenon is in this case determined by the exchange and the relaxation motions in the electron spin system. The nuclear absorption line near ist maximum has a Lorentz shape, since the approximate autocorrelation function assumes the following form for  $T_2^0 << \tau_e$ :

$$\exp\{i\omega_{\mathbf{I}}\mathbf{t} - \mathbf{t}\sum_{\gamma,\beta}\sigma_{\gamma\beta}^{2}\int_{0}^{\infty}\exp[-\tau[T_{\beta}^{-1} - i(\gamma\omega_{\mathbf{I}} + \beta\omega_{\mathbf{S}})] - \tau^{2}\omega_{\mathbf{e}}^{2}/2]d\tau\} + \dots,$$

$$\sigma_{\alpha\beta}^{2} = \sigma_{\alpha\beta,1}^{2} + \sigma_{\alpha\beta,2}^{2}$$
(32)

The factor multiplying  $\gamma$  in the exponent of the exponential determines the position of maximum intensity  $\omega_{\rm I}$  +  $\delta$  <sup>67</sup>, while the factor multiplying [-t] determines the half-width  $\Delta\omega_{\rm g}$ 

$$\Delta\omega_{1_{2}} = \sqrt{(\pi/2)} \ \omega_{e}^{-1} \ \sum_{\gamma=0}^{1} \ \sum_{\beta=-1}^{1} \sigma_{\gamma\beta}^{2} ReL(Z_{\gamma\beta})$$
 (33)

$$\omega_{\rm I} + \delta = \omega_{\rm I} - \sqrt{(\pi/2)} \omega_{\rm e}^{-1} \sum_{\gamma=0}^{1} \sum_{\beta=-1}^{1} \sigma_{\gamma\beta}^2 ImL(Z_{\gamma\beta});$$

$$|\gamma| + |\beta| \neq 0 \tag{34}$$

$$Z_{\gamma\beta} = (\gamma \omega_{I} + \beta \omega_{S} - iT_{\beta}^{-1})/\omega_{e}\sqrt{2}$$
 (35)

$$L(Z) = \exp(-Z^2) - i2W(Z)/\sqrt{\pi}$$
,  $W(Z) = \exp(-Z^2)\int_0^Z \exp(x^2dx)$  (36)

A brief analysis of formulas (33) - (36) is given. In a number of cases (Mm<sup>2+</sup>, Cr<sup>3+</sup>, VO<sup>2+</sup>) the electron relaxation times  $T_{\beta} = T_{1}$ ,  $T_{2}$  are comparatively long, about  $10^{-7}$  to  $10^{-8}$  seconds, so that  $T_{\beta}^{-1} << \omega_{S} \neq 0$ ; therefore in  $Z_{\gamma\beta}$  the imaginary part can be neglected if  $\beta \neq 0$ . Moreover, if  $T_{\beta}\omega_{e} >> 1$ , then the formula for the half-width of the line (33) assumes the following form:

$$\Delta\omega_{\frac{1}{2}} = \sqrt{(\pi/2)} \omega_{e}^{-1} [\sigma_{00}^{2} + \sigma_{10}^{2} + \sum_{\gamma=0,1}^{\Sigma} \sum_{\beta=\pm 1}^{\sigma_{\gamma\beta}} \exp\{-(\gamma\omega_{I} + \beta\omega_{S})^{2}/2\omega_{e}^{2}\}]$$
(37)

analogous to the well known formulas for the half-width of the electron resonance line. <sup>65</sup> For the line shift  $\delta$  one obtains in the present case  $(T_g^{-1} << |\beta\omega_S|, \beta \neq 0)$ 

$$-\delta = \sqrt{2} \omega_{\mathbf{e}} \sum_{\gamma=0}^{\infty} \sum_{\beta=\pm 1}^{\infty} \sigma_{\gamma\beta}^{2} \mathbf{W} [(\gamma \omega_{\mathbf{I}} + \beta \omega_{\mathbf{S}}) / \sqrt{2} \omega_{\mathbf{e}}]$$
(38)

When the relationship  $\gamma \omega_I + \beta \omega_S \simeq \beta \omega_S$  is taken into account, expression (38) may be rewritten as

$$-\delta = \sqrt{2} \omega_e^{-1} S(S+1) [(5/12)\sigma_{IS}^2 - (1/3) < A^2 >] \exp(-y^2) \int_0^y \exp(x^2 dx)$$
 (39)

which reaches a maximum at  $y = \omega_S / \sqrt{2} \omega_e = 0.925$ . Thus by measuring the width (35) and the shift (39) one can find the exchange frequency  $\omega_e$ .

In the opposite case  $T_{\beta}^{-1} >> |\gamma \omega_{\tilde{I}} + \beta \omega_{\tilde{S}}|$  (weak fields) one can set  $Z_{\gamma\beta}$  equal to  $-i\sqrt{2}$   $\omega_{\tilde{e}}T_{\beta}$ . Then the shift  $\delta=0$ , since in such an approximation  $L(Z_{\gamma\beta})$  is real, while the half-width of the line  $\Delta\omega_{\gamma_{\tilde{e}}}$  does not depend upon the constant magnetic field, but will vary markedly as the concentration of the paramagnetic ions is varied:

$$\Delta\omega_{\frac{1}{2}} = \sqrt{(\pi/2)} \ \omega_{e}^{-1} \left[ S(S+1) \left[ (7/12) \sigma_{IS}^{2} + (1/3) < A^{2} > \right] \exp(u^{2}) \right]$$

$$\times \left[ 1 - (2/\sqrt{\pi}) \int_{0}^{u} \exp(-x^{2} dx) \right] + \left[ (13/12) \sigma_{IS}^{2} + (1/3) < A^{2} > \right] \exp(u^{2})$$

$$\times \left[ 1 - (2/\sqrt{\pi}) \int_{0}^{v} \exp(-x^{2} dx) \right] ,$$

$$u = 1/\sqrt{2} \ T_{1}\omega_{e}, \quad v = 1/\sqrt{2} \ T_{2}\omega_{e}$$

$$(40)$$

In the case of weak exchange, when the exchange in the electron spin system is slower than the relaxation motions  $(T_1^{-1}, T_2^{-1} >> \omega_e)$ , formula (40) is inapplicable and the calculation must be repeated neglecting in

(32) the quantity  $\omega_e^2 \tau^2/2$  in comparison to  $\tau/T_\beta$ ; the formulas obtained are not reproduced here since in this case they coincide exactly with (28) and (29) with  $R_{\beta,\alpha}^{-1} = T_{\beta}^{-1}$ . In the case  $\omega_e \simeq T_{\beta}^{-1}$  one should utilize formula (40) and tables of functions for estimating the line width.

Finally, in calculation one could also have taken into account the symmetry of the complex ion as Woessner<sup>69</sup> has done; however, in inorganic complexes this calculation does not appear to be necessary to obtain good agreement between experimental results and theoretical calculated values.

#### IV. Paramagnetic Relaxation in Inorganic Complexes.

In this section a general review of paramagnetic relaxation in inorganic complexes is not attempted, but rather a brief consideration of the theory necessary for interpretation of the spectra of Mo(V) complexes is presented, making reference to the appropriate literature for the mathematical development. For clarity spin-spin and spin-lattice relaxation processes will be treated separately. Spin-spin processes are further divided according to their dependence on the nuclear spin quantum number  $m_{\tilde{I}}$ .

- A. Spin-spin or Longitudinal Relaxation Processes.
  - 1. Nuclear Spin Dependent Relaxation.

Nuclear spin dependent relaxation arises from a distribution of Zeeman and/or hyperfine interactions. The first such nuclear spin dependent relaxation process, observed by McConnell, <sup>70</sup> arises from the averaging of anisotropic Zeeman and hyperfine interactions by the molecular tumbling of the paramagnetic complex in solution. This case has been treated in detail by Kivelson. <sup>15-17,71</sup> The result of the Kivelson derivation modified for the case of an axially symmetric complex is given in Table III.

TABLE III. Coefficients in the Kivelson Expression for Linewidth.

$$T_2^{-1} = \alpha' + \beta m_I + \gamma m_I^2 + \delta m_I^3$$

$$\alpha' = (1/45)\omega_o^2(\Delta g/g)^2\tau_R[4 + 3u] - (1/30)\omega_o(\Delta g/g)bI(I+1)(a/\omega_o)\tau_R[1 + u] + (1/40)b^2I(I+1)\tau_R[3 + 7u - 5uf(a/\omega_o)]$$

$$\beta = (1/15)b\omega_{o}(\Delta g/g)\tau_{R}[4 + 3u] - (1/45)\omega_{o}^{2}(\Delta g/g)^{2}(a/\omega_{o})\tau_{R}[8 + 6u + 6uf]$$
$$- (1/20)b^{2}I(I+1)(a/\omega_{o})\tau_{R}[4 + 3u + 7uf] + (1/40)b^{2}[2I(I+1)-1](a/\omega_{o})\tau_{R}[3 + 2u]$$

$$\gamma = (1/40)b^2 \tau_R [5 - u + 5uf(a/\omega_0)] - (1/30)b\omega_0(\Delta g/g)(a/\omega_0)\tau_R [7 + 5u + 12uf]$$

$$\delta = (1/20)b^{2}(a/\omega_{o})\tau_{R}[1 + u + uf]$$

$$\Delta H = (2/\sqrt{3}) (\hbar/g\beta) T_2^{-1}$$

where

 $\omega_{\alpha}$  = microwave frequency

 $\Delta g = g_{||} - g_{||} = anisotropy of electronic Zeeman tensor$ 

 $\boldsymbol{\tau}_{\boldsymbol{R}}$  = rotational correlation time

b = A - B = anisotropy of the hyperfine tensor

I = nuclear spin quantum number

$$u = 1/(1 + \omega_0^2 \tau_R^2)$$

$$f = \omega_0^2 \tau_R^2 u$$

The second mechanism giving rise to nuclear spin dependent linewidths  $(T_2^{-1})$  is chemical exchange between two species having the same nuclear spin quantum number but different Zeeman and/or hyperfine interactions. A mathematical interpretation of this phenomenon was first attempted by Freed and Fraenkel. More recently Dye and Dalton have considered relaxation involving chemical exchange for species involving large hyperfine interaction. Their expression for  $T_2^{-1}$  is reproduced in Table IV.

A final mechanism capable of giving rise to nuclear spin dependent linewidths involves either a static or dynamic distribution of resonance frequencies arising from a distribution of hyperfine or superhyperfine interactions. 73

- Non-Nuclear Spin Dependent Relaxation Processes (Residual Linewidths).
  - a. Spin-Rotation.

This mechanism was first proposed by  $Hubbard^{74}$  and has been shown by Kivelson and coworkers  $^{16,71}$  to be an important contributor to residual linewidths in dilute solutions of inorganic complexes. The expression derived by Kivelson is as follows:

$$\alpha'' = (\Delta g_{\parallel})^2 + 2\Delta g_{\perp}^2) kT/12\pi r^3 \eta$$

where  $\Delta g_{\parallel} = g_{\parallel} - 2.0023$ ,  $\Delta g_{\perp} = g_{\perp} - 2.0023$ , r is the hydrodynamic molecular radius, and n is the viscosity.

b. Ligand Exchange.

The contribution to  $T_2^{-1}$  from ligand exchange may be represented as  $T_2^{-1} = k[X]$ 

where k is the rate constant for the formation of the complex and [X] is

TABLE IV: Coefficients of  $m_{\scriptscriptstyle T}$  in the Linewidth Expression of Dye and Dalton.

$$T_2(m_I)^{-1} = p_A/T_{2A} + p_B/T_{2B} + p_A^2 p_B^2 (\tau_A + \tau_B) [\alpha + \beta m_I + \gamma m_I^2 + \delta m_I^3 + \epsilon m_I^4]$$

$$\alpha = [F_1 + F_3I(I+1)]^2$$

$$\beta = 2[F_1 + F_3I(I+1)][F_2 + \frac{1}{2}F_4 - I(I+1)F_4]$$

$$\gamma = [F_2 + \frac{1}{2}F_4 - I(I+1)F_4]^2 - 2F_3[F_1 + F_3I(I+1)]$$

$$\delta = 2F_4[F_1 + F_3I(I+1)] - 2F_3[F_2 + \frac{1}{2}F_4 - I(I+1)F_4]$$

$$\varepsilon = 2F_4[F_2 + \frac{1}{2}F_4 - I(I+1)F_4] + F_3^2$$

where

$$F_1 = (\omega_A^{O} - \omega_B^{O})$$

$$F_2 = -(a_A - a_B)$$

$$F_3 = -a_A^2/2\omega_A + a_B^2/2\omega_B$$

$$F_4 = -a_A^{3/2}\omega_A^2 + a_B^{3/2}\omega_B^2$$

and  $p_A$  and  $p_B$  are the fraction of the two species, A and B;  $\tau_A$  and  $\tau_B$  are the mean lifetimes of A and B;  $\tau_{2A}$  and  $\tau_{2B}$  are the exchange-independent transverse relaxation times;  $\omega_A^{\ O}$  and  $\omega_B^{\ O}$  are the transition frequencies in the absence of hyperfine interaction;  $\omega_A$  and  $\omega_B$  are the frequencies of transition involving the hyperfine component  $m_I$ ; and  $a_A$  and  $a_B$  are the hyperfine splitting frequencies.

the concentration of the ligand undergoing exchange.

c. Electron Exchange and Dipolar Broadening.

The mechanisms discussed previously determine  $T_2$  and hence the paramagnetic resonance resonance linewidths in solutions of low paramagnetic ion concentrations. In solutions where the concentration of paramagnetic ion is 1 molar or higher the linewidth is determined by dipolar and exchange interactions.

The exchange interaction between electrons was first considered by  $\mathsf{Dirac}$ ,  $\mathsf{^{75}}$  who demonstrated that the exchange coupling is approximately equivalent to a potential of the form

$$-2\sum_{ij}J_{ij}(S_{i}\cdot S_{j}).$$

The effect, electrostatic in origin, is dictated by symmetry of the orbital wave functions in the representation of the permutation group.

Van Vleck, <sup>76</sup> Pryce and Stevens, <sup>77</sup> and Anderson <sup>66,78</sup> have calculated the combined effect of exchange and dipolar interaction on the linewidth. Since the nature of these calculations has already been demonstrated in the section on nuclear relaxation the topic will not be further pursued.

- B. Spin-Lattice or Longitudinal Relaxation Processes.
  - 1. Processes Independent of Hyperfine Interaction.

Until recently spin-lattice relaxation times were thought to be independent of hyperfine interaction and capable of being represented in the most general form by the following expression:

$$T_1^{-1} = AT + BT^n(J_{n-1})[\theta/T] + C \exp[-\theta/T]$$

where T is the temperature in degrees Kelvin,  $\theta$  is the Debye temperature,

 $J_{n-1}$  is a transport function and A, B, and C are arbitrary coefficients. The first term in the above expression arises from the Van Vleck direct relaxation process. This process involves a phonon-induced spin flip in the ground electronic (orbital) state. The second term arises from the Van Vleck second-order Raman process. This process describes a spin flip resulting from a two-phonon interaction. The third term in the expression for  $T_1^{-1}$  is due to Orbach and is similar to the Van Vleck process except that the spin flip is accompanied by the simultaneous excitation of the electronic state.

The theoretical expressions for the relaxation probabilities for these three processes are given in Table V. It may also be pointed out that a particularly instructive application of these theories to relaxation in inorganic complexes is given by Kivelson. 81

#### 2. Processes Dependent on Hyperfine Interaction.

Recently it has been shown that the modulation of either isotropic hyperfine interaction or anisotropic hyperfine interaction can be an important means of spin-lattice relaxation. 82-86 In these processes the spin-lattice relaxation occurs through the modulation of the hyperfine interaction tensor by phonon or molecular collisions. The process depends upon the difference in magnitude of the tensor representing interaction between the final and initial states, whether or not they are vibration or electronic. The most important mechanisms of this type are a direct vibrational process in which the incoming phonon or colliding molecule excites a vibrational mode of the molecule and simultaneously induces a spin transition, and an Orbach type of mechanism in which the incoming phonon or molecule excites the paramagnetic species electronically and simultaneously induces a spin transition.

TABLE V: Theoretical Expressions for Spin-Lattice Relaxation.

Van Vleck direct process

$$(T_{1e})^{-1} = 64(\lambda/\Delta)^{2}(\phi'q_{o}/\Delta r_{o})^{2}[(\omega_{o}\tau_{c})^{2}\tau_{c}^{-1}]/(1+\omega_{o}^{2}\tau_{c}^{2})$$

Van Vleck-Raman process

$$(T_{1e})^{-1} = 32(\lambda/\Delta)^{2}(\phi'q_{o}/\Delta r_{o})^{4}\tau_{c}^{-1}$$

Orbach process

$$(T_{1e})^{-1} = 16(\lambda/\Delta)^{2}(\phi'q_{o}/\Delta r_{o})^{2}(\Delta/\delta_{on})^{2}\{\tau_{c}^{-1}/[\exp(\hbar\delta_{on}/kT)-1]\}$$

where the symbols are defined in Reference 81.

#### **EXPERIMENTAL**

#### I. Preparation of Complexes.

## [MoOC1<sub>5</sub>]<sup>2-</sup>

Ammonium oxopentachloromolybdate(V) was prepared both by the electrolytic method of James and Wardlaw and by the method of Allen, et al.  $^{20}$ , with preference for the latter method. In addition, the method of Allen was employed for preparation of analogous  $K^+$ ,  $Cu^{2+}$ ,  $C_5H_6N^+$  (pyridinium), and  $Zn^{2+}$  oxopentachloromolybdate complexes. This series of complexes was dissolved in  $D_2O$  (Merck Isotopic Products) saturated with HCl gas for nuclear spin relaxation studies; the concentration of molybdenum in these solutions ranged from 0.01M to 2.0M.

## $[Mo0X_5]^{2}$

Solutions of  $[MoOX_5]^{2-}$  where  $X = F^-$ ,  $Br^-$ , and  $I^-$  were conveniently prepared by dissolution of the  $[MoOCl_5]^{2-}$  salt in the appropriate acid followed by bubbling of the corresponding hydrohalide gas through the solution at 0°C for fifteen minutes.  $K_2[MoOF_5]$  for "doping" in a diamagnetic salt was prepared both by ligand replacement and by the method of Allen, et al. 20 Solutions with cations  $K^+$ ,  $Cu^{2+}$ ,  $NH_4^+$ , and  $Zn^{2+}$  and  $X = F^-$  for nuclear spin echo studies were prepared by ligand replacement.

### $[MoO(NCS)_5]^{2}$

Ammonium oxopentaisothiocyanatomolybdate(V) (assignment of structure based upon observed EPR spectra to be discussed in the Results section) was

prepared by the method of Abraham, et al.  $^{21}$ , a well-known analytical method for Mo(V).  $^{82}$  [MoO(NCS) $_5$ ]  $^{2-}$  could also be prepared by adding KSCN, NaSCN, or NH $_4$ SCN to an alcohol solution of (NH $_4$ ) $_2$ [MoOCl $_5$ ].

### $[MoO(HSO_4)_5]^{2}$

A solution of the oxopentabisulfatomolybdate(V) anion (assignment of structure based upon observed EPR spectra and electrostatic charge considerations) was conveniently prepared by dissolving  $(NH_4)_2[MoOCl_5]$  in an excess of concentrated sulfuric acid. A solution giving an identical EPR spectrum was prepared by reduction of  $K_2MoO_4$  (Alfa Inorganics) or  $(NH_4)_6Mo_7O_24\cdot 4H_2O$  (Mallinckrodt Analyzed Reagent) in hydrochloric acid solution with hydrazine hydrate in HCl solution. The Mo(V) was precipitated as MoO(OH) $_3$  by addition of  $NH_4OH$ . The washed precipitate was then dissolved in concentrated sulfuric acid.

### $Mo_2O_3(SO_4)_2$

Molybdenum trioxydisulfate was prepared both by electrolysis with platinized platinum electrodes of a concentrated sulfuric acid solution of  $[\text{MoO}_2(\text{SO}_4)_2]^{2-}$  and more conveniently by reduction with a stream of  $\text{H}_2\text{S}$  gas of a concentrated sulfuric acid solution containing 14.4g (0.1 mole) molybdenum trioxide (Merck and Co.).

### $MoOC1SO_4$

Molybdenum oxochlorosulfate, characterized by chlorine hyperfine lines in the EPR spectrum, was prepared by adding to the sulfuric acid solution of  ${\rm Mo_2O_3(SO_4)_2}$  small amounts of saturated aqueous NaCl, KCl, or concentrated HCl so the  ${\rm Cl^-/SO_4^{\ 2^-}}$  ratio was between 1/20 and 1/10.

### $MoOC1_3$

Molybdenum oxytrichloride was prepared by solvolysis of  $\mathrm{MoCl}_5$  (K & K

Laboratories) in liquid sulfur dioxide. 5.5g (0.02 mole) MoCl<sub>5</sub> was placed in a 300-ml 3-necked round bottom flask equipped with dry ice condenser and inlets for prepurified nitrogen and sulfur dioxide. The flask was placed in an acetone-dry ice bath and SO<sub>2</sub> gas was admitted until about 100 ml of condensate had accumulated. The excess SO<sub>2</sub> was then allowed to evaporate, the flask being swept with prepurified nitrogen until the solid MoOCl<sub>3</sub> was dry. The MoOCl<sub>3</sub> was dried at room temperature under reduced pressure for 24 hours before being used. Commercial MoOCl<sub>3</sub> (Climax Molybdenum Co.) was used in later experiments.

### $[MoO(H_2PO_4)_5]^{2}$

A species tentatively characterized on the basis of EPR spectroscopy and electrostatic charge considerations as the oxopentakis(dihydrogenphosphato)-molybdate(V) anion resulted upon dissolution of (NH<sub>4</sub>)<sub>2</sub>[MoOCl<sub>5</sub>] in concentrated phosphoric acid.

### ${^{C}_{5}}^{H}_{6}{^{N}}[^{Mo}(^{OCH}_{3})_{2}{^{X}_{4}}]$

Pyridinium tetrachlorodimethoxomolybdate(V), as well as the corresponding tetramethylammonium and quinolinium salts, was prepared by the method of McClung, et al.  $^{14}$  The preparation of  $[(CH_3)_4N][Mo(OCH_3)_2Br_4]$  and  $[(n-C_4H_9)_4N][Mo(OCH_3)_2I_4]$  as well as  $(NH_4)[Mo(OCH_3)_2F_4]$  by procedures analogous to those employed for the synthesis of  $[(CH_3)_4N][Mo(OCH_3)_2Cl_4]$  were attempted, yielding crystalline solids, but EPR examination of N,N-dimethylformamide (DMF) solutions of the solids (bromide and iodide) indicated mixed halide ligand substitution. The solid obtained from addition of a dry methanol solution of ammonium fluoride to a methanol solution of molybdenum pentachloride was insoluble in organic solvents, and EPR examination of the solid showed it

to be diamagnetic. The synthesis of a thiocyanato complex was attempted by a method analogous to that for the preparation of  $[(CH_3)_4N][Mo(OCH_3)_2Cl_4]$ , by employing  $NH_ASCN$  (Baker Analyzed Reagent) instead of  $[(CH_3)_AN]C1$ . 5.5g (0.02 mole)  $MoCl_{\varsigma}$  (Climax Molybdenum Co.) was placed in a 500-ml 3-necked round bottom flask which was swept with helium. Methanol which had been refluxed over magnesium turnings was distilled with helium sweep into the flask containing  $\operatorname{MoCl}_{\varsigma}$  and was also distilled into a flask equipped with sidearm stopcock containing 7.6g (0.1 mole)  $NH_ASCN$  which had been dried under vacuum. The  $NH_4SCN$  solution was added dropwise to the  $MoCl_5$  solution which had been immersed in an acetone-dry ice bath. The solid product was filtered under helium, washed with cold ether, and dried under vacuum for 24 hours. EPR examination of this complex showed it to be isotropic, the nitrogen superhyperfine lines indicating the presence of three  $^{14}\mathrm{N}$  nuclei in the coordination sphere. A formula consistent with the observed EPR spectra is [Mo(NCS)<sub>3</sub>Cl<sub>3</sub>], but this characterization must be regarded as tentative.

Thiocyanate complexes with axial symmetry were prepared by adding NaSCN, KSCN, or NH<sub>4</sub>SCN (in excess) to methanol or dimethylformamide solutions of pyridinium tetrachlorodimethoxomolybdate(V).

Solutions of sulfate and phosphate complexes possessing axial symmetry were prepared by dissolution of  $C_5H_6N[Mo(0CH_3)_2Cl_4]$  in concentrated sulfuric and phosphoric acids respectively. The composition of such complexes was not determined in the solid state, but the ligands in the xy plane (z is the axial molecular axis) apparently are bonded to the molybdenum through the oxygen, on the basis of EPR characterization of the solution species.

#### Mo(V) Complexes with Ligands Containing Phosphorus

Addition of molybdenum pentachloride (Climax Molybdenum Co.) to tri-n-butylphosphate (Eastman Organic Chemicals) resulted in the formation of complexes tentatively characterized as  $[Mo[(BuO)_3PO]Cl_5]$  and  $[Mo[(BuO)_3PO]_2Cl_4]^+$  on the basis of EPR data.

Dissolution of molybdenum pentachloride in diethylhydrogenphosphite (Victor Chemical Co.) resulted in the formation of a series of complexes differing in ligand substitution. The concentration of each species (as measured by EPR) varied in a regular manner as the concentration of MoCl<sub>5</sub> was changed. The nature of the equilibria of this series of complexes will be discussed in later sections.

Addition of molybdenum pentachloride to diethyldithiophosphoric acid (abbreviated DDPA) (Aldrich Chemical Co.) or the addition of DDPA to a hydrochloric acid solution containing  $[MoOCl_5]^{2-}$  resulted in the formation of a complex the EPR spectral features of which are consistent with the formula  $[Mo(Cl)_5SPS(OC_2H_5)_2]^-$ , both phosphorus and chlorine superhyperfine structure being observed in the EPR spectrum. Extraction of this latter complex with ethanol resulted in the disappearance of chlorine superhyperfine structure, an effect which may be attributed to the replacement of chloride ligands with ethoxide ligands. Addition of DDPA to a sulfuric acid solution containing  $[MoO(HSO_4)_5]^{2-}$  resulted in the formation of a complex giving an EPR spectrum consistent with the formula  $[Mo(HSO_4)_5SPS(OC_2H_5)_2]^{-}$ .

No attempt to characterize these complexes by chemical means was made.

#### II. Solvent Purification.

Methanol, ethanol, acetone, and dimethylformamide were purified for preparation of EPR samples. Dimethylformamide (DMF) and acetone were purified and degassed by a repetitive melt-pump-freeze technique and subsequently distilled into a vessel which was swept with prepurified nitrogen. Methanol was dried by refluxing with magnesium turnings and subsequent distillation in a nitrogen-swept storage vessel; ethanol was dried by refluxing with sodium and distillation into a similar storage container. Ether was dried by refluxing over sodium followed by distillation.

#### III. Crystal Preparation.

For EPR and spin echo studies, crystals of molybdate salts substituted into diamagnetic hosts were prepared. Crystals of  $(NH_4)_2[InCl_5 \cdot H_2O]$  containing a range of concentrations of  $(NH_4)_2[MoOCl_5]$  from 0.1 mole percent to 1.9 mole percent as an impurity were grown by cocrystallization of the molybdate and indate from hydrochloric acid solution, crystals of  $(NH_4)_2[InBr_5 \cdot H_2O]$  with  $(NH_4)_2[MoOBr_5]$  being prepared by an analogous procedure. Crystal structure information is given by Wentworth and Piper.  $^{24}$ 

Crystals containing about 0.01 mole percent to 0.1 mole percent  $[MoOF_5]^{2-}$  in  $K_2NbOF_5 \cdot KHF_2$  were made by dissolving  $K_2[MoOCl_5]$  in concentrated HF, then bubbling HF gas through the solution at 0°C for conversion of  $[MoOCl_5]^{2-}$  to  $[MoOF_5]^{2-}$ , followed by cocrystallization of  $[MoOF_5]^{2-}$  with the appropriate amount of  $K_2NbOF_5 \cdot KHF_2$  (prepared by the method of Balke and Smith<sup>88</sup>; commercial  $K_2NbOF_5$  obtained from Alfa Inorganics was used in later experiments). Crystals identical in appearance and EPR spectral features were obtained by use of  $K_2[MoOF_5]$  solid prepared by the method of Allen, et al. 20 as the source of molybdenum impurity in the host crystal.

 $K_2[MoOF_5]$  was also substituted into a  $K_2SnF_6 \cdot 2H_2O$  host ( $K_2SnF_6$  obtained from Alfa Inorganics) at a concentration between 0.1 mole percent and 1.0 mole percent. Since a high concentration of was necessary to suppress polymerization of the potassium hexafluorostannate (at 48 to 72 hour intervals during the crystallization period HF gas was bubbled gently through the crystallization solution by means of a gas dispersion tube) and since the host crystallizes in monoclinic plates  $^{89}$  only small crystals were obtained.

The most satisfactory host for the  $[MoOF_5]^{2-}$  in this investigation was found to be  $K_3T1F_6 \cdot 2H_2O$ . By cocrystallization of  $K_2[MoOF_5]$  with this host, crystals larger in size than the fluorostannate crystals were obtained with a molybdenum concentration between 0.1 mole percent and 1.0 mole percent.

#### IV. Reference Standards.

Five reference standards were commonly employed for calibration of magnetic field and frequency and monitoring of passage conditions.

Potassium peroxylamine disulfonate, K<sub>2</sub>NO(SO<sub>3</sub>)<sub>2</sub>, was prepared by the method of Palmer; <sup>90</sup> potassium pentacyanonitrosylchromate(I) hydrate, K<sub>3</sub>Cr(CN)<sub>5</sub>NO·H<sub>2</sub>O, was synthesized by the procedure of Griffith, et al. <sup>91</sup> In addition, an aqueous solution of vanadyl sulfate (Fisher Scientific Co.) and a 0.1% pitch in KCl as well as a 0.00033% pitch in KCl standard Varian reference standards were employed. Diphenylpicrylhydrazyl (DPPH) (Aldrich Chemical Co.) was conveniently used by gluing small crystals of the free radical to the outside of sample tubes. Pertinent magnetic tensors for these standards are recorded in the literature. <sup>26,92,93</sup>

#### V. Preparation of Samples for EPR.

For EPR relaxation and equilibrium studies, a weighed quantity of molybdate was placed in a glass container similar to that described by Dalton<sup>92</sup> so the solution could be prepared without exposure to air. An alternate technique for filling EPR tubes consisted of temporarily sealing the tubes filled by a hypodermic syringe in the dry box with wax or with polyethylene caps. The tubes were then sealed with a torch below the temporary seal.

For spin echo studies the solution samples were prepared in the dry box, since the sample tubes were of a diameter too large for convenient sealing with a torch.

#### VI. Instrumental.

#### A. Electron Paramagnetic Resonance Measurements.

Electron paramagnetic resonance measurements were made at frequencies from 9.2 to 9.5 kMc by using a Varian X-band spectrometers. Measurements at 35.0 to 35.5 kMc were made by using a Varian K-band spectrometer.

Measurements at 77°K were made by using the Varian nitrogen dewar assembly. Variable temperature measurements were made by using the Varian variable temperature accessory.

When searching for ligand superhyperfine structure, special care was taken to assure that there was no distortion of the resonance lines from instrumental effects. Consequently, for these studies microwave power and modulational amplitudes were kept at a minimum. Slow passage conditions were employed and dielectric loss was minimized as much as possible by judicious choice of solvent.

#### B. Electron Spin Relaxation Measurements.

Electronic relaxation times were measured by both the saturation and electron spin echo techniques. The saturation measurements were performed at 9.2 kMc on a Varian EPR spectrometer. The electron spin echo spectrometer employed permitted electron spin echo measurements to be made either by the classical 90°-180°-90° pulse sequence technique or by the "picket" technique. The picket technique delivers a string or picket of 10 to 20 pulses instead of the initial 90° pulse of the classical sequence. This insures complete saturation in the initial step of the sequence, thus combating such spurious relaxation processes as cross relaxation or spin diffusion. 94-97 Unlike the nuclear spin echo experiment to be described later, the pulse angle could be varied only by changing the pulse amplitude. Care was taken to ensure that the first pulse was a 90° pulse. The angle of the other pulses is less crucial. Measurements were made at 4.2°K, 77°K, and 298°K by using the appropriate dewar assembly and refrigerant.

#### C. Nuclear Spin Relaxation Measurements.

Nuclear spin-lattice relaxation times  $(T_{1N})$  were measured by a 90°-180°-90° pulse sequence. In these experiments the pulse angle could be varied by changing either the pulse amplitude or pulse width. Molecular diffusion prevented use of this method for measurement of nuclear spin-spin relaxation times  $(T_{2N})$ . Nuclear spin-spin relaxation times were measured by either the spin echo "picket" technique of Carr and Purcell<sup>98</sup> or by wide line NMR with Varian 60 Mc/sec and 100 Mc/sec instruments. The nuclear spin echo spectrometer employed was a variable frequency spectrometer permitting measurements to be made at 3.09, 4.4, 16.33, and 28.7 Mc/sec.

D. Electron Nuclear Double Resonance Measurements.

ENDOR measurements were made at 4.2°K. Varian EPR spectrometers served to provide the saturating microwave field. The radiofrequency equipment was largely "homemade". In general, the best ENDOR signals were obtained from the central or outermost components of the hyperfine spectrum.

#### VII. Computer Programs.

A. Programs to Calculate Hyperfine and g Tensors from EPR Spectra.

Several computer programs were employed to obtain A and g values from EPR spectra. The data reported in this thesis were obtained by using a program written by Mr. Vincent A. Nicely of this laboratory. This program is based upon the modified Breit-Rabi equation discussed in the Theoretical section.

B. Program to Obtain Linewidth Parameters from EPR Linewidth Data.

The nuclear spin dependence of the EPR linewidths was determined by evaluating the coefficients of the following expression;

$$T_2^{-1} = C_0 + C_1 m_1 + C_2 m_1^2 + C_3 m_1^3$$
.

A least squares fitting sequence of the above expression to the experimental data was employed. This program was obtained from Mr. Jay D. Rynbrandt 99 of this laboratory.

C. Program to Obtain Linewidth Parameters from Magnetic Anisotropy
Data and Solution Viscosities.

Several programs were written which calculate  $\alpha'$ ,  $\alpha''$ ,  $\beta$ ,  $\gamma$ , and  $\delta$  from experimental values for  $\langle g \rangle$ ,  $g_{\parallel}$ ,  $g_{\perp}$ ,  $\langle a \rangle$ , A, B,  $\omega_S$ , n, r, and T, which are in the notation of Kivelson. A plotter subroutine which presents the respective hyperfine components as derivatives of Lorentzian absorptions permits comparison of the experimental and theoretical spectra.

D. Program to Synthesize the EPR Spectra of Frozen Glasses and Polycrystalline Samples.

Lefebvre and Maruani<sup>45</sup> have written a rather general and effective program to accomplish this task. Their program, document 8275, was obtained from ADI Auxiliary Publication Project, Photoduplication Service, Library of Congress, Washington, D. C., and modified to synthesize Mo(V) spectra.

E. Program to Synthesize the ENDOR Spectra of Frozen Glasses and Polycrystalline Materials.

A program taking into account nuclear dipolar, electron-nuclear hyperfine interaction through second order, and quadrupolar interactions was written, but further work must be done before this program can be used for effective analysis of experimental spectra.

F. Additional Programs.

Additional programs were written for calculation of molecular orbital coefficients from various methods in the literature  $^{14,100,101}$  and symmetry constants for a series of molybdates were evaluated by the method of Culvahouse, et al.  $^{102}$ 

#### **RESULTS**

- I. Molybdenyl Halide Complexes.
  - A. Solution and Frozen Glass Spectra.

## $[MoOF_5]^2$

The EPR spectra of  $[{\rm MoOF}_5]^{2-}$  in 38% hydrofluoric acid are shown in Figure 3. Fluorine superhyperfine structure is observed on both the central line from the molybdenum isotopes  $^{92}{\rm Mo}$ ,  $^{94}{\rm Mo}$ ,  $^{96}{\rm Mo}$ ,  $^{98}{\rm Mo}$ , and  $^{100}{\rm Mo}$  (I = 0) and on the hyperfine components arising from interaction of the paramagnetic electron with  $^{95}{\rm Mo}$  and  $^{97}{\rm Mo}$  nuclei (I = 5/2). As shown in Figure 3, the superhyperfine structure consists of five equally spaced lines; however, the signal heights of the superhyperfine lines are not in the ratio 1:4:6:4:1. The variations in signal heights occur because the linewidths of the superhyperfine components depend upon the nuclear spin quantum number  $^{\rm m}{\rm I}$ . The  $^{\rm m}{\rm I}$  dependence of the linewidth results from averaging of g tensors and superhyperfine interaction tensors by tumbling of the complex in solution, as is discussed by Kivelson and coworkers.  $^{15-17}{\rm If}$  the areas rather than the signal heights of the superhyperfine components are considered, the intensity ratios 1:4:6:4:1, as is theoretically predicted, are observed.

The number of components together with the fact that their intensities are in the ratio 1:4:6:4:1 indicates that the paramagnetic electron interacts with the four equatorial fluorine nuclei of the  $[MoOF_{\varsigma}]^{2-}$  complex.

The observed fluorine superhyperfine interaction is only slightly dependent upon temperature, the concentration of  $[MoOF_5]^{2-}$ , and the pH of the solution (the electron paramagnetic resonance spectra were examined in HF

and mixtures of HF and DF prepared by bubbling HF gas into D<sub>2</sub>O) and vary only from 12.4 to 13.5 gauss over the entire range of conditions under which spectra were recorded.

A typical spectrum of  $[MoOF_5]^{2-}$  in a frozen acid glass is shown in Figure 3. The spectra of acid glasses is rather sensitive to the concentration of  $[MoOF_5]^{2-}$  and the pH of the solution used to prepare the glass. Although fluorine superhyperfine interaction is observed in the frozen glasses it is too complex to permit first order analysis, <u>i.e.</u>, the intensity ratios cannot be determined without the aid of computer simulation of the spectra.

# $[MoOC1_5]^{2-}$

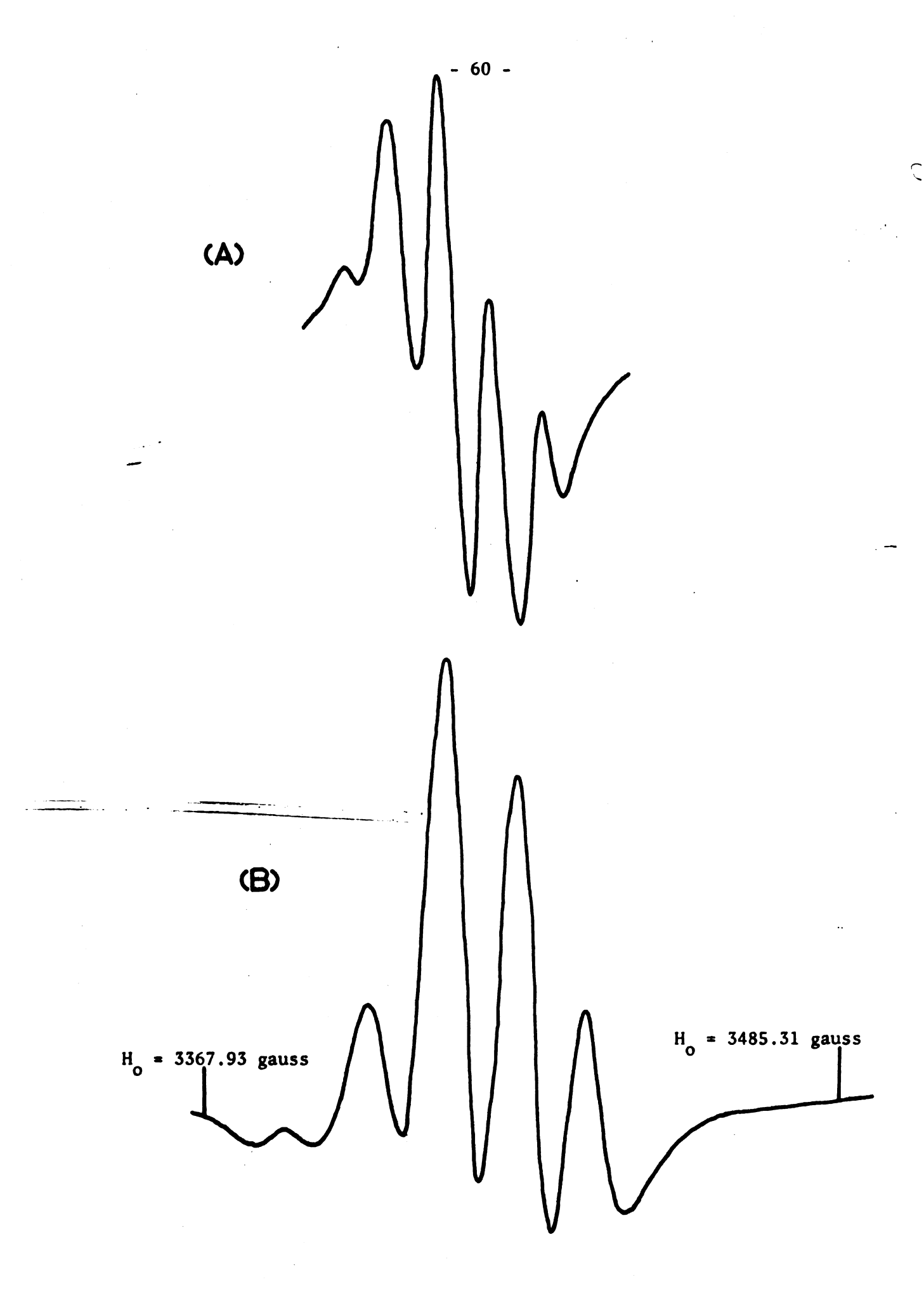
The solution and frozen glass spectra of this complex are in good agreement with those already reported.  $^{4}$ ,  $^{10}$ 

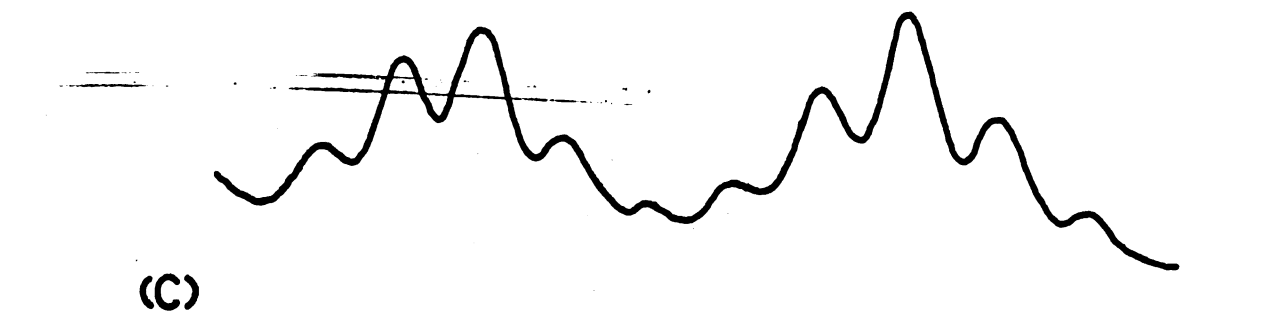
### $[MoOBr_5]^{2}$

Bromine superhyperfine interaction in solutions of the  $[MoOBr_5]^{2-}$  complex was not observed; however, in agreement with Kon and Sharpless  $^{10}$  and Dowsing and Gibson  $^4$ , bromine superhyperfine structure for this complex in frozen acid glasses was observed. The spectra did not appear to be particularly sensitive to the concentration of  $[MoOBr_5]^{2-}$  or the pH of the solution used to prepare the glass. A typical spectrum showed no detectable superhyperfine interaction of the molybdenum parallel hyperfine components or on the  $g_{\parallel}$  absorption; however, the  $g_{\perp}$  absorption displayed a bromine superhyperfine structure consisting of thirteen nearly equally spaced lines (see Figure 4). Dowsing and Gibson  $^4$  suggest that the paramagnetic electron interacts with four equivalent bromine nuclei. However, the hyperfine interaction may be interpreted as arising from two equivalent bromine nuclei. Then the thirteen lines may be

Figure 3. The EPR Spectra of  $[MoOF_5]^2$  in Solutions and Frozen Glasses of Hydrofluoric Acid.

- (A) A first derivative presentation of the fluorine superhyperfine structure on the central line corresponding to the electron in complexes containing  $^{92}$ Mo,  $^{94}$ Mo,  $^{96}$ Mo,  $^{98}$ Mo, or  $^{100}$ Mo nuclei (I = 0). The spectrum was taken at -80°C.
- (B) A second derivative presentation of the spectrum in (A).
- (C) A second derivative presentation of the fluorine superhyperfine structure on the m $_{\rm I}$  = +5/2 and m $_{\rm I}$  = +3/2 components of the  $^{95}$ Mo and  $^{97}$ Mo hyperfine components.
- (D) First derivative presentation of the spectrum of  $[MoOF_5]^{2-}$  in a frozen acid glass at 77°K.





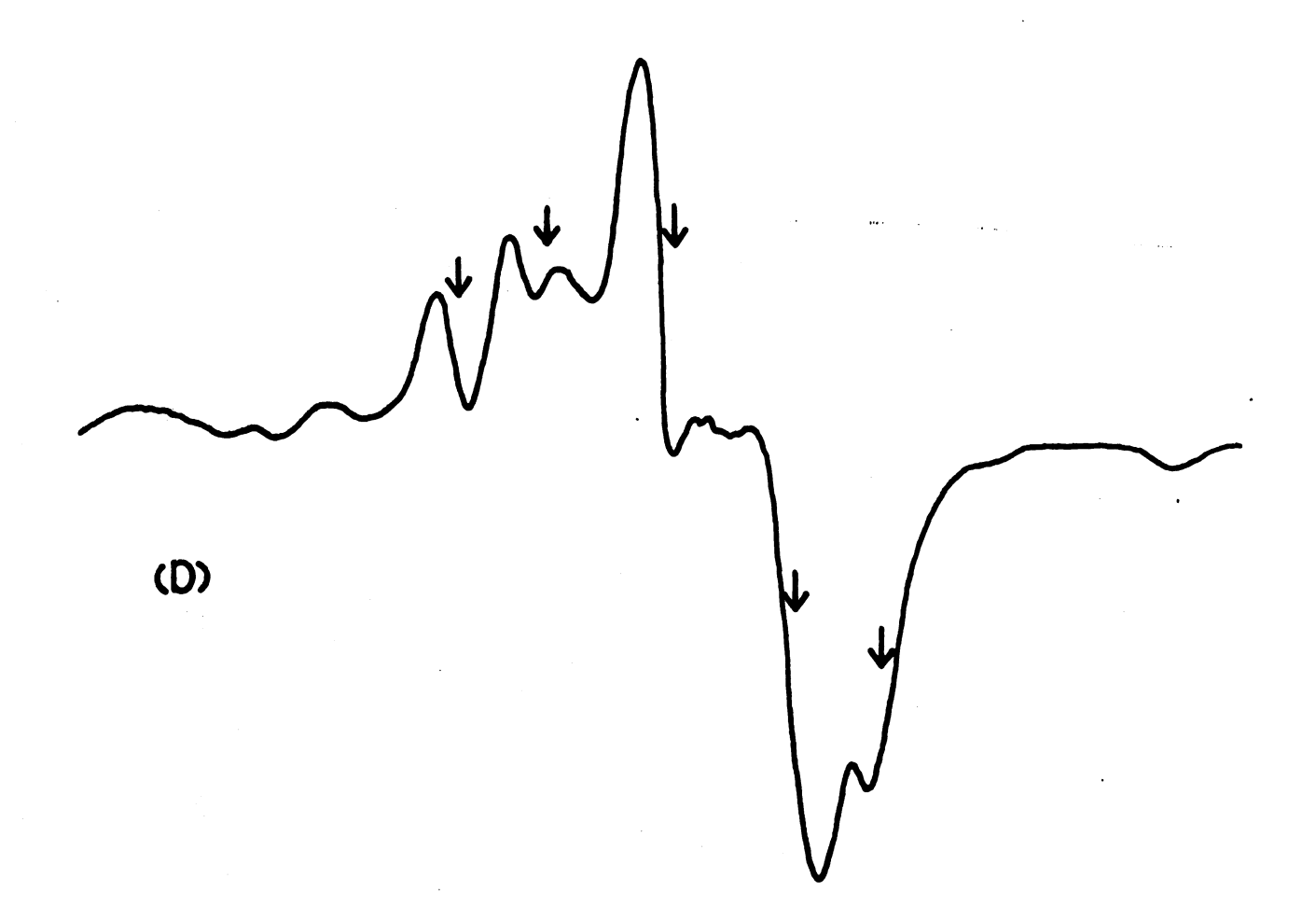


Figure 4. EPR Spectrum of  $[MoOBr_5]^{2-}$  in a frozen acid glass at 77°K. First derivative presentation.



shown to arise from the near degeneracy of the molybdenum perpendicular hyperfine components and the bromine superhyperfine components.

# $[MoOI_5]^{2}$

Although ligand superhyperfine interaction was observed for this complex in concentrated HI solution, the separation of the molybdenum hyperfine components was smaller than for other molybdenyl halide complexes. This resulted in considerable overlap of the superhyperfine components, making quantitative measurements of either the molybdenum hyperfine interaction or iodine superhyperfine interaction impossible.

The values of the magnetic tensor elements measured from solution and frozen glass spectra of the molybdenyl halides are given in Tables VI and VII.

B. Single Crystal and Polycrystalline Spectra.

Prior to discussion of the single crystal EPR spectra of molybdenyl halide complexes, it is necessary to indicate clearly the coordinate system to which the magnetic tensor elements refer.

The Zeeman and metal hyperfine interaction tensors can be thought of as having their origin at the molybdenum nucleus. To calculate the theoretical expressions for the elements of the Zeeman and hyperfine interaction tensors from molecular orbital theory, it is convenient to take the z axis along the molybdenum-oxygen bond. The x and y axes are located in the plane formed by the four equatorial halide ligands.

This coordinate system permits unambiguous specification of Zeeman and metal hyperfine tensor elements but does not permit unambiguous specification of ligand superhyperfine tensor elements. To consider ligand superhyperfine interaction a coordinate system which has its origin at the ligand nucleus rather

TABLE VI. Magnetic Tensor Elements of Mo(V) Complexes.

Complex	<b>∆</b> 0	<del></del>	<u></u>	<a><a><a><a><a><a><a><a><a><a><a><a><a>&lt;</a></a></a></a></a></a></a></a></a></a></a></a></a>	A cm <sup>-1</sup> x 10 <sup>-4</sup>	В
$(NH_4)_2[MoOC1_5]$ in $(NH_4)_2[InC1_5 H_2O]$	1.9477	1.9632	1.9400	46.6	74.7	32.6
[MoOC1 <sub>5</sub> ] <sup>2-</sup>	1.949	1.970	1.938	47.0	74.6	30.5
MoOC1 <sub>3</sub>	1.945	1.965	1.940	50.9	76.1	47.1
$(\mathrm{NH_4})_2[\mathrm{MoOBr_5}]$ in $(\mathrm{NH_4})_2[\mathrm{InBr_5}$ $\mathrm{H_2O}]$	1.993	2.090	1.945	41.7	0.99	30°0
$[MoOBr_S]^{2-}$	1.993	2.090	1.945	41.5	0.99	30.0
$K_2^{MOOF}_5$ in diamagnetic host crystals	1.906	1.874	1.918	65.4	8.66	48.2
$[MoOF_5]^{2-}$	1,905	1.874	1.918	62.2	7.66	48.3
[MoOI <sub>5</sub> ] <sup>2-</sup>	2.058					
$[MoO(NCS)_5]^{2}$	1.938	1.932	1.944	44.5	68.4	33.6
$[MoC1_{3}(NCS)_{3}]^{-}$	1.940			46.2		
$C_5H_6N[Mo(0CH_3)C1_4]$ in DMG + acetone <sup>a</sup>	1.999	2.000	1.998		71.0	

TABLE VI, continued.

Complex	⟨ø⟩	<u></u>	<del>_</del>	<a>&gt;</a>	A cm <sup>-1</sup> x 10 <sup>-4</sup>	B B
$C_{SH_6}N[Mo(OCH_3)_2C1_4]$ in pyridine	1,9374			42.8		
$C_{5}H_{6}N[Mo(0CH_{3})_{2}C1_{4}]$ in $NH_{4}SCN/CH_{3}OH$	1.937	1.932	1.944	45.0	68.5	34.0
$MoOC1SO_4$	1.935	1.927	1.940	48.8	72.5	34.0
$Mo_2O_3(SO_4)_2$	1.925	1.920	1.928	55.7	80	44
$C_5H_6N[Mo(0CH_3)_2C1_4]$ in $H_2SO_4$	1.963	1,992	1,948	38.5	43.1	36.2
$C_{5}H_{6}N[Mo(OCH_{3})_{2}C1_{4}]$ in $H_{3}PO_{4}$	1.921	1,893	1.935	54.9	93.0	35.4
$[Mo(C1)_{5}SPS(OC_{2}H_{5})_{2}]^{-}$ in DDPA solution	1.963	1.992	1.949	37.4	59.5	26.4
$[Mo(HSO_4)_5 SPS(OC_2H_5)_2]^-$ in $H_2 SO_4$ + DDPA solution	1.970	2.001	1.955	37.9	59.8	26.5
$[Mo(OC_2H_5)_5SPS(OC_2H_5)_2]^-$ in ethanol + DDPA solution	1.970	2.001	1.955	37.9	59.8	26.5

TABLE VI, continued.

Complex	<b>⇔</b> 0 <b>∀</b>	₩ 	₩	<a>&gt; A</a>	A cm <sup>-1</sup> x 10 <sup>-4</sup>	<b>B</b>
$[Mo[(Bu0)_3P0]C1_5]$ in $(Bu0)_3P0$ solution	1.946	1.960	1.960 1.939 46.8	46.8	73.9	33.2
$[Mo[(C_2H_5O)_2PO]Cl_5]^-$ in $(C_2H_5O)_2POH$ solution	1.945	1.945 1.960 1.942 48.1	1.942	48.1	74.7	36.3

The uncertainties in the g values range between 0.002 and 0.0005 and the uncertainties in the hyperfine values range between 0.05 and 0.3 cm  $^{-1}$  x  $10^{-4}$ .

 $^{\mathbf{a}}$ DMG is the abbreviation for dimethylglyoxime.

 $^{
m b}_{
m DDPA}$  is the abbreviation for diethyldithiophosphoric acid.

Elements of the Ligand Superhyperfine Interaction Tensor. TABLE VII.

Sample	Liganda	A <sub>x</sub> (L)	A <sub>y</sub> (L)	A <sub>z</sub> (L)	A <sub>S</sub> (L)	A <sub>p</sub> (L)	$A_{\mathbf{p_x}}(L)$
				cm <sup>-1</sup> x	x 10-4		
$(\mathrm{NH_4})_2[\mathrm{MoOCl}_5]$ (single crystal)	Eq. <sup>b</sup> 35 <sub>C1</sub> ,37 <sub>C1</sub>	0.0	6.34	0 ° 0	(2.1) <sup>c</sup>	(-2.1)	(0.0)
$(\mathrm{NH_4})_2[\mathrm{MoOCl}_5]$ (diluted powder) d	Eq. 35 <sub>C1</sub> ,37 <sub>C1</sub>	0.0	6.34	0.0	(2.6)	(-2.1)	(0.0)
$(C_5H_6N)[Mo(OCH_3)_2C1_4]$ (diluted powder)	Eq. 35 <sub>C1</sub> , 37 <sub>C1</sub>	0.0	0.9	0.0	(2.0)	(-2.0)	(0.0)
$\begin{array}{llllllllllllllllllllllllllllllllllll$	35 <sub>C1,</sub> 37 <sub>C1</sub>				9.03		
$\begin{array}{llllllllllllllllllllllllllllllllllll$	35 <sub>C1,</sub> 37 <sub>C1</sub>				9.03		
${\tt MoOCISO}_4$ in ${\tt NaCI/H}_2{\tt SO}_4$	35 <sub>C1</sub> , 37 <sub>C1</sub>				9.03		
$(\mathrm{NH_4})_2[\mathrm{MoOBr}_5]$ (single crystal)	Eq. 79 <sub>Br,</sub> 81 <sub>Br</sub>	0.0	36.1	0.0	(12.0)	(-12.0)	(0.0)

TABLE VII, continued.

	c						
Sample	Liganda	$A_{\mathbf{X}}(L)$	A <sub>y</sub> (L)	$A_{z}(L)$	A <sub>S</sub> (L)	$^{ m A}_{ m p_y}$ (L)	$A_{\mathbf{p_x}}^{\mathbf{L}}$ (L)
				cm -1	x 10-4		
$(\mathrm{NH_4})_2[\mathrm{MoOBr}_5]$ (diluted powder) d	Eq. 79 <sub>Br,</sub> 81 <sub>Br</sub>	0.0	36.0	0.0	(12.0)	(-12.0)	(0.0)
[MoOBr <sub>5</sub> ] <sup>2-</sup> in HBr frozen glass	Eq. 79 <sub>Br,</sub> 81 <sub>Br</sub>	0.0	36.1	0.0	(12.0)	(-12.0)	(0.0)
[MoOF <sub>5</sub> ] <sup>2-</sup> in aq. HF solution	Eq. 19 <sub>F</sub>				11.1		
$ ext{K}_2[ ext{MoOF}_5]$ (single crystal)	$_{ m Eq.}$ $^{19}_{ m F}$	-16.9	50.7	0.0	(11.3)	(-16.9)	(5.6)
$ extbf{K}_2[ extbf{MoOF}_5]$ (diluted powder)	$^{ m Eq.}$ $^{19}_{ m F}$	-16.9	50.7	0.0	(11.3)	(-16.9)	(5.6)
$\left[  ext{MoOF}_{ ext{S}}  ight]^{2-}$ in aq. HClO $_{ ext{4}}$ solution	$_{ m Eq.}$ $^{19}_{ m F}$				11.1		
$[MoOF_3Cl_2]^{2-}$ in HF + HCl + HCl0 <sub>4</sub> solution	$^{19}_{ m F}$				11.1		
$[MOOF_2C1_3]^{2-}$ in HF + HC1 + HC10, solution	$^{19}_{ m F}$				11.2		

TABLE VII, continued.

Sample	Liganda	A <sub>X</sub> (L)	A <sub>y</sub> (L)	$A_{z}(L)$	A <sub>S</sub> (L)	A Py (L)	A <sub>px</sub> (L)
				cm-1	x 10 <sup>-4</sup>		
$[MoOFC1_4]^{2-}$ in HF + HC1 + HC10 <sub>4</sub> solution	$^{19}_{ m F}$				11.3		
$[MoOF_3Br_2]^2$ in HF + HBr + HClO <sub>4</sub> solution	$^{19}_{ m F}$				11.1		
$[MoOF_2Br_3]^2$ in HF + HBr + HClO <sub>4</sub> solution	$^{19}_{ m F}$				11.1		
$[MoOFBr_4]^{2-}$ in HF + HBr + HClO <sub>4</sub> solution	$^{19}_{ m F}$				11.1		
$[MoOF_3I_2]^{2-}$ in HF + HI + HClO <sub>4</sub> solution	$^{19}_{ m F}$				11.1		
$[MoOF_3(HSO_4)_2]^{2-}$ in HF + $H_2SO_4$ + HClO <sub>4</sub> solution	$^{19}_{ m F}$				11.1		
$[Mo(C1)_{5}SPS(OC_{2}H_{5})_{2}]^{-}$	$^{31}$ p	36.4	36.4	35.3	36.0	(-0.37)	(-0.37)
in ether solution and frozen glass	Eq. 35 <sub>C1</sub> , <sup>37</sup> <sub>C1</sub>	0.0	8.2	0.0	(2.7)	(-2.7)	0.0

TABLE VII, continued.

Sample	Liganda	$A_{\mathbf{X}}(L)$	$A_{\mathbf{y}}(\mathbf{L})$	A (L)	A <sub>S</sub> (L)	$A_{p_{y}}^{(L)}$	$A_{\mathbf{p_x}}^{\mathbf{L}}$
				cm-1 x	x 10-4		
$[Mo(C1)_S SPS(OC_2H_S)_2]^-$ in $CCI_4$ solution	$^{31}_{ m p}$				36.0		
[Mo(C1) <sub>S</sub> SPS(OC <sub>2</sub> H <sub>S)2</sub> ] in DDPA solution	$^{31}_{ m p}$				36.0		
$[Mo(HSO_4)_5 SPS(OC_2H_5)_2]^-$ in $H_2 SO_4$ + DDPA solution	$^{31}$ p	36.5	36.5	35.5	36.2	(-0.33)	(-0.33)
$[Mo(OC_2H_5)_5SPS(OC_2H_5)_2]^-$ in $C_2H_5OH + DDPA$ solution	$^{31}_{ m p}$	36.5	36.5	35.5	36.2	(-0.33)	(-0.33)
[Mo[(Bu0) <sub>3</sub> P0]C1 <sub>5</sub> ]	Eq. 35 <sub>C1</sub> , 37 <sub>C1</sub>	1		, •	2.2		

'The ligand nuclei involved in the superhyperfine interaction.

 $^{\mathsf{C}}$ Parentheses indicate that the value is calculated rather than measured directly.

<sup>d</sup>Diluted powder prepared by grinding up single crystals of molybdate complex in diamagnetic host.

<sup>e</sup>DDPA is abbreviation for diethyldithiophosphoric acid.

<sup>&</sup>lt;sup>b</sup>Eq. refers to the equatorial ligands.

than the metal nucleus must be considered. A local coordinate system on an equatorial halide ligand  $^{103}$  with the x' axis along the Mo-X bond, the z' axis parallel to the symmetry axis of the complex (the Mo-O bond) and y' chosen to form a right-handed coordinate system is defined. The spherical polar angles  $\theta$  and  $\phi$  relate the external magnetic field vector to the z' and y' axes respectively. Next the individual complexes are considered.

$${\rm (NH_4)_2[MoOC1_5]} \ {\rm in} \ {\rm (NH_4)_2[InC1_5 \cdot H_2O]}$$

At ambient temperatures ligand superhyperfine interaction was not observed in the EPR spectra of single crystals of  $(NH_4)_2[MoOCl_5]$  in  $(NH_4)_2[InCl_5 \cdot H_2O]$  at any orientation of the magnetic field with respect to the quantization axes of the magnetic tensors.

The electronic Zeeman and metal hyperfine tensors obey the relationships

$$g = (g_z^2 \cos^2 \theta + g_x^2 \sin^2 \theta \cos^2 \phi + g_y^2 \sin^2 \theta \sin^2 \phi)^{\frac{1}{2}}$$

$$gA(Mo) = (A_z^2 g_z^2 \cos^2 \theta + A_x^2 g_x^2 \sin^2 \theta \cos^2 \phi + A_y^2 g_y^2 \sin^2 \theta \sin^2 \phi)^{\frac{1}{2}}$$

The orientation for which  $\theta=0$  gives rise to the spectrum corresponding to  $g_z$  and  $A_z$  while those orientations for which  $\theta=\pi/2$ ,  $\phi=0$ ,  $\pi/2$  give rise to the "double spectra" corresponding to  $(g_x,A_x)$  and  $(g_y,A_y)$ . The values of the g and A(Mo) tensors calculated from the angular variation of the absorption frequencies of the molybdenum hyperfine components are given in Table VI.

As the temperature is lowered, chlorine superhyperfine structure begins to appear. In general this superhyperfine structure is quite complex but readily interpretable spectra are obtained for certain orientations.

At the orientation for which  $\theta$  = 0, the chlorine superhyperfine structure is characterized by the A<sub>Z</sub> component of the chlorine superhyperfine interaction

tensor. Since no chlorine structure was observed for this orientation, it is assumed that A(C1) is less than 1 gauss.

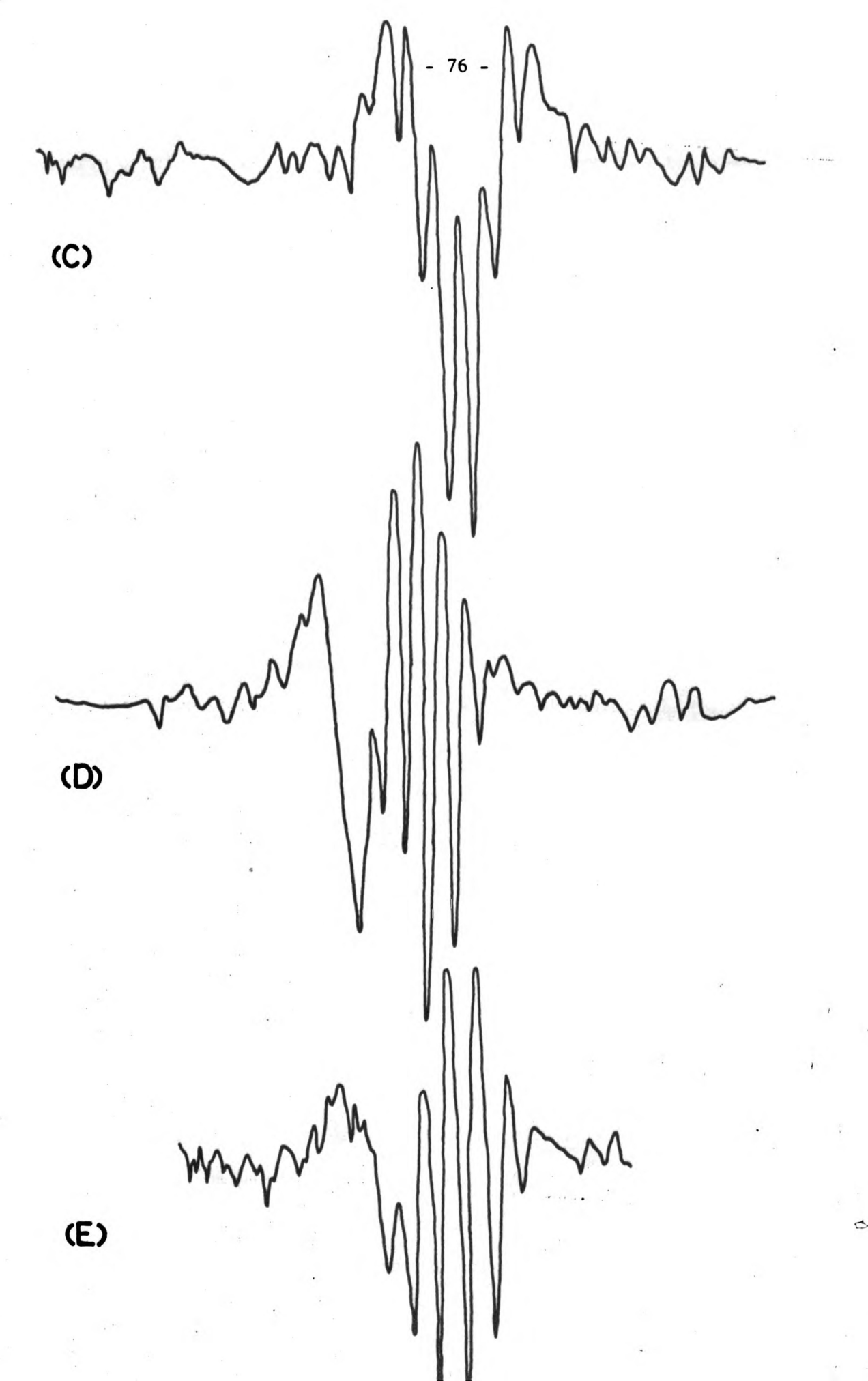
For  $\theta = \pi/2$  and  $\phi = 0$  one would expect the chlorine superhyperfine structure to be determined by the  $A_{v}(C1)$  and  $A_{x}(C1)$  components. If  $A_{x} \neq A_{v}$  and neither  $A_{x}$ nor  $\mathbf{A}_{\mathbf{y}}$  are equal to zero one would expect to observe forty-nine superhyperfine components on each of the molybdenum absorptions (For this orientation there exist two inequivalent sets of equivalent chlorine nuclei for which I = 3).  $A_{x}(C1)$ is the interaction characteristic of the set of chlorine nuclei for which the external field  $\vec{H}$  lies along the line connecting them, Cl-Mo-Cl. A<sub>v</sub>(Cl) is the interaction characteristic of the set of chlorine nuclei for which the external field is perpendicular to the line connecting them. It is expected that the intensities of these superhyperfine components would alternate as the crystal is rotated with respect to the magnetic field  $\vec{H}$ . If  $A_x(C1) = A_v(C1)$  or either  $A_x$ or  $A_{_{\mathbf{V}}}$  is equal to zero one would expect the chlorine superhyperfine structure to consist of seven equally spaced lines of separation  $A_{v}(C1)$  or  $A_{x}(C1)$  and with intensity ratios 1:6:15:20:15:6:1. Experimentally, this latter case appears to be observed, as shown in Figure 5. Since the separation of the seven lines for this orientation is 7.0  $\pm$  0.1 gauss, it is clear that A and A have the values of 0 and 7.0 gauss. It is not possible to determine experimentally which value corresponds to each value of the superhyperfine interaction tensor. Since the  $p_y$  orbitals on the chlorine ligand can bond with the  $b_2(d_{xy})$  orbital containing the unpaired electron on the central metal ion, one expects  $A_y(C1)$  to be the larger ligand superhyperfine constant. Thus  $A_v(C1)$  is assigned the value 7.0 ±  $^{0.1}$  gauss and  $\rm A_{_{X}}(C1)$  the value 0.0  $^{\pm}$  1.0 gauss.

Next the orientation for which  $\theta=\pi/2$  and  $\phi=\pi/4$  is considered. For this orientation all four equatorial chlorines are equivalent. Hence, one would expect

Figure 5. EPR Spectra of a Single Crystal of  $(NH_4)_2[MoOCl_5]$  in  $(NH_4)_2[InCl_5 \cdot H_2O]$ .

The EPR spectra of a single crystal containing  $[MoOCl_5]^{2-}$  were recorded as a function of the orientation of the magnetic field H with respect to the quantization axes of the chloride superhyperfine tensor. Spectra were recorded at  $77^{\circ}$ K using a second derivative presentation.

- (A) Spectrum for the orientation  $\theta$  = 0,  $\phi$  = 0°.
- (B)  $\theta = 0$ ,  $\phi = 45^{\circ}$ .
- (C)  $\theta = 0$ ,  $\phi = 20^{\circ}$ .
- (D)  $\theta = 0$ ,  $\phi = 75^{\circ}$ .
- (E)  $\theta = 0$ ,  $\phi = 90^{\circ}$ .



to observe a chlorine superhyperfine structure consisting of thirteen equally spaced lines with separation

$$A_{\pi/4}(C1) = [A_{y}(C1)^{2}\cos^{2}(\pi/4) + A_{x}(C1)^{2}\sin^{2}(\pi/4)]^{\frac{1}{2}}$$

and of intensity ratios 1:4:10:20:31:40:44:40:31:20:10:4:1. As can be seen from Figure 6

$$A_{\pi/4}(C1) \simeq A_y(C1)\cos(\pi/4);$$

hence the conclusion that  $A_{x}(C1) < |1|$  gauss | is reinforced.

Further indication of the magnitudes of  $A_X(C1)$  and  $A_X(C1)$  is provided by studying the observed chlorine splitting as a function of  $\phi$  in the xy plane. The results are summarized in Figures 5 and 6 and in Table VII. The chlorine splitting was also examined as a function of  $\theta$  in the yz plane.

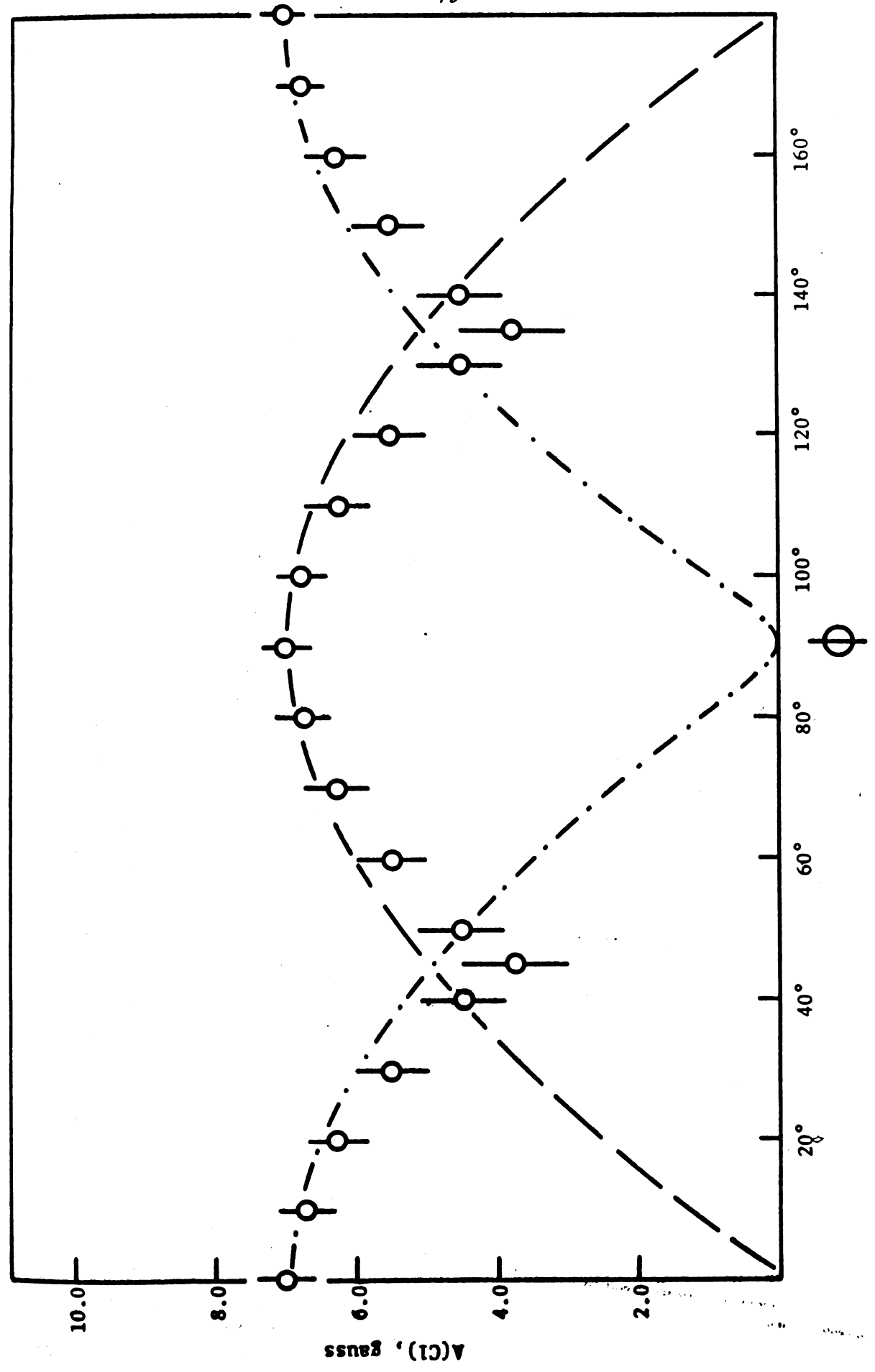
Chlorine superhyperfine structure has also been ovserved in polycrystalline samples of  $(NH_4)_2[MoOCl_5]$  in  $(NH_4)_2[InCl_5 \cdot H_20]$  which were prepared by powdering single crystals. Theoretically the superhyperfine structure observed for polycrystalline samples would be expected to be similar to the single crystal spectra observed for the orientations  $\theta = \pi/2$ ,  $\phi = 0$ , and  $\theta = \pi/2$ ,  $\phi = \pi/2$ , as is observed (see Figure 7). Computer simulation of spectra by using the values  $A_{\chi}(Cl) = 7.0$  gauss and  $A_{\chi}(Cl) = A_{\chi}(Cl) = 0.0$  gauss gave good agreement with the experimental spectra, as is shown in Figure 7.

$$(NH_4)_2[MoOBr_5]$$
 in  $(NH_4)_2[InBr_5 \cdot H_2O]$ 

As with the chloride complex, ligand superhyperfine structure was not observed at ambient temperatures and the best resolution of the bromine superhyperfine structure was obtained at temperatures of approximately 77°K. The spectra observed for single crystals of the bromide complex in  $(NH_4)_2[InBr_5 \cdot H_20]$  were very similar to those observed for the chloride complex.

Figure 6. The Variation of the Chlorine Superhyperfine Interaction as a Function of the Orientation of the External Magentic Field with respect to the Quantization Axes of the Chlorine Superhyperfine Tensor.

Circles denote experimental points and vertical bars indicate limits of error. — — line indicates theoretical variation of A(Cl) for one pair of equivalent chlorines assuming  $A_x(Cl) = 0$  and  $A_y(Cl) = 7$  gauss. — — — line indicates theoretical variation of A(Cl) for the other pair of equivalent equatorial chlorines for the same conditions.



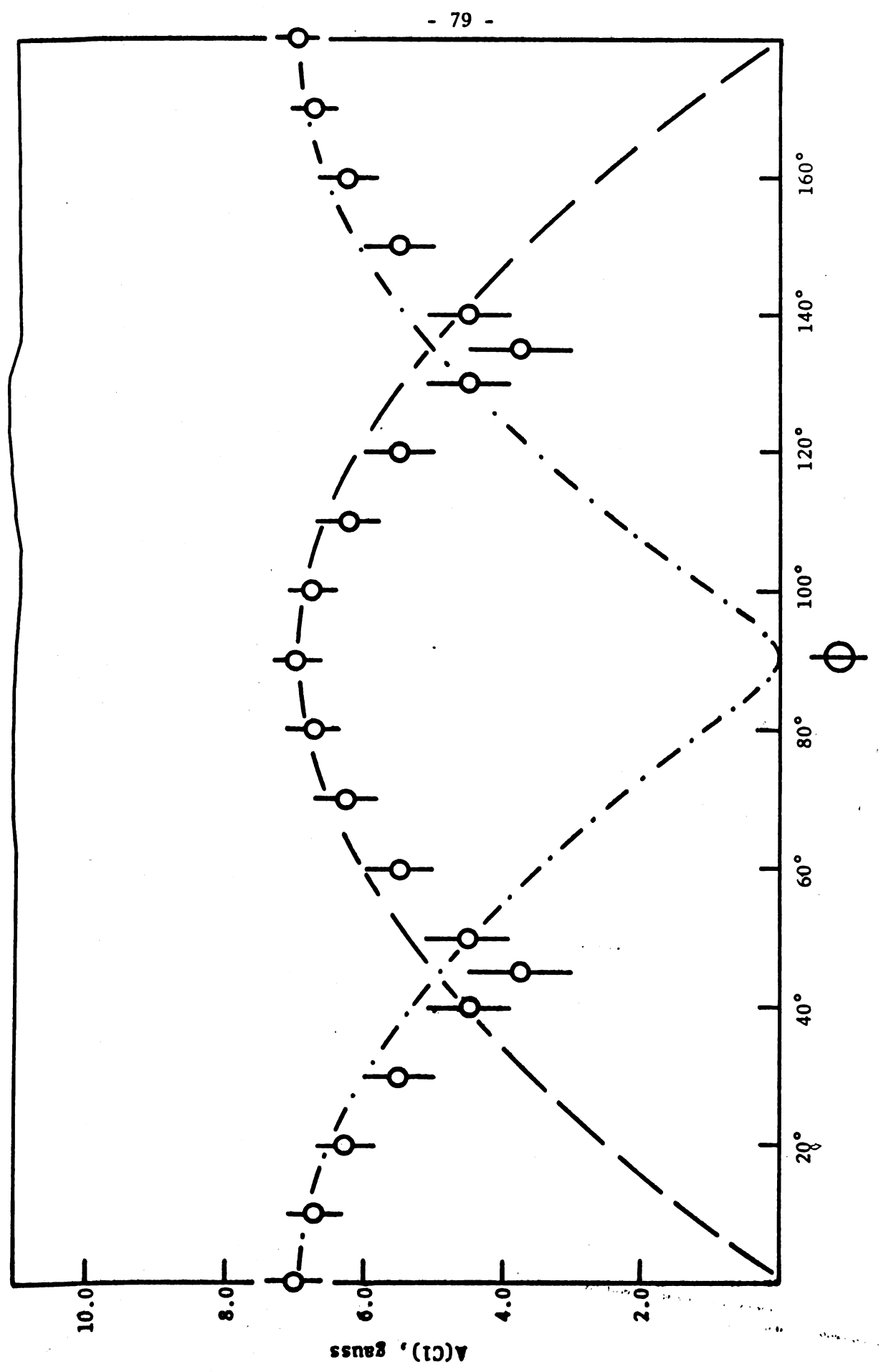
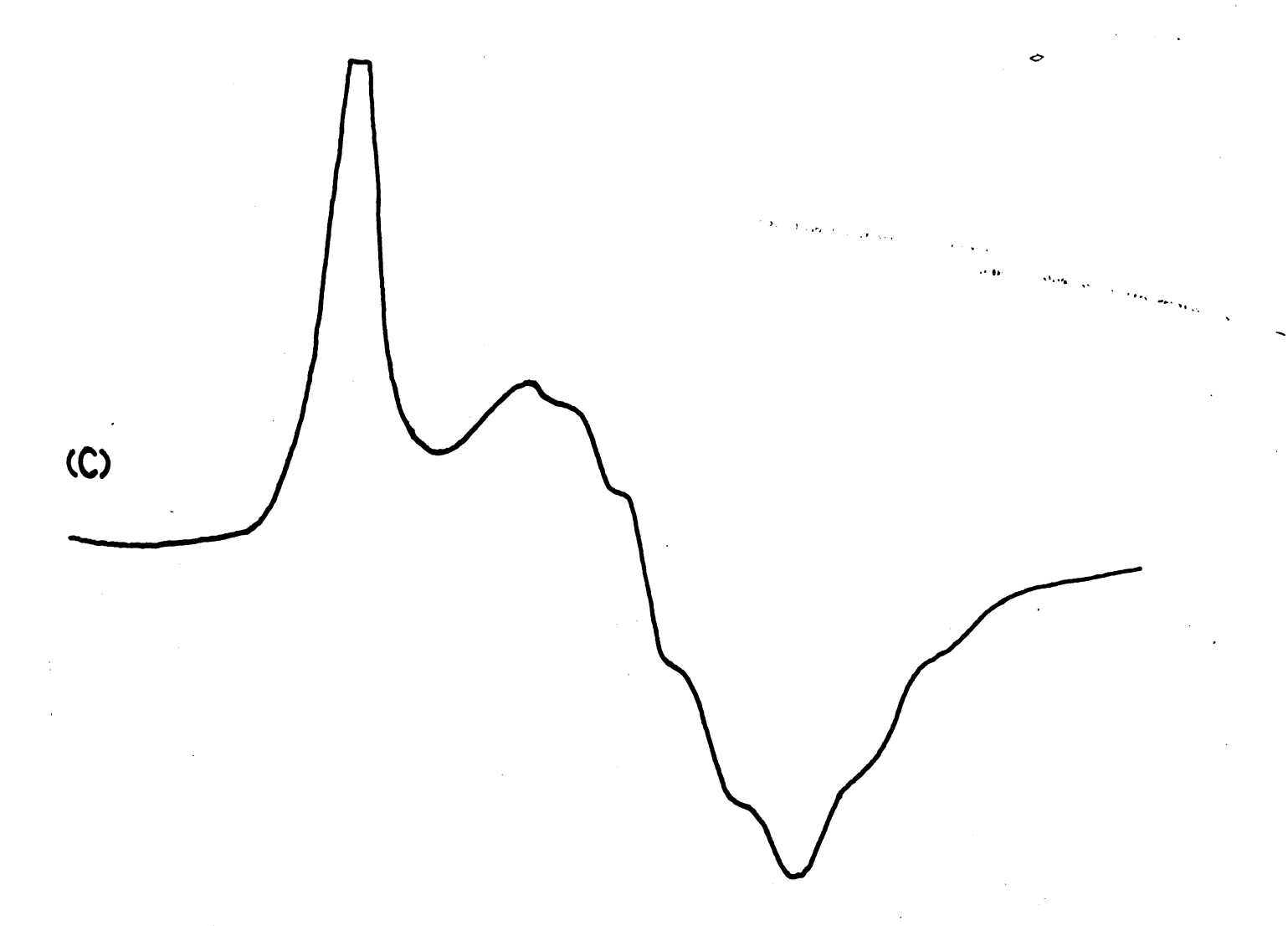


Figure 7. EPR Spectra of Polycrystalline  $(NH_4)_2[MoOCl_5]$  in  $(NH_4)_2[InCl_5 \cdot H_2O]$  at  $77^{\circ}K$ .

- (A) First derivative spectrum.
- (B) Second derivative presentation. The gain was reduced in order to keep the  $g_{\parallel \parallel}$  absorption from exceeding the limits of the chart paper.
- (C) Computer simulation employing the values given in Tables VI and VII.



At  $\theta=0$  no bromine superhyperfine structure was observed, indicating that  $A_z(Br)\simeq 0$  gauss. At  $\theta=\pi/2$  and  $\phi=0$  the spectrum consisted of seven equally speced lines while at  $\theta=\pi/2$  and  $\phi=\pi/4$  the spectrum consisted of thirteen equally spaced lines. These observations together with the intensity ratios and the magnitude of the observed splittings for various orientations lead to the conclusion that  $A_z(Br)\simeq 0$  gauss,  $A_y(Br)=40\pm 1$  gauss, and  $A_y(Br)\simeq 0$  gauss.

The spectra of polycrystalline samples of  $(NH_4)_2[MoOBr_5]$  in  $(NH_4)_2[InBr_5 \cdot H_2 0]$  are also very similar to those observed for the chloride complex, as would be expected on the basis of the single crystal results as is shown in Figure 8.

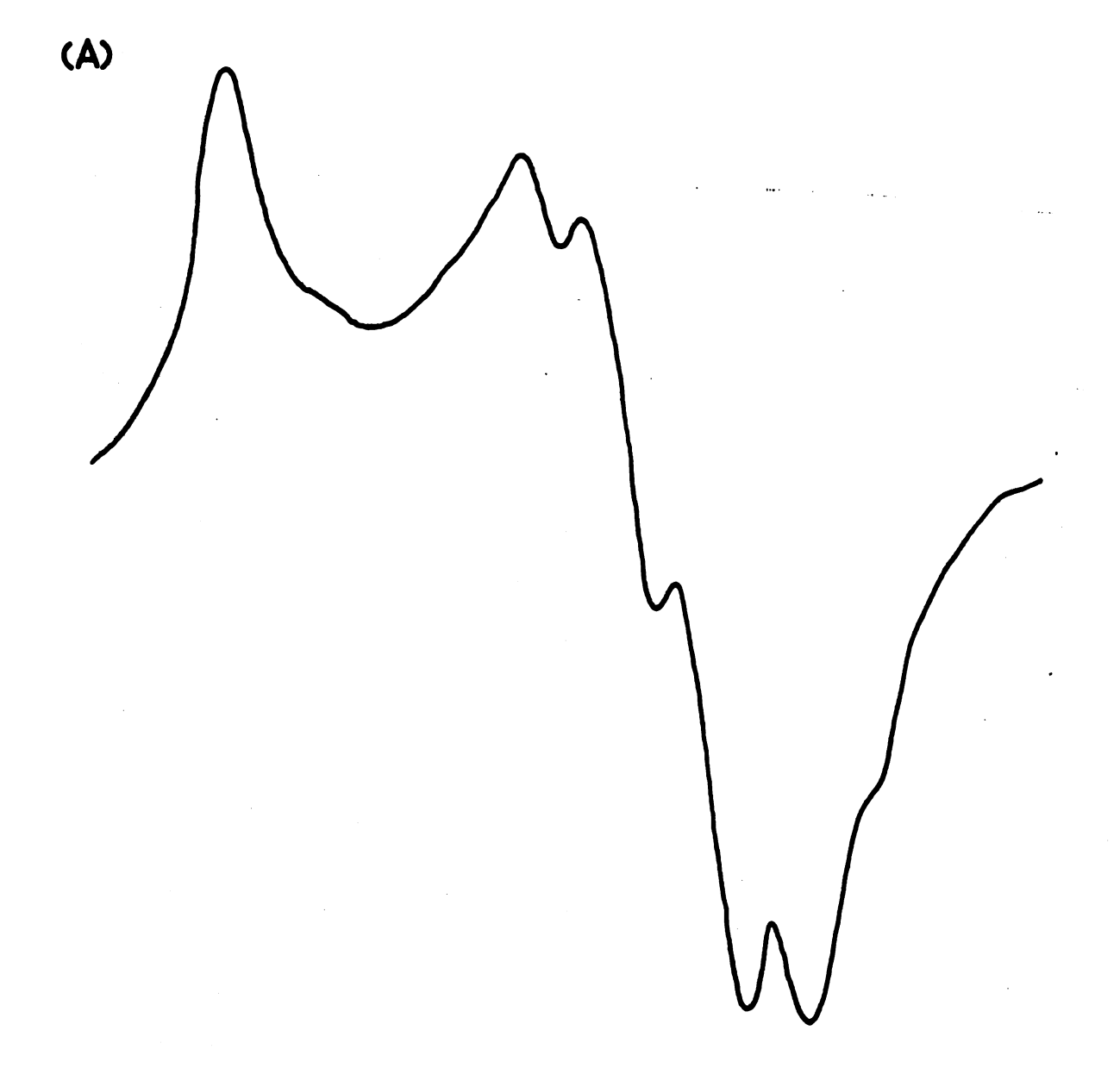
### $K_2[MoOF_5]$ in Diamagnetic Hosts

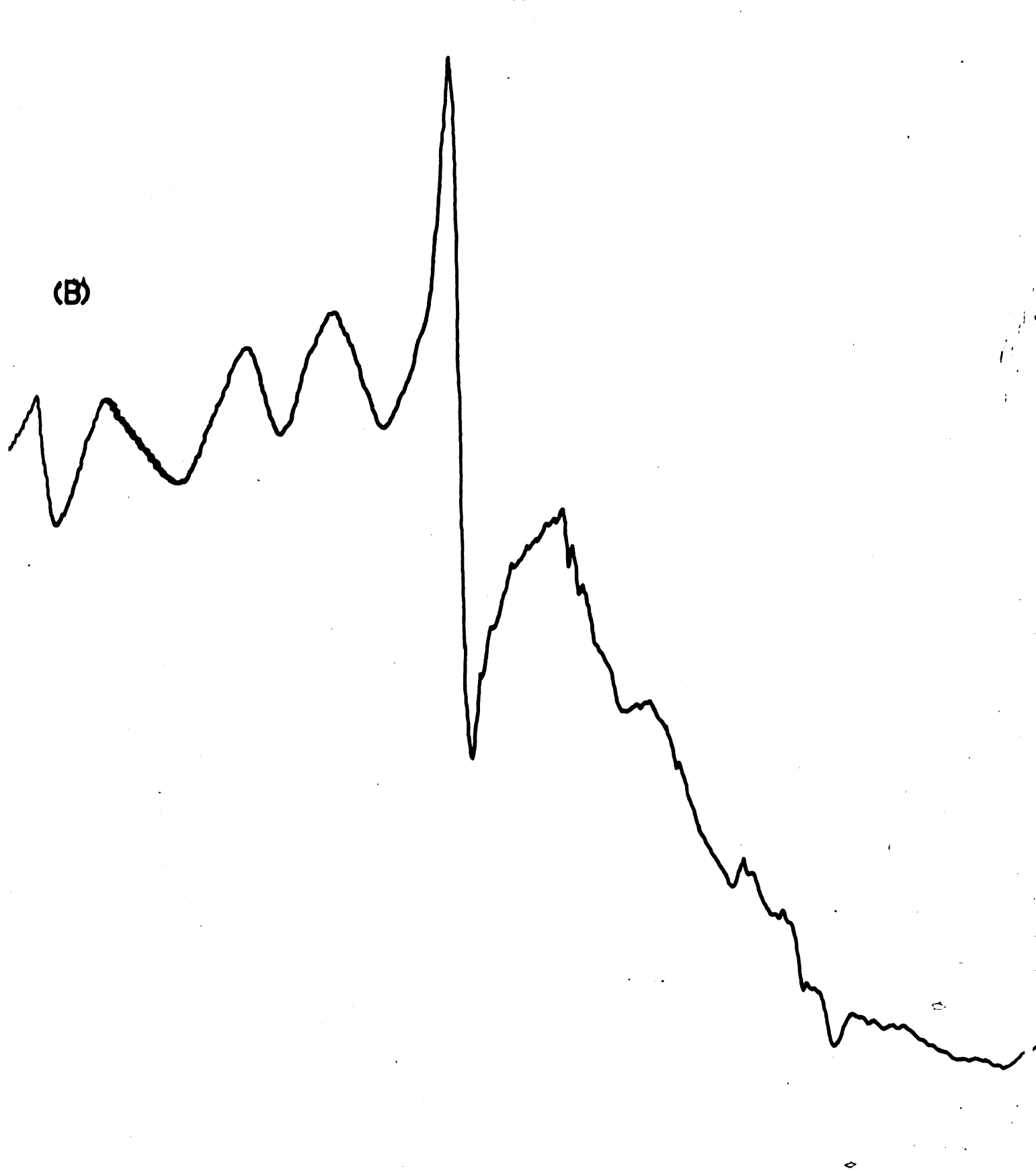
More difficulty was encountered in obtaining single crystals containing the [MoOF $_5$ ]  $^{2-}$  anion than was the case for the corresponding chloride and bromide complexes. The concentration of  $K_2$ [MoOF $_5$ ] in the diamagnetic hosts  $K_2$ NbOF $_5$ ·KHF $_2$ ,  $K_2$ SnF $_6$ ·2H $_2$ O, and  $K_3$ T1F $_6$ ·2H $_2$ O was in general substantially less than in the starting solutions from which the crystals were grown. In addition there was a certain degree of randomness of the orientation of the [MoOF $_5$ ] $^{2-}$  in the crystals studied. Preliminary recording of the EPR spectra of crystals containing the fluoride complex facilitated selection of crystals which gave reasonable EPR spectra. These selected crystals were studied in greater detail.

As with the chloride and bromide complexes, the best resolution of ligand superhyperfine structure occurred at temperatures in the region of 77°K. Even though I = 1/2 for fluorine as compared to I = 3/2 for chlorine and bromine nuclei, the superhyperfine structure observed for dilute single crystals of  ${}^{K}_{2}[\text{MoOF}_{5}]$  was in general quite complex. Again it is helpful to consider

Figure 8. EPR Spectra of Polycrystalline  $(NH_4)_2[MoOBr_5]$  and  $K_2[MoOF_5]$  in Diamagnetic Hosts.

- (A) Spectrum of  $(NH_4)_2[MoOBr_5]$  in  $(NH_4)_2[InBr_5:H_2O]$ .
- (B) Spectrum of  $K_2[MoOF_5]$  in a diamagnetic host.





particular orientations of the magnetic field with respect to the quantization axes of the magnetic tensors.

At  $\theta=0$  no fluorine superhyperfine structure was observed, indicating that  $A_Z(F)\cong 0$ . For  $\theta=\pi/2$  and  $\phi=0$  or  $\pi/2$  the fluorine superhyperfine structure on the central molybdenum line consisted of nine components of nearly equal separation (approximately 19 gauss). For the case of  $A_Y(F)\neq A_X(F)$  and neither  $A_Y(F)$  nor  $A_X(F)$  equal to zero one would expect to observe nine superhyperfine lines with the intensity ratios 1:2:1:2:4:2:1:2:1. As is shown in Figure 9, this is approximately (but only approximately) the case for experimental spectra. These results would imply that  $A_Y(F)=-58$  gauss and  $A_X(F)=19$  gauss. The values are in good agreement with the superhyperfine interaction constant obtained from solution spectra.

The polycrystalline spectra of diamagnetically diluted  $\rm K_2[MoOF_5]$  shown in Figure 8 is in good agreement with the single crystal spectra.

### II. Mixed Halide Complexes.

The spectra of a number of mixed pentahalomolybdenyl complexes were observed in solution. Since the magnetic parameters for a number of these have already been reported, accurate measurements were not attempted on those complexes already studied (Table II). The results of the measurements made in this investigation are summarized in Table VIII.

III. Mo(V) Complexes with Ligands Containing Phosphorus.

## Complexes Formed by Ligand Substitution with $H_3PO_4$

Dissolution of  $(NH_4)_2[MoOCl_5]$  or  $C_5H_6N[Mo(OCH_3)_2Cl_4]$  in concentrated  $H_3PO_4$  resulted in the formation of complexes which are of axial symmetry, as evidenced

Figure 9. The EPR spectra of a Single Crystal of  ${\rm K_2MoOF_5}$  in  ${\rm K_3T1F_6 \cdot 2H_2O}$  at 77°K.

- (A)  $\theta=0^{\circ}$ ,  $\phi=0^{\circ}$ .
- (B)  $\theta=0^{\circ}$ ,  $\phi=45^{\circ}$ .

TABLE VIII. Equilibrium Constants and Magnetic Tensors for Mixed Complexes.

Species	Complex	<g></g>	<a><sup>a</sup></a>	Keq
1	[Mo[(EtO) <sub>2</sub> PO]C1 <sub>5</sub> ]	1.945	48.1	1.61 x 10 <sup>-2</sup>
2	[Mo[(EtO) <sub>2</sub> PO] <sub>2</sub> C1 <sub>4</sub> ]	1.938	52.5	
3	[Mo[(EtO) <sub>2</sub> PO] <sub>3</sub> C1 <sub>3</sub> ]	1.929	55.9	$5.57 \times 10^{-3}$
4	[Mo[(EtO) <sub>2</sub> PO] <sub>4</sub> Cl <sub>2</sub> ]	1.919	60.9	$1.45 \times 10^{-3}$
5	[Mo[(EtO) <sub>2</sub> PO] <sub>5</sub> C1]	1.910		$3.15 \times 10^{-4}$
Species	Complex	Isotropic	Zeeman Tensor,	<g></g>
Species	Complex	Isotropic X=C1 <sup>-</sup> ,Y=I		<g> X=Br<sup>-</sup>,Y=I<sup>-</sup></g>
Species 1	Complex [MoOX <sub>5</sub> ] <sup>2-</sup>			
		X=C1 <sup>-</sup> ,Y=1		X=Br <sup>-</sup> ,Y=I <sup>-</sup>
1	[MoOX <sub>5</sub> ] <sup>2-</sup>	X=C1 <sup>-</sup> ,Y=I 1.949		X=Br,Y=I 1.993
2	$[MoOX_5]^{2}$	X=C1 <sup>-</sup> ,Y=I 1.949 1.977		X=Br <sup>-</sup> ,Y=I <sup>-</sup> 1.993 2.008
1 2 3	$[MoOX_5]^{2-}$ $[MoOX_4Y]^{2-}$ $[MoOX_3Y_2]^{2-}$	X=C1 <sup>-</sup> ,Y=I 1.949 1.977 2.002		X=Br, Y=I  1.993  2.008  2.027

 $a_{\text{In units of cm}^{-1} \text{ x } 10^{-4}}$ 

by the observed EPR spectra of frozen glasses containing these complexes (see Figure 10). This observation together with electrostatic charge considerations suggests that the complexes formed are most likely  $[MoO(HPO_4)_5]^{2-}$  and  $[Mo(OCH_3)_2(H_2PO_4)_4]^{-}$ . The magnetic tensors measured from solution and frozen glass spectra are given in Table VI. A careful investigation of the spectra as a function of temperature and solvent composition failed to reveal any phosphorus or hydrogen superhyperfine interaction. This result is not unexpected since it is certainly reasonable to expect the bonding of the  $[H_2PO_4]^{-}$  to molybdenum to involve molybdenum-oxygen bonding. It may be recalled that oxygen rather efficiently restricts the flow of paramagnetic electron density to atoms more remote from the paramagnetic ion.

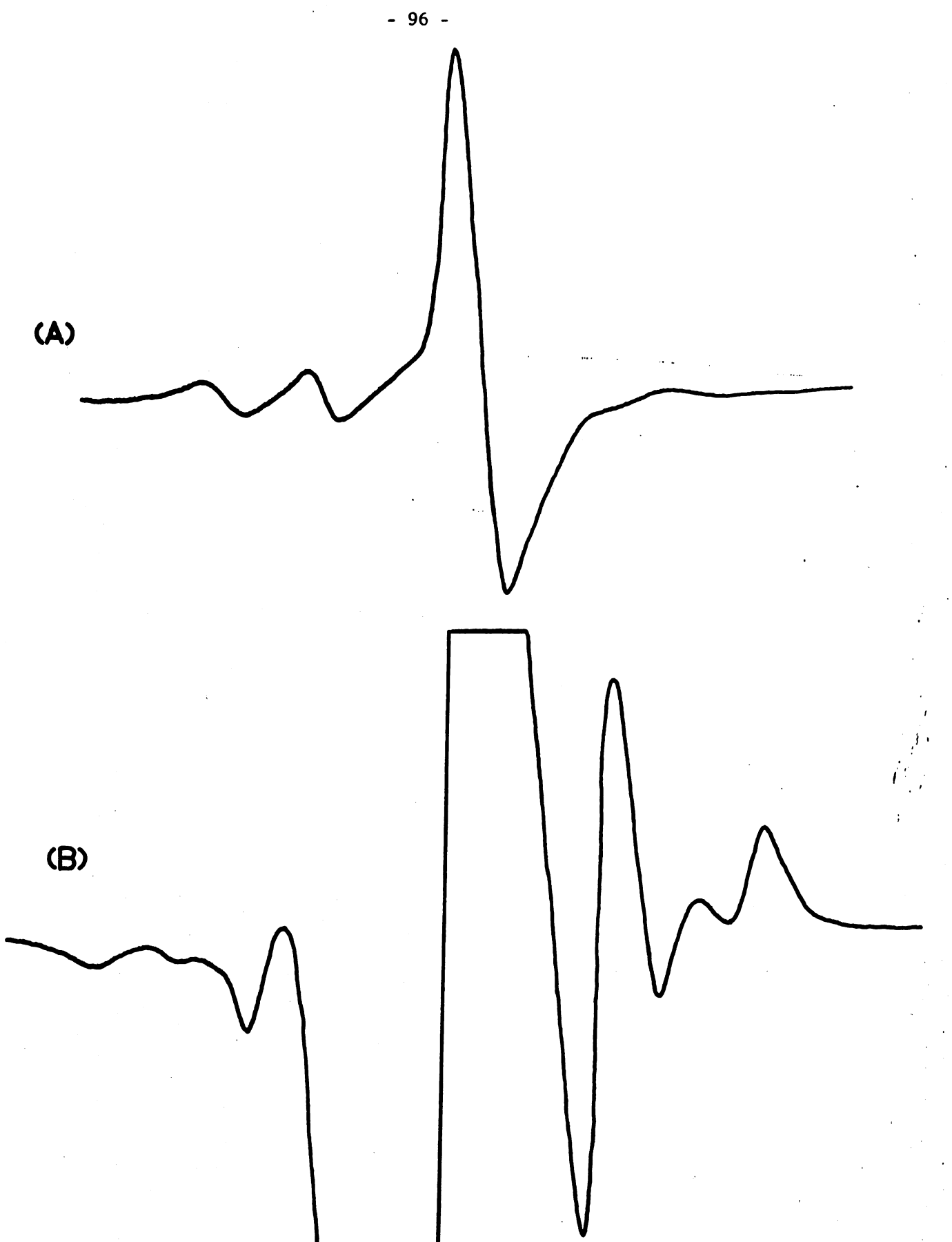
#### Compounds Formed with Phosphate Salts

 $C_5H_6N[Mo(OCH_3)_2Cl_4]$  dissolved in solutions of  $CH_3OH$  or DMF saturated with  $Na_3PO_4$  or  $K_3PO_4$  yielded EPR spectra very similar to those obtained by dissolution of the complex in phosphoric acid. Magnetic tensors are given in Table VI. Complexes Formed with  $(BuO)_3PO$ 

Dissolution of molybdenum pentachloride in tri-n-butylphosphate resulted in the formation of a complex of axial symmetry, as indicated by EPR examination. A careful study of the EPR spectra of this complex as a function of temperature revealed the presence of chlorine superhyperfine structure. The overlap of superhyperfine absorptions prohibited determination of the number of chlorine superhyperfine lines and their ratios. On the basis of a consideration of Zeeman and hyperfine value in comparison with those of other complexes leads to tentative identification of the complex as [Mo[(BuO)<sub>3</sub>PO]Cl<sub>5</sub>]. In very dilute solutions of MoCl<sub>5</sub> in (BuO)<sub>3</sub>PO (approximately 10<sup>-3</sup> to 10<sup>-4</sup> molar) the appearance of another paramagnetic Mo(V) complex was observed. The g value of

Figure 10. EPR Spectra of a Complex Formed by Adding  $(NH_4)_2[MoOCl_5]$  to  $H_3PO_4$ .

- (A) A first derivative presentation taken at 298°K.
- (B) Spectrum of the frozen glass at 77°K; first derivative presentation.



this complex was less than that of the complex predominant at higher  $MoCl_5$  concentrations. These observations together with the established successive ligand substitution reactions shown to occur for other Mo(V) complexes allows the tentative formulation of the second complex as  $[Mo[(BuO)_3PO]_2Cl_4]^+$ . Complexes Formed with  $(EtO)_2POH$ 

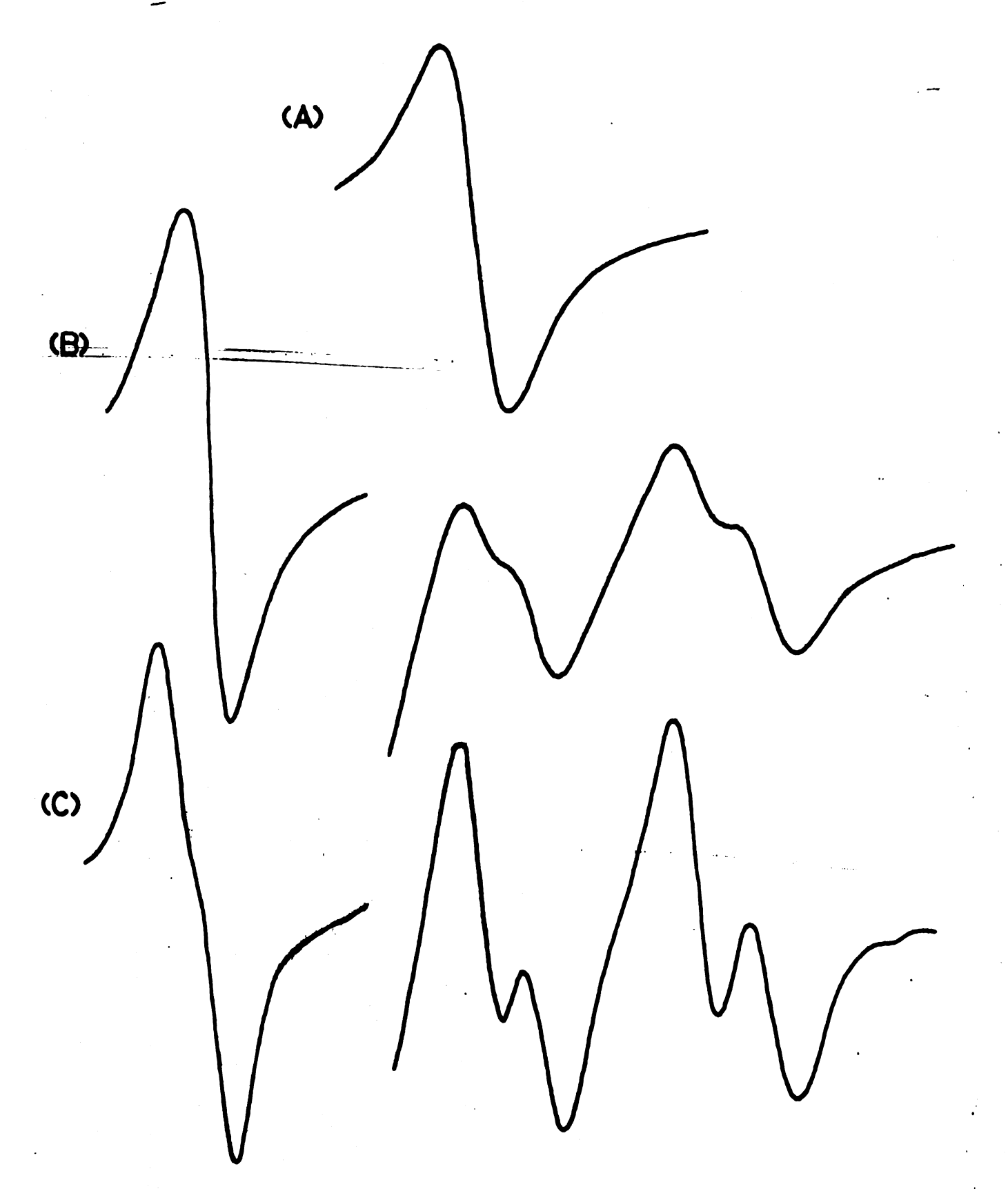
The addition of molybdenum pentachloride to diethylhydrogenphosphite resulted in the formation of five complexes containing Mo(V). The relative concentrations of these five complexes varied as the ratio of MoCl<sub>5</sub> to (EtO)<sub>2</sub>POH was altered. Typical spectra are shown in Figure 11. The variation of the concentrations of these species with MoCl<sub>5</sub> concentration and a consideration of their hyperfine and Zeeman tensors leads to the conclusion that these complexes result from the stepwise replacement of chloride ions by (EtO)<sub>2</sub>PO ligands. The nature of the spectra of frozen glasses leads to formulation of these five complexes as [Mo[(EtO)<sub>2</sub>PO]Cl<sub>5</sub>], [Mo[(EtO)<sub>2</sub>PO]<sub>2</sub>Cl<sub>4</sub>], [Mo[(EtO)<sub>2</sub>PO]<sub>3</sub>Cl<sub>3</sub>], [Mo[(EtO)<sub>2</sub>PO]<sub>4</sub>Cl<sub>2</sub>], and [Mo[(EtO)<sub>2</sub>PO]<sub>5</sub>Cl]. The magnetic tensors for these complexes are given in Table VI and the equilibrium constants for the successive substitution reactions are given in Table VIII.

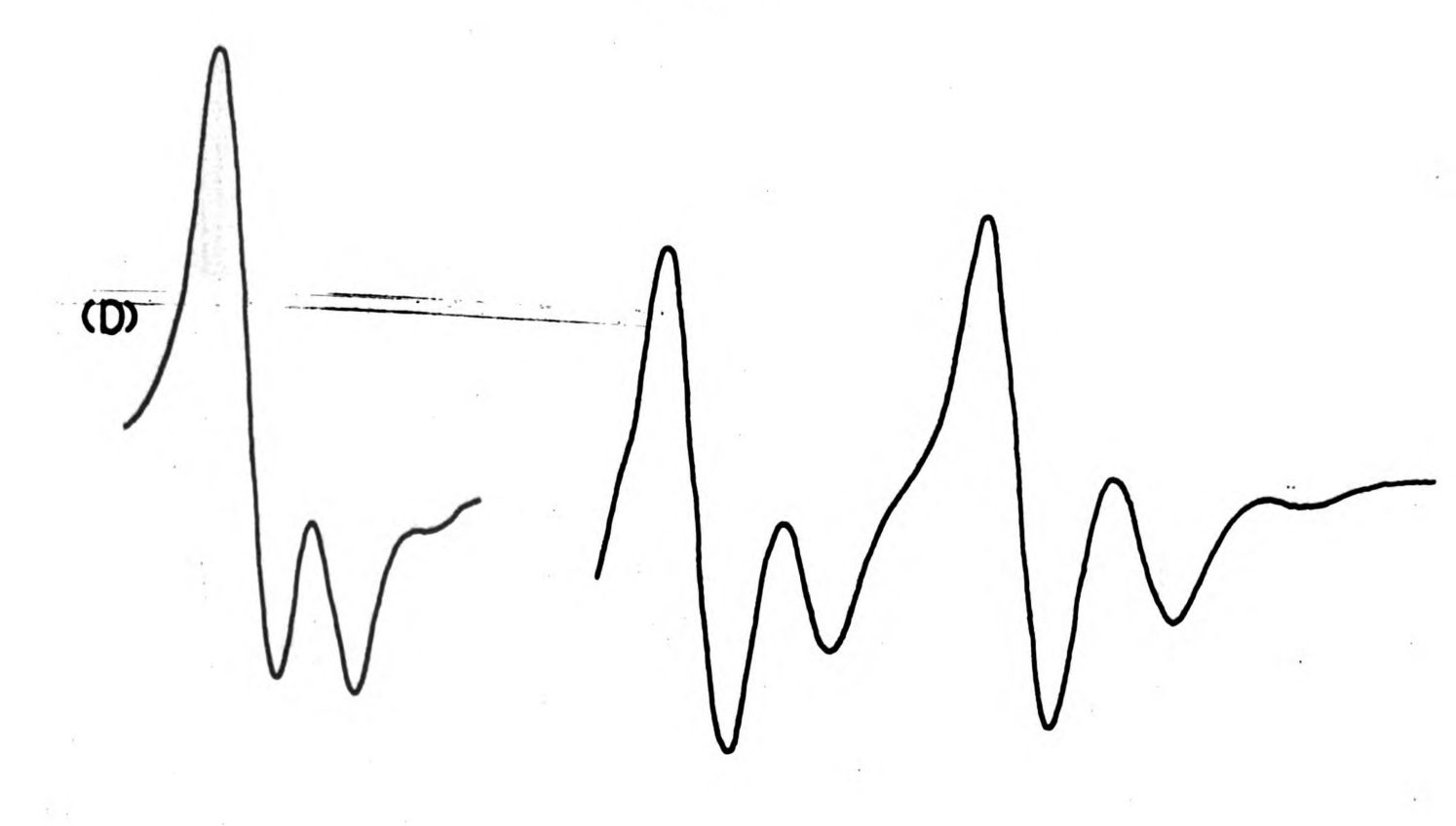
A study of the spectra of these complexes as a function of temperature indicated that the equilibria are temperature dependent. No attempt was made to determine the activation enthalpies and entropies from the temperature variation of the equilibrium constants.

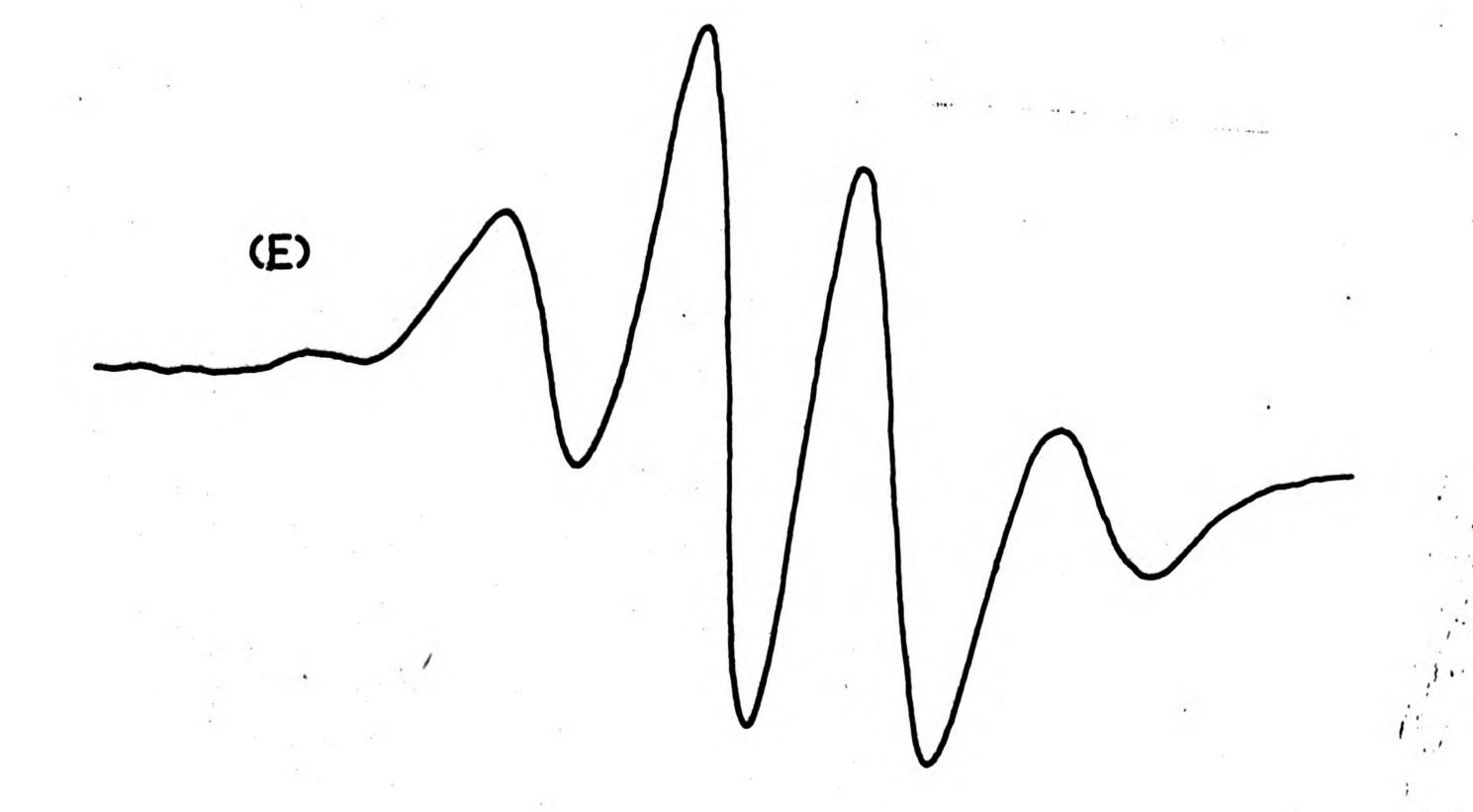
### Complexes Formed with DDPA

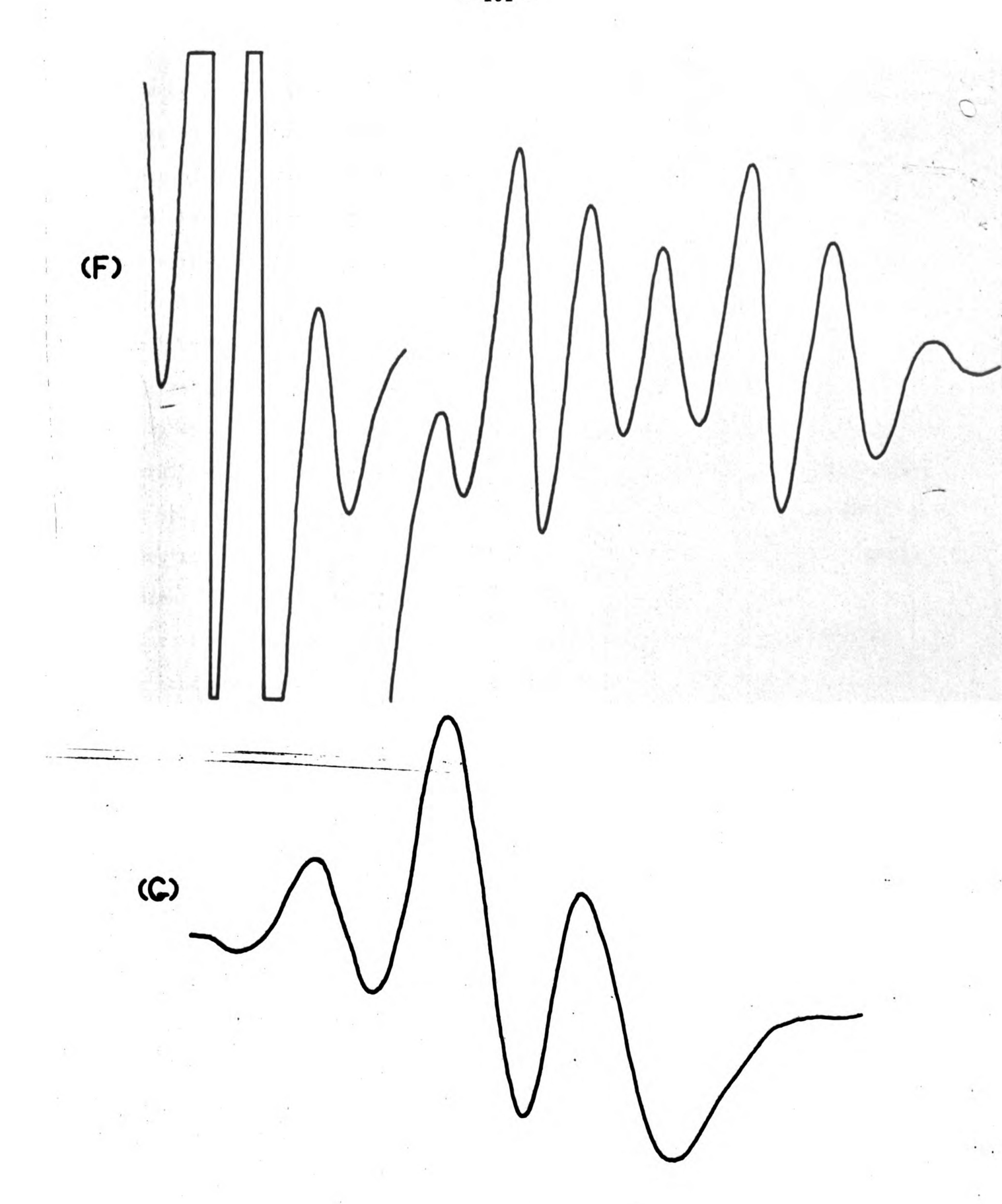
A complex characterized as  $[MoCl_5SPS(OC_2H_5)_2]^-$  by the observation of both phosphorus and chlorine superhyperfine interaction could be prepared by either addition of  $MoCl_5$  to DDPA or by addition of DDPA to a concentrated HCl solution containing  $[MoOCl_5]^{2-}$ . The paramagnetic species  $[MoCl_5SPS(OC_2H_5)_2]^-$  could be

- Figure 11. EPR Spectra of Complexes Containing (EtO) $_2$ PO as a Ligand in (EtO) $_2$ POH Solution.
- (A) First derivative EPR spectrum for a 0.25M solution of MoCl $_5$  in (EtO) $_2$ POH at 298°K. Only the m $_I$  = 0 absorption is shown, where m $_I$  is the molybdenum nuclear spin quantum number.
- (B) First derivative EPR spectrum for a 0.125M solution of MoCl $_5$  in (EtO) $_2$ POH at 298°K. The m $_{\rm I}$  = 0, m $_{\rm I}$  = -3/2, and m $_{\rm I}$  = -5/2 components are shown. The upfield components were recorded at increased gain.
- (C) First derivative EPR spectrum for a 0.05M solution of  $MoCl_5$  in (EtO)<sub>2</sub>POH at 298°K. The m<sub>I</sub> = 0, m<sub>I</sub> = -3/2, and m<sub>I</sub> = -5/2 components are shown. The upfield components were recorded at increased gain.
- (D) First derivative EPR spectrum for a 0.025M solution of  $MoCl_5$  in (EtO)<sub>2</sub>POH at 298°K. The m<sub>I</sub> = 0, m<sub>I</sub> = -3/2, and m<sub>I</sub> = -5/2 components are shown. The upfield components were recorded at increased gain.
- (E) First derivative EPR spectrum for a 0.01M solution of  $MoC1_5$  in (EtO)<sub>2</sub>POH at 298°K. Only the  $m_T$  = 0 component is shown.
- (F) First derivative EPR spectrum for a 0.01M solution of MoCl<sub>5</sub> in (EtO)<sub>2</sub>POH at 298°K. The  $\rm m_I$  = 0,  $\rm m_I$  = -3/2, and  $\rm m_I$  = -5/2 absorptions are shown. The upfield transitions were recorded at high gain.
- (G) First derivative EPR spectrum for a 0.005M solution of MoCl $_5$  in (EtO) $_2$ POH at 298°K. Only the m $_{\rm I}$  = 0 component is shown.









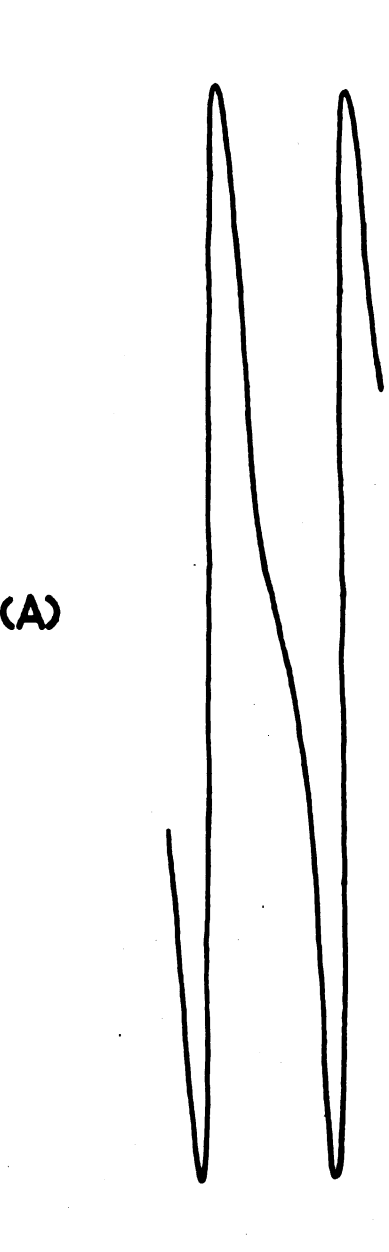
extracted by a wide range of organic solvents. The observed electron paramagnetic resonance spectra of this complex appeared to be relatively insensitive to the nature of the solvent (typical spectra are shown in Figure 12) with the exception that in ethanol the disappearance of chlorine superhyperfine structure together with the change in Zeeman and hyperfine tensor magnitudes indicate that the chlorine ligands are probably replaced by the ethoxide group.

Each of the phosphorus perpendicular superhyperfine components in the frozen glass spectra of  $[MoCl_5SPS(OC_2H_5)_2]^-$  are further split into seven components by two equivalent chlorines. Since this structure largely results from the spatial orientations  $\theta = \pi/2$ ,  $\phi = 0$  and  $\phi = \pi/2$ , the observed seven-component chlorine splitting was interpreted as indicative of interaction of the paramagnetic electron with the four equivalent equatorial chloride ligands. The spectra also indicate that the components of the chlorine superhyperfine interaction parallel to the molybdenum-phosphorus bond and along the molybdenum-equatorial chlorine bond are nearly zero. The large anisotropic chlorine hyperfine interaction is thus attributed to the component of the chlorine superhyperfine tensor perpendicular to the molybdenum-phosphorus and molybdenum-equatorial chlorine bonds. This assignment is consistent with the symmetry of metal and ligand orbitals which are capable of substantial overlap.

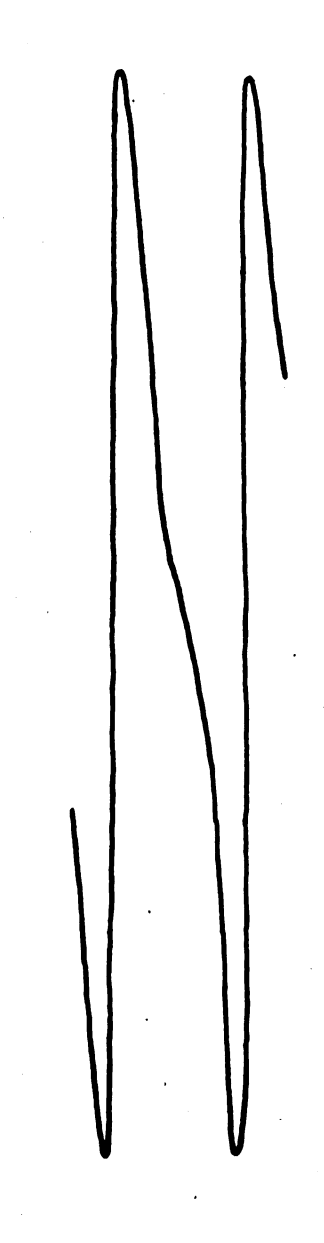
The addition of DDPA to a sulfuric acid solution containing  $[MoO(HSO_4)_5]^{2-}$  resulted in the formation of a complex which on the basis of phosphorus superhyperfine interaction and on the observed values of the Zeeman and hyperfine tensors may be interpreted structurally to be  $[Mo(HSO_4)_5SPS(OC_2H_5)_2]^{-}$ . Typical spectra are shown in Figure 12. The magnetic tensors determined from the observed spectra are given in Tables VI and VII.

Figure 12. EPR Spectra of Complexes Containing (EtO)<sub>2</sub>PSS as a Ligand.

- (A) EPR spectrum of  $[{\rm MoCl}_5{\rm SPS}({\rm OC}_2{\rm H}_5)_2]^-$  in diethyl ether at 298°K showing the phosphorus superhyperfine interaction on the m $_{\rm I}$  = 0 and m $_{\rm I}$  = -5/2 components of the molybdenum hyperfine interaction. A first derivative presentation is shown; the gain was increased for recording of the superhyperfine interaction on the m $_{\rm I}$  = -5/2 component.
- (B) EPR spectrum of  $[MoCl_5SPS(OC_2H_5)_2]^-$  in a frozen glass of diethyl ether at 77°K. A first derivative presentation of the superhyperfine interaction on the  $m_I = 0$  component is shown. Chlorine superhyperfine structure from two equivalent chlorines is visible on the perpendicular components of the phosphorus superhyperfine interaction.
- (C) First derivative presentation of EPR spectrum of  $[Mo(HSO_4)_5SPS(OC_2H_5)_2]^-$  in a mixture of  $H_2SO_4$  and  $(EtO)_2PSSH$  at  $298^\circ K$ .
- (D) First derivative presentation of the EPR spectrum of  $[Mo(HSO_4)_5SPS(OC_2H_5)_2]^-$  in a frozen glass of  $H_2SO_4$  and  $(EtO)_2PSSH$  at  $77^\circ K$  showing the phosphorus superhyperfine interaction on the parallel and perpendicular  $m_I = 0$  components and on the parallel  $m_I = -5/2$  component. Gain was increased for recording of the upfield component.



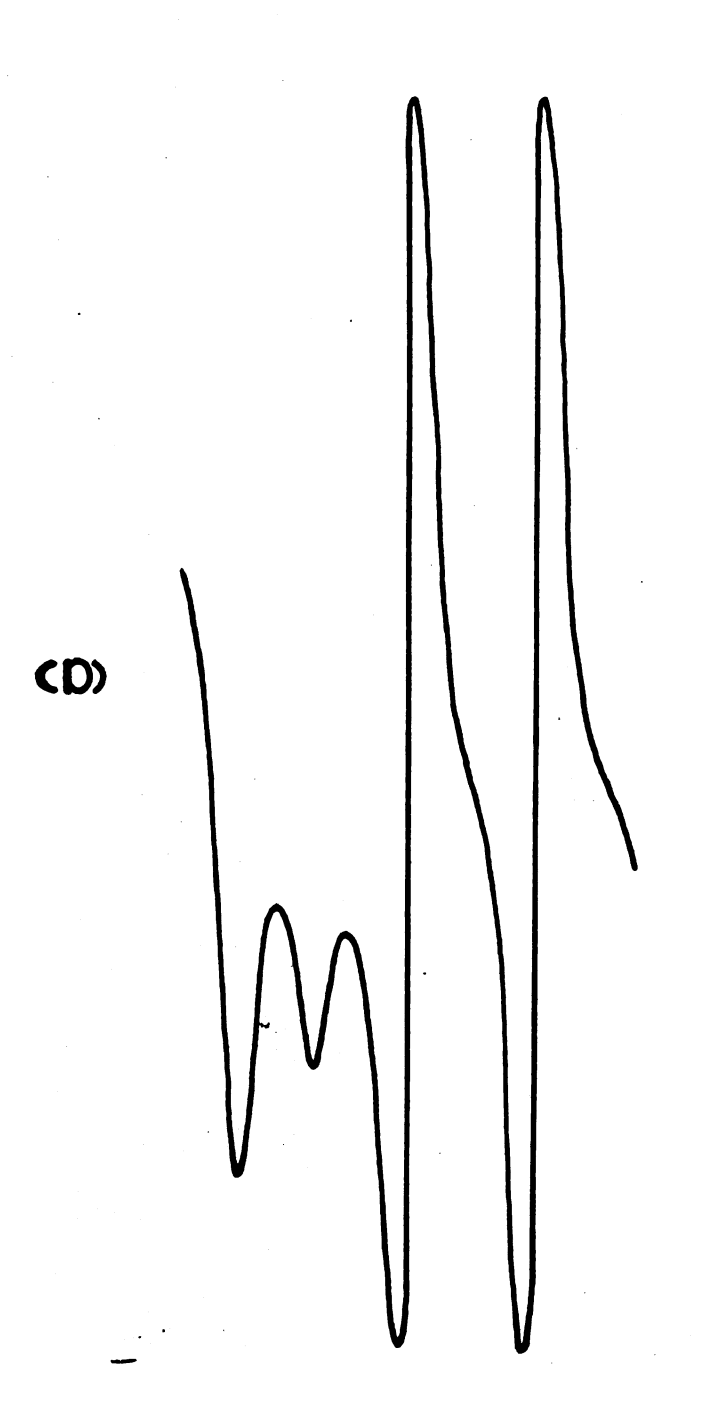


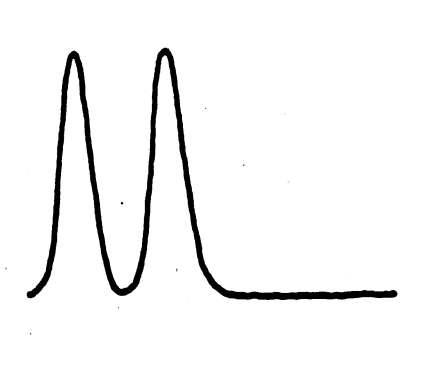


(C)



Ç,





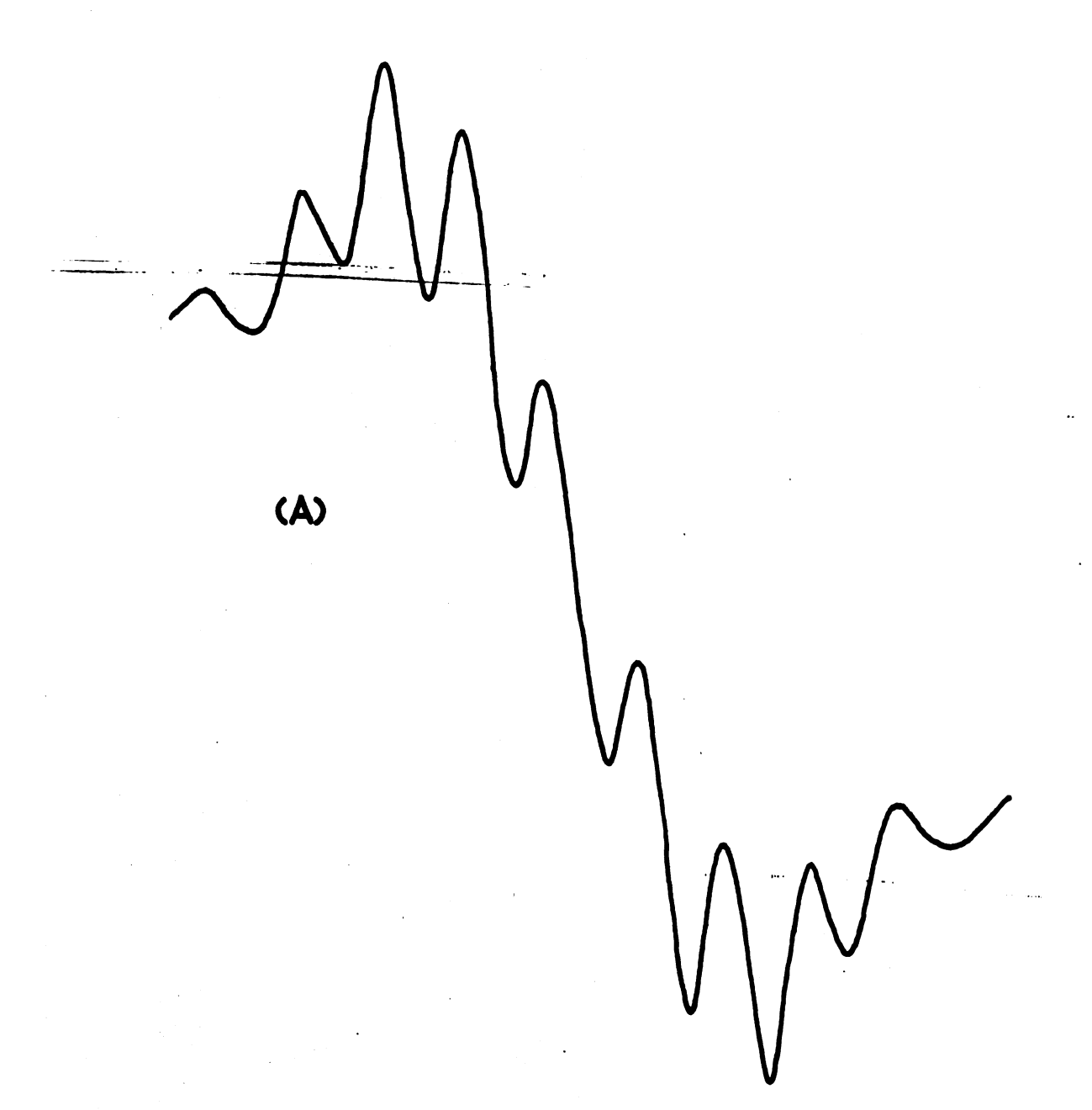
IV. Mo(V) Complexes with Ligands Containing Nitrogen.

# $[MoO(NCS)_5]^{2-}$

Upon cooling a 2M perchloric acid solution of  $(NH_4)_2[MoO(NCS)_5]$  to -25°C, nitrogen superhyperfine interaction was observed on the molybdenum hyperfine components and on the central line arising from interaction of the molybdenum isotopies for which I = 0 with the paramagnetic electron. This superhyperfine structure, shown in Figure 13, consists of 9 equally spaced lines having the approximate intensity ratios 1:8:28:56:70:56:28:8:1, indicating the interaction of the paramagnetic electron with four equivalent nitrogen nuclei. When the temperature was either raised or lowered the linewidths of the superhyperfine components increased. The linewidths of the nitrogen superhyperfine components are approximately equal at -25°C, an observation which indicates that both the spin-rotation and anisotropic rotational relaxation mechanisms are factors in determining the linewidth. The increase in linewidth (as the temperature is increased) is viewed as resulting from the action of the spin-rotational mechanism while the increase in linewidth with decreasing temperature results from the operation of the anisotropic rotational mechanism. That best resolution of the nitrogen superhyperfine structure occurs at a temperature at which the linewidths are equal indicates that the anisotropic rotational mechanism may be somewhat more important.

Observation of the spectrum of  $[MoO(NCS)_5]^{2-}$  in a frozen  $HClO_4$  glass indicated the complex to be of axial symmetry (see Figure 14). The measured magnetic tensors are given in Tables VI and VII.

- Figure 13. Nitrogen Superhyperfine Interaction in Mo(V) Complexes Containing Thiocyanate as a Ligand.
- (A) First derivative EPR spectrum of  $[MoO(NCS)_5]^{2-}$  in 2M HClO $_4$  at -25°C showing the nitrogen superhyperfine interaction on the m $_{\rm I}$  = 0 component of the molybdenum spectrum.
- (B) First derivative EPR spectrum of complex tentatively formulated as  $[Mo(OCH_3)_2(NCS)_4]^-$  in dimethylformamide at -70°C showing the nitrogen superhyperfine structure on the  $m_T = 0$  absorption.



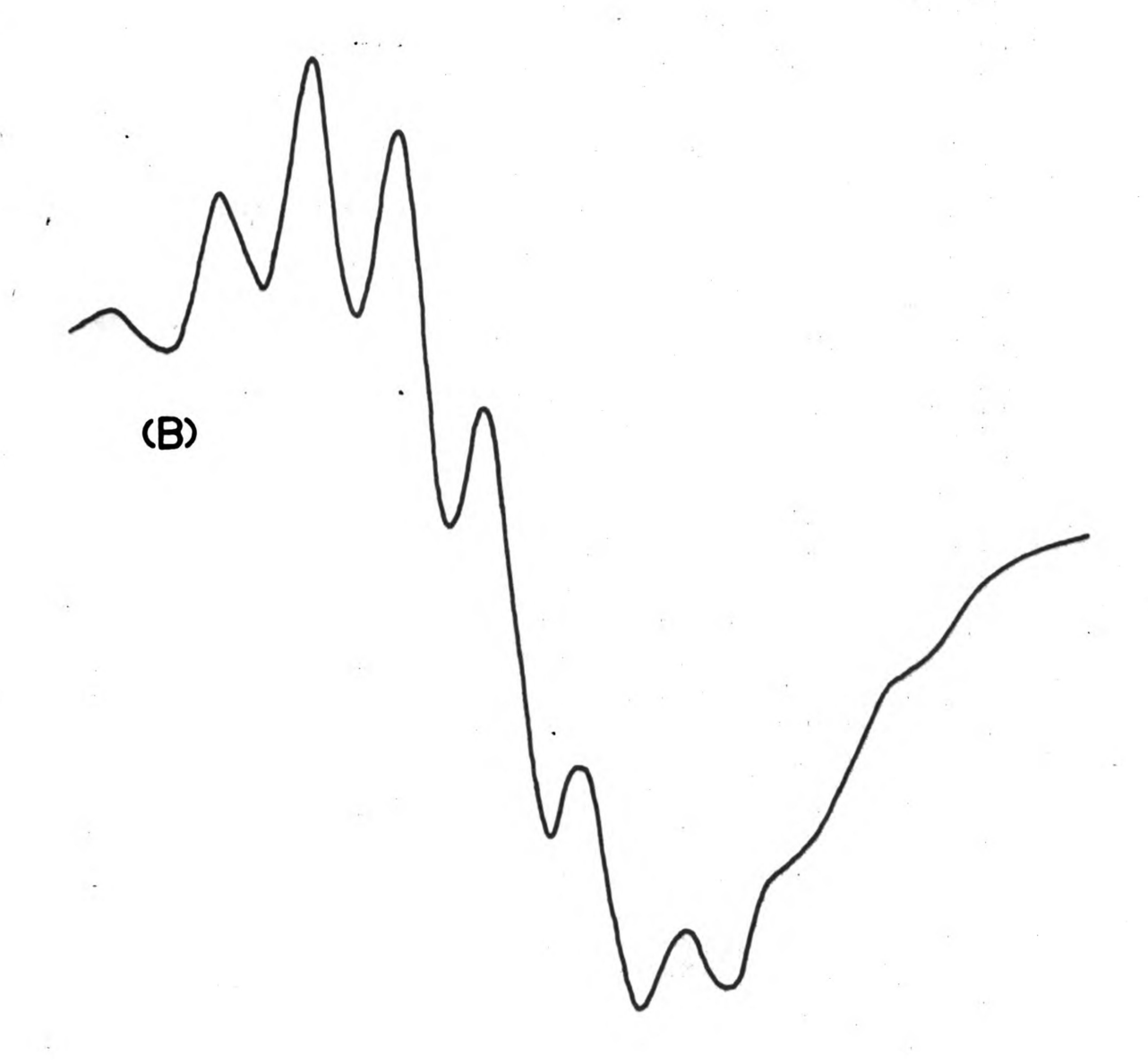
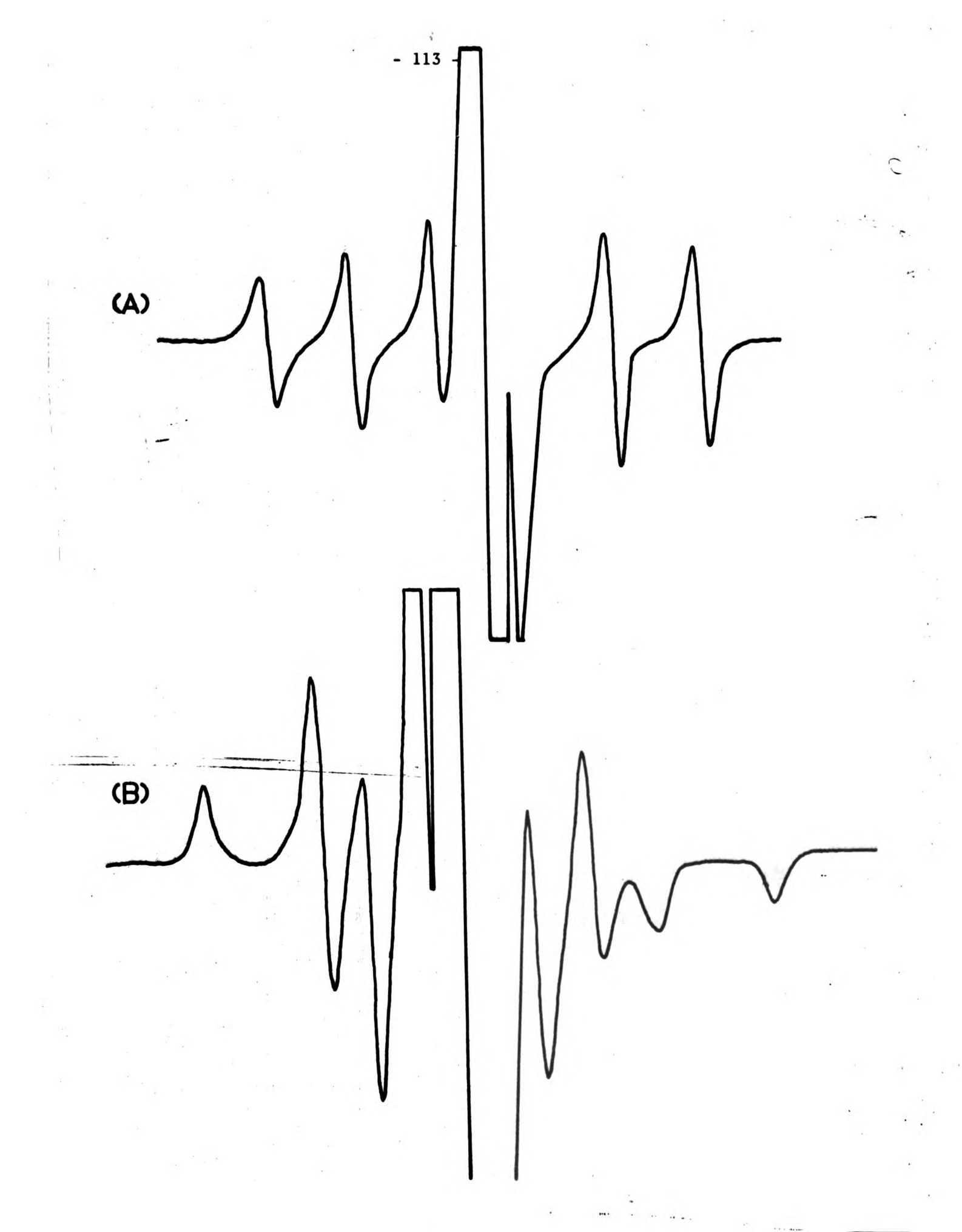


Figure 14. Solution and Frozen Glass EPR Spectra of  $[MoO(NCS)_5]^{2-}$ .

- (A) First derivative EPR spectrum of  $[MoO(NCS)_5]^{2-}$  in 2M HClO<sub>4</sub> at 298°K.
- (B) First derivative EPR spectrum of a frozen glass of [MoO(NCS) $_5$ ]  $^{2-}$  in HClO $_{A}$ .



# $^{\text{C}_5\text{H}_6\text{N}[\text{Mo}(\text{OCH}_3)_2\text{Cl}_4]}$ Dissolved in NH<sub>4</sub>SCN/CH<sub>3</sub>OH and NH<sub>4</sub>SCN/DMF

The spectra of  $C_5H_6N[Mo(OCH_3)_2Cl_4]$  dissolved in methanol saturated with  $NH_4SCN$  demonstrated the presence of an axially symmetrical complex. The magnetic tensors for this complex are given in Table VI. Nitrogen superhyperfine interaction was not observed at any temperature over a range from  $77^{\circ}K$  to  $300^{\circ}K$ .

Upon dissolution of  $C_5H_6N[Mo(OCH_3)_2Cl_4]$  in a solution of DMF saturated with  $NH_4SCN$  and cooling of the resultant solution to  $-70^{\circ}C$  a nitrogen superhyperfine structure similar to that recorded for  $(NH_4)_2[MoO(NCS)_5]$  in perchloric acid was observed, a typical spectrum being shown in Figure 13. Nine equally spaced nitrogen superhyperfine lines were observed on each molybdenum component. As with the  $[MoO(NCS)_5]^{2-}$  complex, either raising or lowering the temperature resulted in an increase in the nitrogen superhyperfine linewidths accompanied by less resolution of the superhyperfine structure. Unlike the  $[MoO(NCS)_5]^{2-}$  complex, it will be noted that the linewidths of the superhyperfine components in the spectra of the complex formed from  $C_5H_6N[Mo(6CH_3)_2Cl_4]$  are not equal at the temperature of best resolution. These unequal linewidths indicate that the spin-rotational mechanism determines the resolution of the superhyperfine structure. The linewidth variations observed for the components of the nitrogen superhyperfine structure indicates that this interaction is anisotropic in nature.

Observation of the spectrum of the complex formed from  $C_5H_6N[Mo(0CH_3)_2Cl_4]$  at 77°K in a DMF glass resulted in the spectrum shown in Figure 14. The nature of this spectrum clearly indicates that the complex is of axial symmetry, the values of the magnetic tensors being given in Table VI.

## $[Mo(X)_3(NCS)_3]^-$

Dissolution of molybdenum pentachloride in a methanol solution saturated

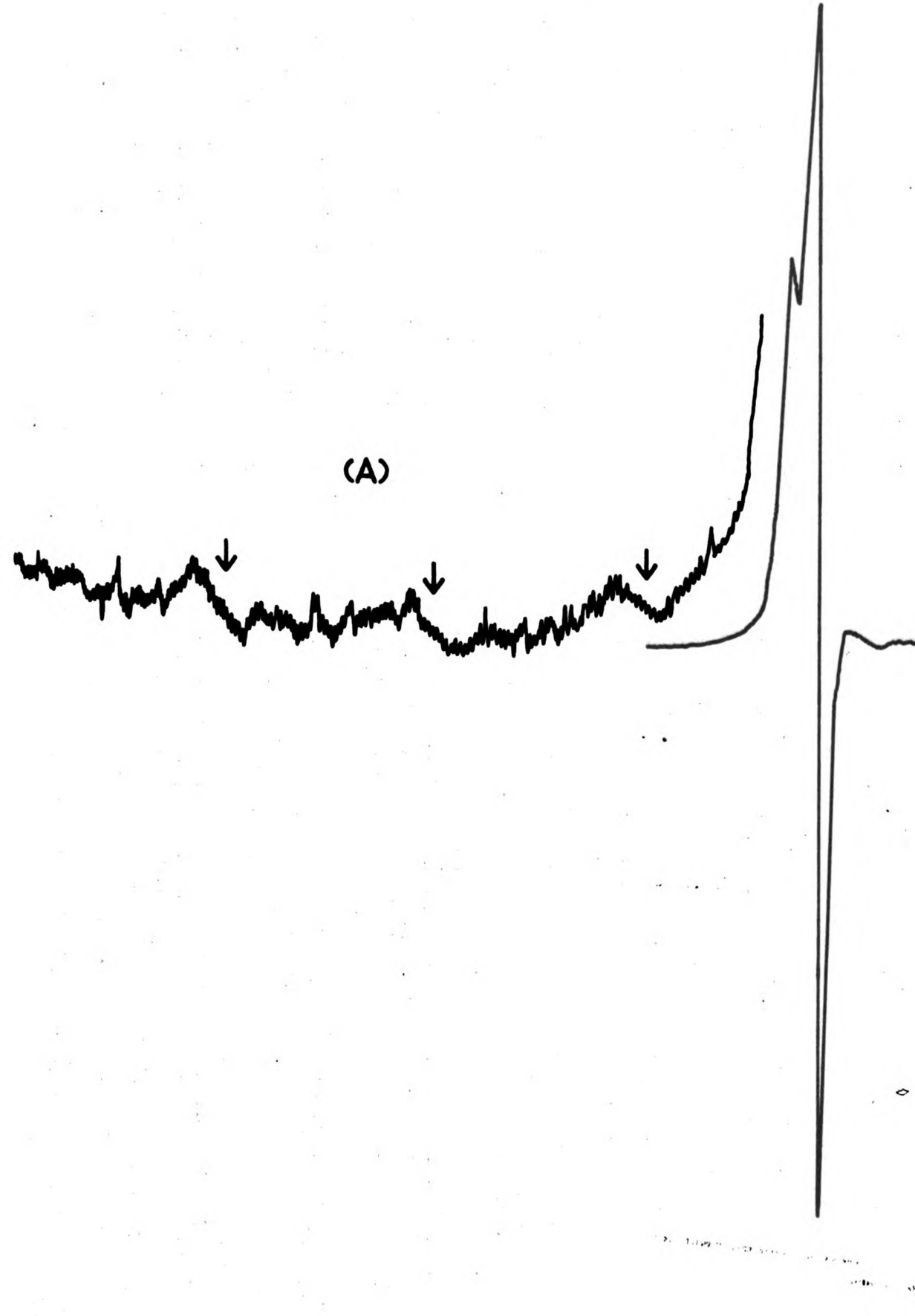
with NH<sub>4</sub>SCN resulted in the formation of a complex which gave the same EPR spectrum in solution and in the frozen glass. Thus an isotropic distribution of ligands in the complex must be involved. When this complex was dissolved in DMF and the EPR spectrum of the resulting solution examined, a nitrogen superhyperfine structure consisting of seven equally spaced lines in the intensity ratios 1:6:15:20:15:6:1 was observed. This indicates the interaction of the paramagnetic electron with 3 equivalent nitrogen nuclei; the complex may be tentatively formulated as  $[Mo(X)_3(NCS)_3]^-$  where  $X = CH_3O^-$  or  $C1^-$ . Since no distortion from spherical symmetry is observed in the spectrum of the frozen glass, one may further conclude that only the <u>cis</u> isomer is present. The measured magnetic tensors are given in Tables VI and VII.

### $C_5H_6N[Mo(OCH_3)_2Cl_4]$ in Dimethylglyoxime/Acetone

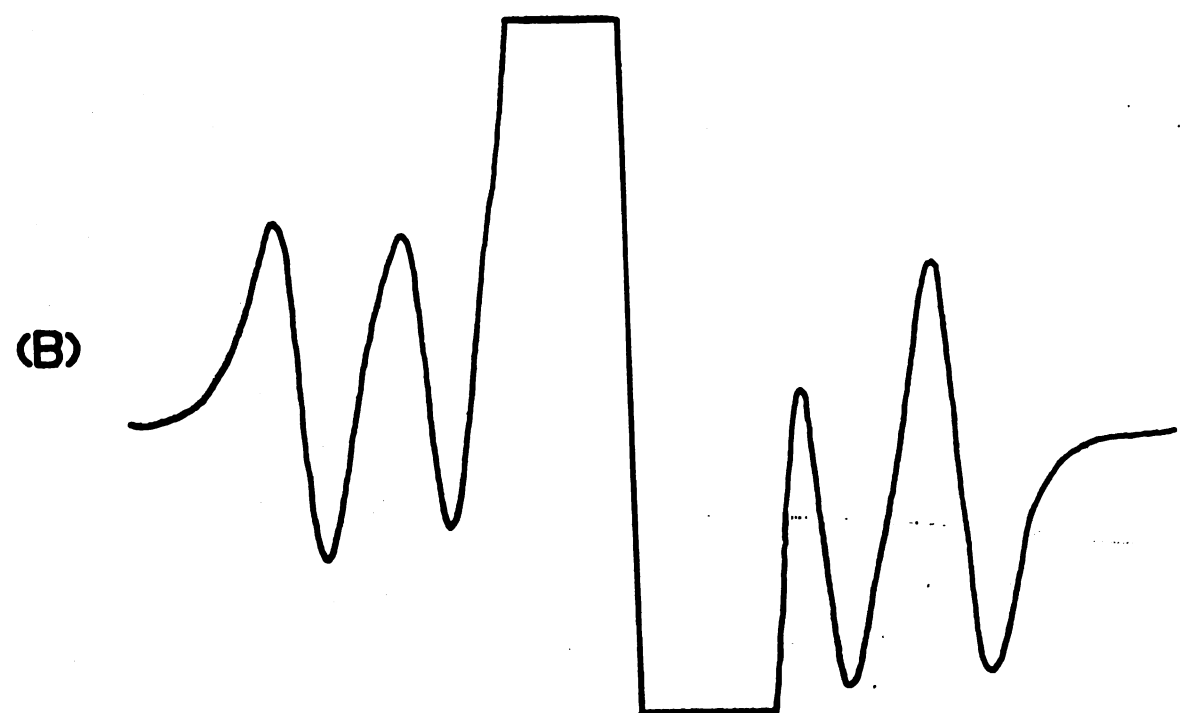
The addition of  $C_5H_6N[Mo(OCH_3)_2Cl_4]$  to a solution of acetone saturated with dimethylglyoxime (DMG) resulted in precipitation of a solid which gave the EPR spectrum reproduced in Figure 15. Since the g values for this material are very different from those of the original complex, the coordination of DMG to molybdenum may be inferred. Further support for this contention is obtained by recording the spectrum of the DMG complex in acetone at 77°K. When solutions of  $C_5H_6N[Mo(OCH_3)_2Cl_4]$  in acetone are frozen only a single broad line is observed in the EPR spectra as the result of the formation of a polycrystalline powder rather than a glass. When the DMG complex is added to acetone and the solution is frozen a polycrystalline powder also results. However, the EPR spectra observed is well resolved and corresponds to the spectra usually observed for frozen glasses. In the study of the EPR spectra of the DMG complex over the temperature range from 77°K to 300°K an unevenness of the molybdenum hyperfine

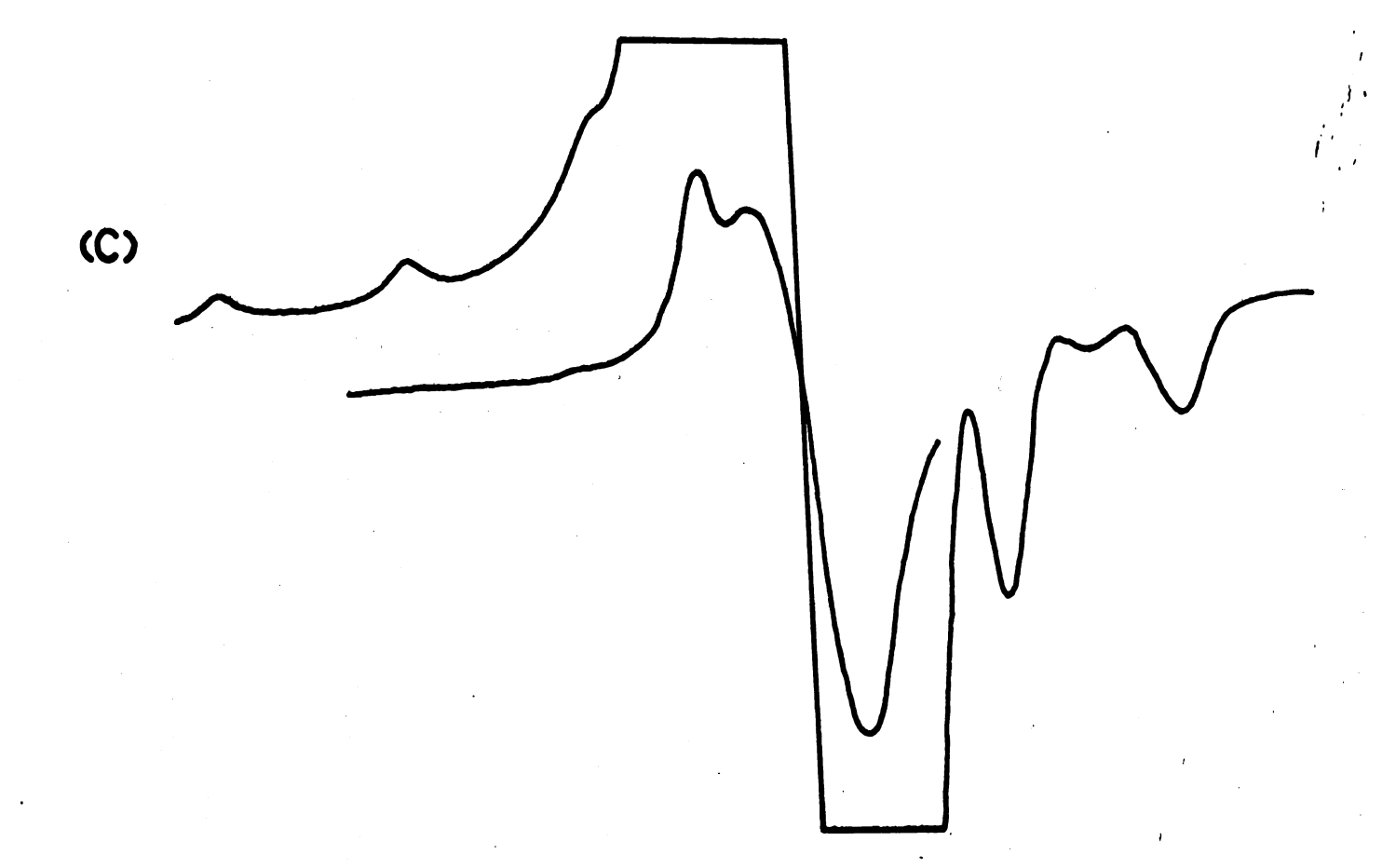
Figure 15. EPR Spectra of Complex Containing Dimethylglyoxime as a Ligand.

- (A) Spectrum of the undiluted powder of the complex containing dimethylglyoxime (DMG) as a ligand. The first derivative presentation shown was recorded at 298°K. Arrows indicate unusual hyperfine components.
- (B) First derivative EPR spectrum of the complex containing DMG in a solution of acetone at 298°K.
- (C) First derivative EPR spectrum of the DMG complex in a frozen powder of the acetone solution (acetone forms a polycrystalline material rather than a glass upon freezing) at 77°K. Gain was adjusted so that all features of the spectrum would be visible.



0





lines was noted. This may be indicative of unresolved nitrogen superhyperfine interaction.

## ${\rm C_5H_6N[Mo(OCH_3)_2Cl_4]}$ in Pyridine

Several typical spectra obtained for solutions of  $C_5H_6N[Mo(OCH_3)_2Cl_4]$  dissolved in pyridine are shown in Figure 16. The change in hyperfine and g tensor magnitudes indicates that pyridine is coordinating to the molybdenum in these complexes. The spectra shown in Figure 16 indicate that at least three different complexes containing pyridine can be formed by varying the relative concentrations of chloride ion and pyridine. Furthermore, the spectra indicate that at least two of these complexes possess axial symmetry. Sufficient time for study of the equilibria in detail was not available.

V. Mo(V) Complexes with Ligands Containing Sulfur.

# $[MoO(HSO_4)_5]^{2-}$

The EPR spectrum of  $[MoO(HSO_4)_5]^{2-}$  in concentrated  $H_2SO_4$  was recorded over a temperature range from 77°K to 350°K. The low field molybdenum hyperfine lines are better resolved than the upfield lines of the same  $|m_{\rm I}|$ , which is consistent with the spin-rotational and anisotropic rotational modulation of the hyperfine interaction and a negative sign of the g tensor.

# $^{\mathrm{C}_5\mathrm{H}_6\mathrm{N}[\mathrm{Mo}(\mathrm{OCH}_3)_2\mathrm{Cl}_4]}$ in $^{\mathrm{H}_2\mathrm{SO}_4}$

The EPR spectrum of  $C_5H_6N[Mo(OCH_3)_2Cl_4]$  in concentrated  $H_2SO_4$  was, within experimental error, identical to that observed for  $[MoO(HSO_4)_5]^{2-}$ .

# $Mo_2O_3(SO_4)_2$

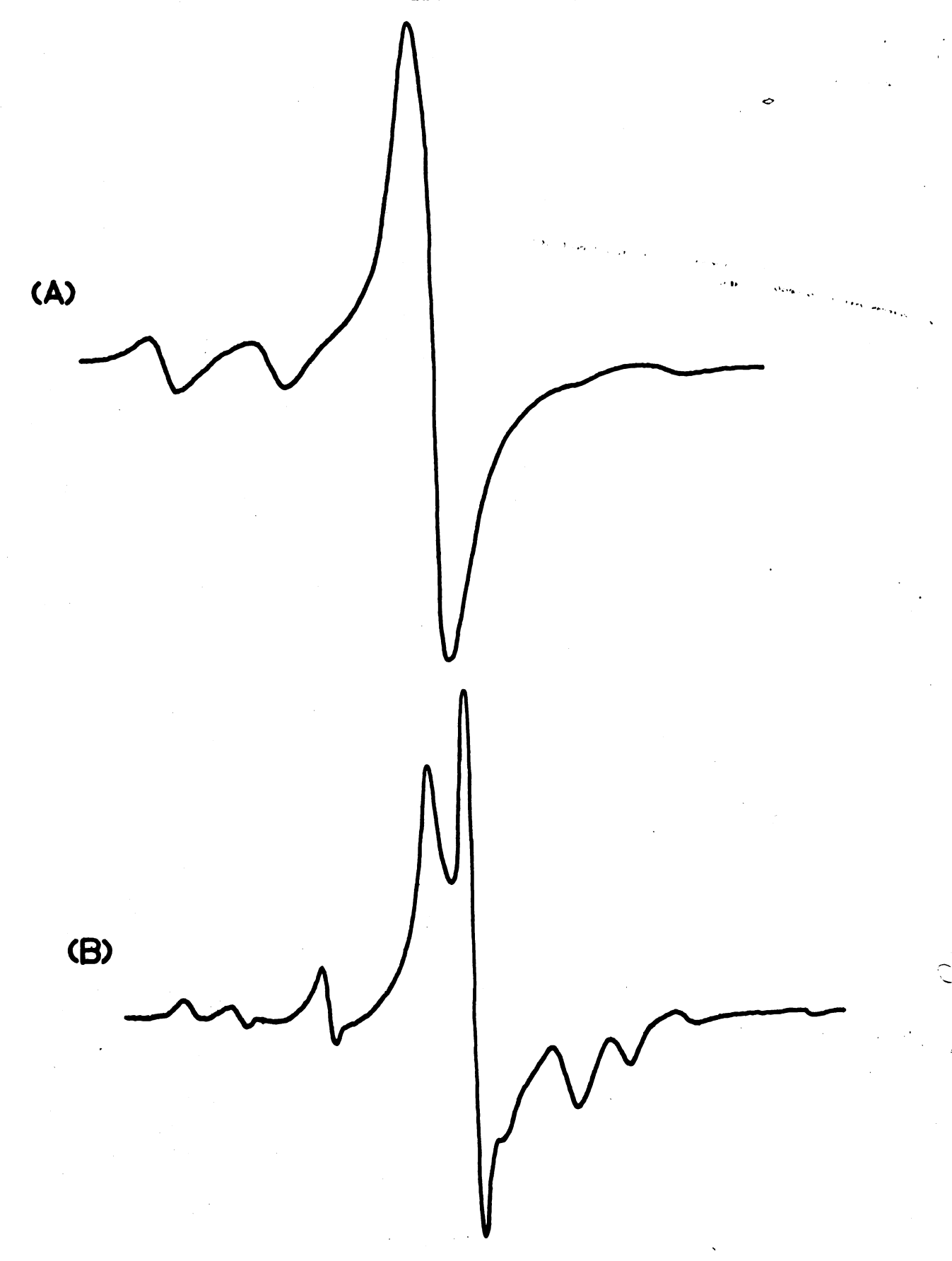
The large  $m_I$  dependence of the linewidth of the sulfuric acid solution (see Figure 17) of  $Mo_2o_3(So_4)_2$  indicates a large rotational radius and therefore possibly a dimeric complex.

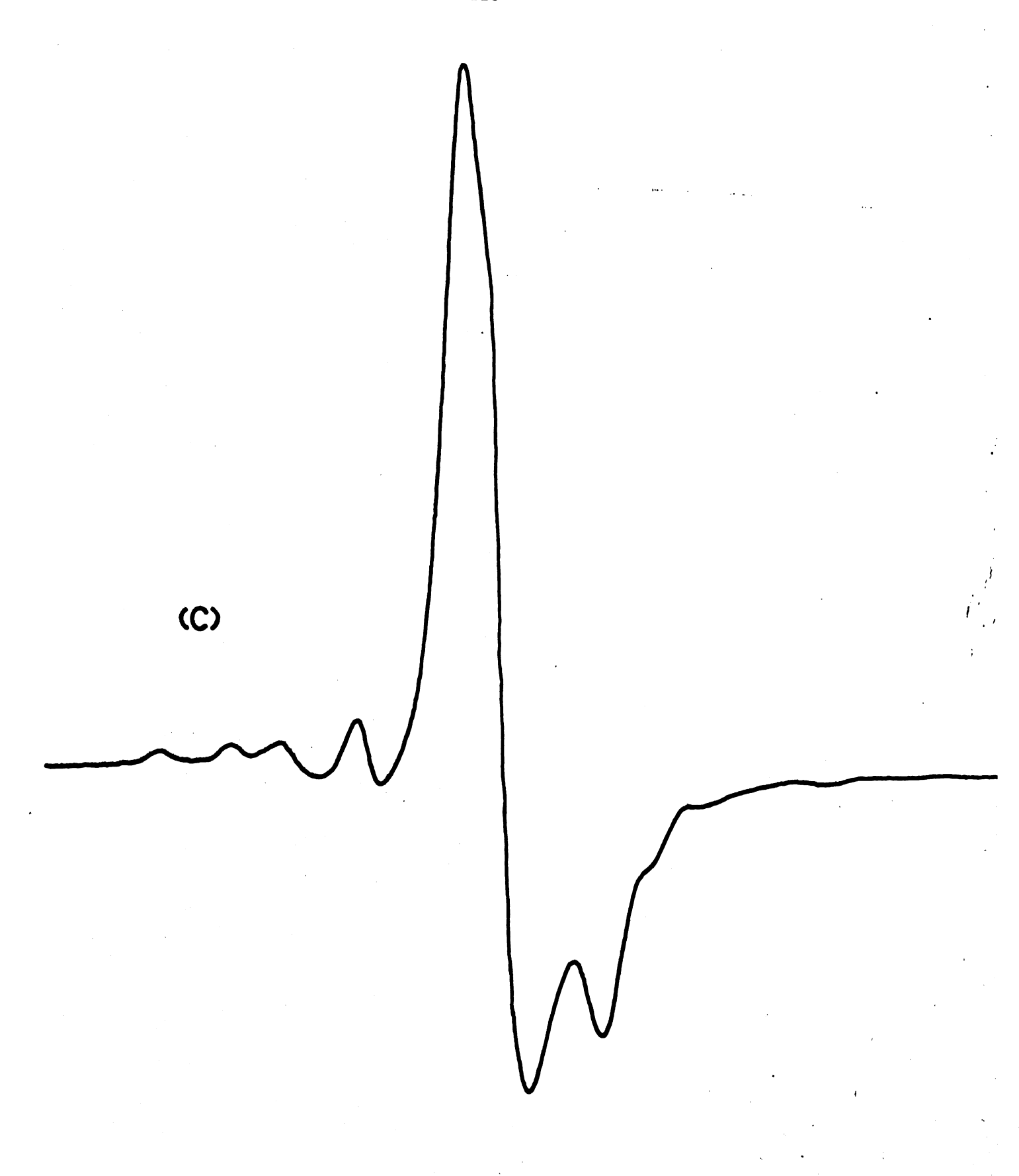
Figure 16. EPR Spectra of Complexes Containing Pyridine as a Ligand.

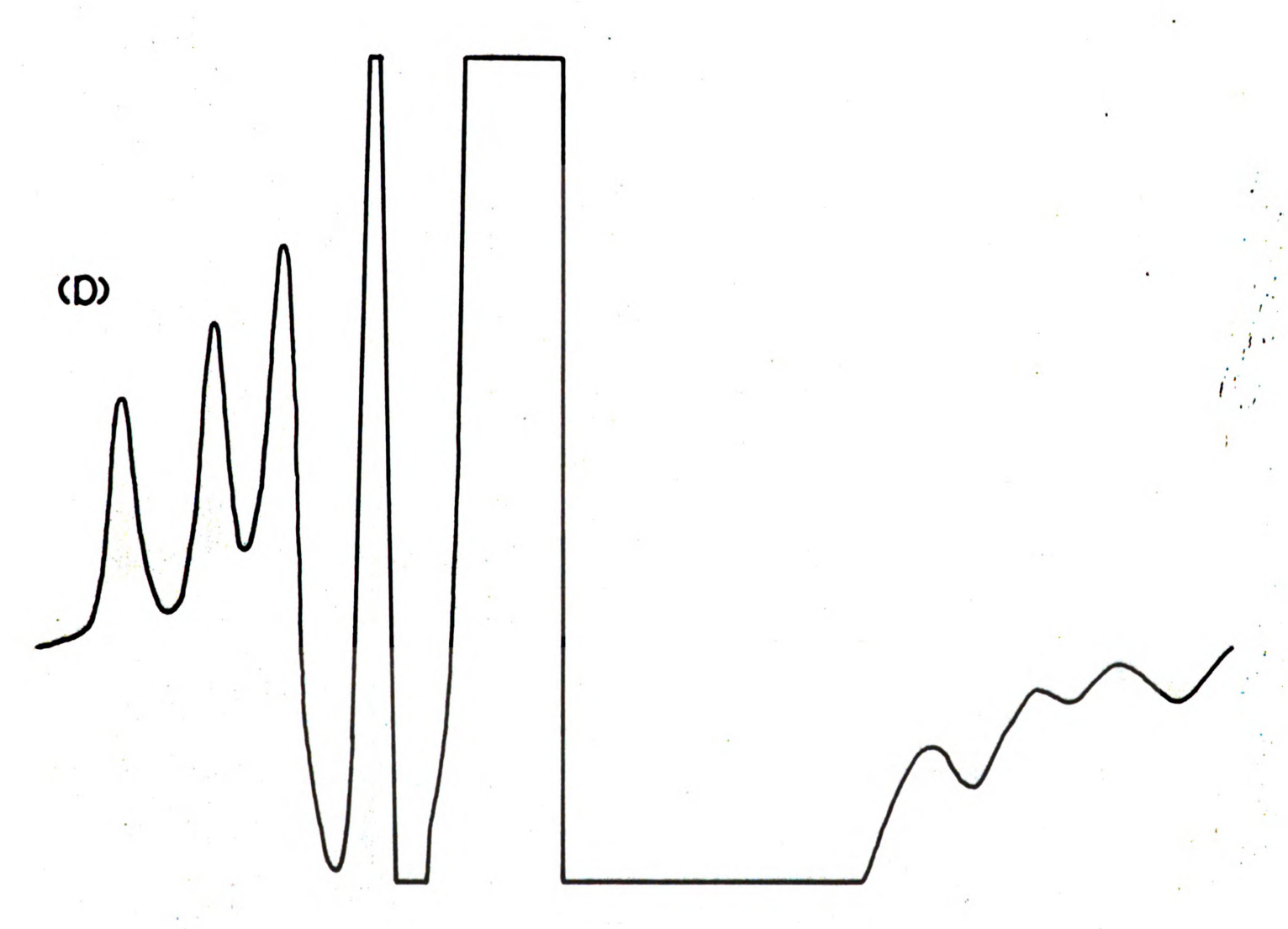
- (A) First derivative EPR spectrum of  ${\rm C_5H_6N[Mo(OCH_3)_2Cl_4]}$  dissolved in pyridine at 298°K. Sample 1.
- (B) First derivative EPR spectrum of the central portion of the EPR spectrum of Sample 1 at 77°K.
- (C) First derivative EPR spectrum of a second sample of  ${\rm C_5H_6N[Mo(OCH_3)_2Cl_4]}$  dissolved in pyridine at 77°K. Low field and central portions of the EPR spectrum are shown. The low field portion was recorded at greatly increased gain.
- (D) First derivative EPR spectra of a third sample of  ${\rm C_5H_6N[Mo(OCH_3)_2Cl_4]}$  in pyridine at 77°K. Two recordings are shown with the gain settings adjusted so that all the pertinent features are visible.

Relative concentrations of molybdenum in these samples are as follows: Sample 1 < Sample 2 < Sample 3. Figure 17. EPR Spectra of  $Mo_2O_3(SO_4)_2$ .

- (A) First derivative EPR spectrum of  $Mo_2O_3(SO_4)_2$  in  $H_2SO_4$  at 25°C.
- (B) First derivative EPR spectrum of  $Mo_2O_3(SO_4)_2$  in  $H_2SO_4$  at -50°C.
- (C) First derivative EPR spectrum of  ${\rm Mo_2O_3(SO_4)_2}$  in a frozen glass of  ${\rm H_2SO_4}$  at 77°K.
- (D) First derivative EPR spectrum of  ${\rm Mo_2O_3(SO_4)_2}$  in a frozen glass of  ${\rm H_2SO_4}$  at 77°K. Spectrum recorded at increased gain.







### $MoOC1SO_4$

As small amounts of saturated aqueous sodium chloride, potassium chloride, or concentrated hydrochloric acid were added to the concentrated sulfuric acid solution of 0.01 molar  $Mo_2O_3(SO_4)_2$ , chlorine hyperfine lines were observed in the EPR spectra of these solutions, each molybdenum line being split into four components by interaction with the  $^{35}C1$ ,  $^{37}C1$  nuclei (I = 3/2) as is shown in Figure 18. The optimum concentration range for observation of ligand hyperfine splitting at room temperature was at  $[{\rm Cl}^-]/[{\rm H}_2{\rm SO}_4]$  ratios between 1/20 and 1/10. As the concentration of  ${\rm C1}^-$  was increased so that the ratio  ${\rm [C1}^-]/{\rm [H_2SO_4]}$ approached unity, the EPR pattern gave the same magnetic tensors as the [MoOCl<sub>5</sub>]<sup>2-</sup> complex. Within experimental error, the spectrum for a solution of  $MoOCl_3$  $(5 \times 10^{-3} \text{M})$  in concentrated  $\text{H}_2\text{SO}_4$  was identical in appearance and in measured tensor elements to that observed for  $Mo_2O_3(SO_4)_2$  containing small amounts of C1. On the basis of the ligand splitting, one chlorine must be in the coordination sphere, implying a formulation of the complex as  $MoOC1SO_4$ . The chlorine superhyperfine linewidths as well as those of molybdenum hyperfine components show a dependence upon nuclear spin I, indicating the existence of an axial field gradient in this complex. The magnetic tensors of this complex as well as the oxosulfate precursor are given in Tables VI and VII.

#### VI. Nuclear Relaxation Results.

The electron-nuclear dipolar hyperfine interaction for protons, deuterons, and fluorine nuclei with the paramagnetic complex  $[{\rm MoOF}_5]^{2-}$  in  ${\rm HF/D}_2{\rm O}$  solution, for the protons and deuterons associated with the  $[{\rm MoOCl}_5]^{2-}$  complex in  ${\rm HCl/D}_2{\rm O}$  solutions, and for the protons of the  $[{\rm Mo(OCH}_3)_2{\rm Cl}_4]^-$  complex in methanol was measured from the shift of the NMR absorption frequency in the presence of the

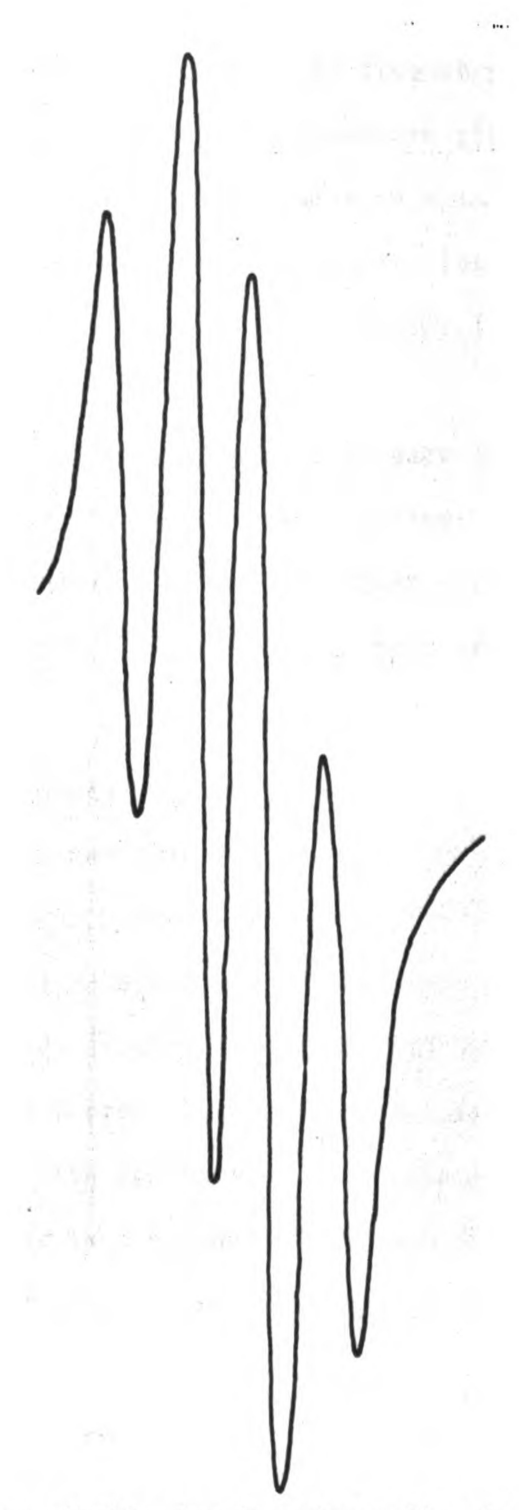


Figure 18. EPR Spectrum of Chlorine Superhyperfine Interaction in MoOC1SO4.

First derivative presentation on the  $m_{I} = 0$  absorption of molybdenum. Spectrum was recorded for MoOC1SO<sub>4</sub> in a HC1/H<sub>2</sub>SO<sub>4</sub> solution at 298°K. Note the dependence of the linewidths upon the chlorine nuclear spin quantum number.

respective paramagnetic complex compared to the frequency in the absence of the paramagnetic material. The results of this study are given in Table IX.

The nuclear spin-lattice  $T_{1N}$  and nuclear spin-spin  $T_{2N}$  relaxation times are given in Figure 19 as a function of paramagnetic ion concentration and radio-frequency field for solutions of the  $[MoOF_5]^2$ ,  $[MoOCl_5]^2$ , and  $[Mo(OCH_3)_2Cl_4]^2$  complexes respectively.

Varying the cation in the solids used to prepare solutions of the above anions had no effect upon the observed relaxation times. In the case of the  $[\text{MoOF}_5]^2$  and  $[\text{MoOCl}_5]^2$  complexes, relaxation times were also measured as a function of acid concentration. The results of these measurements are summarized in Figure 20.

#### VII. Electron Relaxation Results.

- A. Electron Relaxation Measurements by Pulse and Saturation Measurements.

  The results of these measurements are summarized in Table X.
- B. Electron Relaxation Measurements by Lineshape Analysis.

In most of the complexes studied the molybdenum hyperfine components are of Gaussian lineshape in the frozen glass and Lorentzian in solution. The former result is consistent with the fact that the linewidths in the solid state in most cases are determined by unresolved ligand superhyperfine interaction. The thermal modulation in solution is apparently sufficient to result in Lorentzian lineshapes.

The dominant relaxation mechanisms in the complexes possessing axial or lower symmetry appear to be the rotational modulation of an anisotropic hyperfine tensor and g-tensor as well as spin rotation. The equations of Kivelson et al. 15,16 predicted the experimental linewidths with the best accuracy for

TABLE IX. Contact Frequency Shifts for Some Mo(V) Complexes.

Complex	Nuclei	(A <sub>N</sub> /h)
[MoO(HC1) <sub>5</sub> ] <sup>5+</sup> or [MoOC1 <sub>5</sub> (H <sub>2</sub> O) <sub>2</sub> ] <sup>2-</sup>	1 <sub>H</sub>	3.5 x 10 <sup>5</sup> cps <sup>a</sup>
[MoO(DC1) <sub>5</sub> ] <sup>5+</sup> or [MoOC1 <sub>5</sub> (D <sub>2</sub> O) <sub>2</sub> ] <sup>2-</sup>	2 <sub>D</sub>	5.0 x 10 <sup>4</sup> cps <sup>a</sup>
[MoO(HF) <sub>5</sub> ] <sup>5+</sup> or [MoOF <sub>5</sub> (H <sub>2</sub> O) <sub>2</sub> ] <sup>2-</sup>	1 <sub>H</sub>	4.0 x 10 <sup>5</sup> cps <sup>a</sup>
[MoO(DF) <sub>5</sub> ] <sup>5+</sup> or [MoOF <sub>5</sub> (D <sub>2</sub> O) <sub>2</sub> ] <sup>2-</sup>	2 <sub>D</sub>	5.5 x 10 <sup>4</sup> cps <sup>a</sup>
[MoO(HF) <sub>5</sub> ] <sup>5+</sup> or [MoOF <sub>5</sub> (H <sub>2</sub> O) <sub>2</sub> ] <sup>2-</sup>	19 <sub>F</sub>	4.2 x 10 <sup>8</sup> cps <sup>b</sup>
[Mo(OCH <sub>3</sub> ) <sub>2</sub> C1 <sub>4</sub> ]	1 <sub>H</sub>	$(1/0 \times 10^4 \text{ cps})^{a,c}$

<sup>&</sup>lt;sup>a</sup>Calculated from the observed NMR contact shift and the formula:

$$\Delta v/v = -(A_N/h)(\gamma_e/\gamma_N)(g\beta S(S+1)/3kT)$$
,

where  $\Delta\nu$  is the NMR shift; (A<sub>N</sub>/h) is the electron-nuclear coupling constant;  $\nu$  is the resonant frequency (100 Mc); g is the Lande g factor;  $\beta$  is the Bohr magneton; S is the electron spin; and  $(\gamma_e/\gamma_N)$  is the ratio of the magnetogyric ratios for the electron and nucleus (see references 56 and 64).

<sup>&</sup>lt;sup>b</sup>Calculated from superhyperfine structure observed in the electron paramagnetic resonance spectra.

<sup>&</sup>lt;sup>C</sup>Assignment of shifted peak was  $\underline{\text{not}}$  confirmed by observing the NMR spectra of the complex in  $\text{CD}_{3}\text{OD}$ .

- Figure 19. The Nuclear Spin-Lattice  $\mathbf{T}_{1N}$  and Nuclear Spin-Spin  $\mathbf{T}_{2N}$  Relaxation Times as a Function of Paramagnetic Ion Concentration and Radiofrequency Field.
- (A)  $T_{1N}$  and  $T_{2N}$  as a function of paramagnetic ion concentration for solutions of  $[MoOF_5]^{2-}$ ,  $[MoOCl_5]^{2-}$ , and  $[Mo(OCH_3)_2Cl_4]^{-}$ . Circles indicate data for  $[Mo(OCH_3)_2Cl_4]^{-}$  in  $CH_3OH$  solution. Triangles indicate data for  $[MoOCl_5]^{2-}$  in concentrated HCl solution. Squares indicate data for  $[MoOF_5]^{2-}$  in concentrated HF solution.
- (B) Frequency dependence of the relaxation times  $T_{1H}$  and  $T_{2H}$  (indicated by circles) and  $T_{1D}$  and  $T_{2D}$  (indicated by triangles) for a solution of  $[MoOCl_5]^2$ -in a mixture of HCl and DCl.

ν<sub>I</sub> (x 10<sup>6</sup> cps)

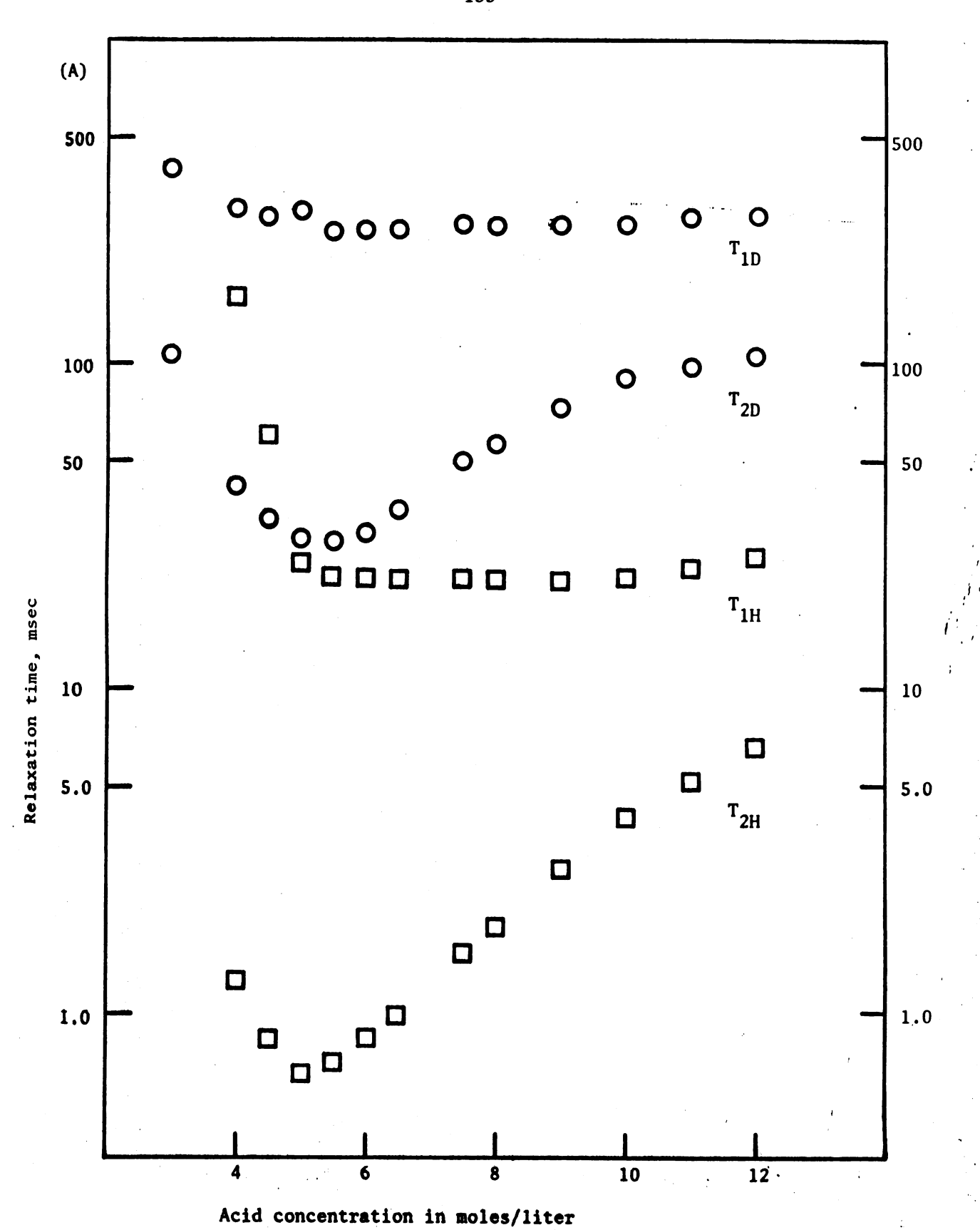
Figure 20. Electronic and Nuclear Relaxation Times as a Function of Acidity of the Solution for  $[MoOCl_5]^{2-}$  in a Mixture of HCl and DCl.

(A) Relaxation times of protons and deuterons as a function of acid concentration of the solution. The concentration of Mo(V) is 0.2M.

Circles indicate data for  $\mathbf{T}_{1D}$  and  $\mathbf{T}_{2D}.$ 

Squares indicate data for  $T_{1H}$  and  $T_{2H}$ .

(B)  $T_{2e}^{-1}$  and  $T_{2,ex,H}$  for a 0.2M  $[MoOCl_5]^{2-}$  solution as a function of HCl concentration.



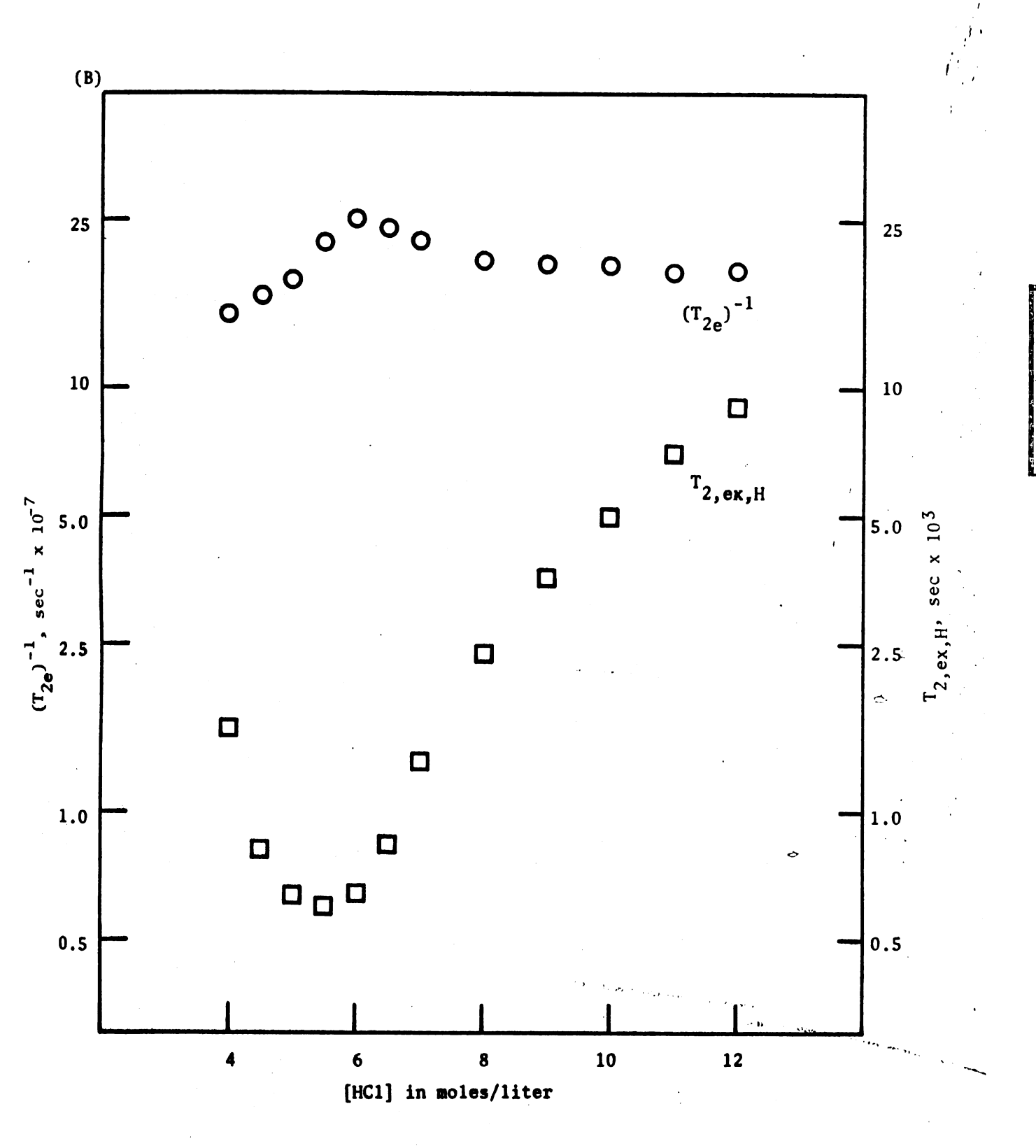


TABLE X. Electronic Relaxation Times.

Complex	Temp.	T <sub>2e</sub> (sec)	T <sub>le</sub> (sec)
MoOC1 <sub>3</sub>	77°K	$3.4 \times 10^{-6}$	$8.5 \times 10^{-6}$
[MoOC1 <sub>5</sub> ] <sup>2-</sup>	77°K	$1.6 \times 10^{-6}$	$1.5 \times 10^{-5}$
[MoOBr <sub>5</sub> ] <sup>2-</sup>	77°K	$1.0 \times 10^{-6}$	1.1 x 10 <sup>-6</sup>
	4.2°K	$1.5 \times 10^{-2}$	1.1 x 10 <sup>-6</sup>

the  $[MoO(HSO_4)_5]^{2-}$  and  $[Mo(OCH_3)_2Cl_4]^{-}$  complexes in noncoordinating solvents. Deviation in the other cases is probably due to unresolved ligand superhyperfine splitting.

For concentrations of paramagnetic ions above about  $5 \times 10^{-2} M$  the linewidths were broadened by electron exchange; this topic will be elaborated upon later.

#### VIII. ENDOR Measurements.

The results of the ENDOR measurements of  $[{\rm MoOF}_5]^{2-}$  are presented in Table VII.

#### CONCLUSIONS

- I. Halooxomolybdate(V) Complexes.
  - A. Ligand Superhyperfine Interaction.

The ligand superhyperfine interaction involving the equatorial halide ligands could arise from three sources. (1) It could result from Fermi contact interaction with paramagnetic electron density localized in a halide s orbital. This interaction would be isotropic and would be expected to account for the isotropic part of the halide superhyperfine interaction tensor. It should be noted that the hyperfine interaction of a paramagnetic electron in a halide s orbital is very large and hence only a small electron density in such an orbital can give rise to a finite splitting. (2) The superhyperfine interaction could arise from dipole-dipole interaction of the halide nuclei with paramagnetic electron density in a molybdenum orbital.

The electron-nuclear dipolar contribution is proportional to r<sup>-3</sup> where r is the distance separating the electron and nuclear dipoles. In the case of most molybdenum complexes r would be expected to be greater than 2.0 Å and hence it is doubtful that this type of electron-nuclear dipolar interaction could account for the observed superhyperfine interaction. (3) The ligand superhyperfine interaction could arise from electron-nuclear dipolar hyperfine interaction which is the result of a finite paramagnetic electron density in the p orbitals of the halide ligands. It is most reasonable that this type of dipolar interaction accounts for the anisotropic parts of the ligand superhyperfine interaction tensors. Assuming this to be true, the anisotropic part of the superhyperfine interaction tensor may be expressed as

$$A_{p} = (2/5) g_{\perp} \beta g_{N} \beta_{N} \langle r^{-3} \rangle |\rho_{p}|.$$

The spin density in the halide p orbitals was calculated by using this equation.

The results are presented in Table XI.

Next the implications of the spin densities calculated in Table XI in terms of molybdenum-ligand bonding will be considered. Spin density in the ligand  $p_x$  orbital can most logically arise from in-plane  $\pi$  bonding involving the molybdenum  $b_2(\text{primarily } d_{xy})$  and ligand  $b_2(\text{primarily } p_y)$  orbitals. Since the paramagnetic electron is assumed to be localized primarily in the ground state  $b_2(d_{xy})$  orbital it is reasonable that a fairly large paramagnetic density would be expected to reach the ligand  $b_2(p_y)$  orbital.

The explanation of spin density in the ligand  $p_x$  orbital cannot be rationalized in terms of bonding involving the  $b_2$  orbitals. The ground state  $b_2$  orbital is of the wrong symmetry to overlap appreciably with the ligand  $p_x$  orbitals. Therefore configurational interaction involving an excited molybdenum  $b_1(d_x^2-y^2)$  orbital must be considered. Bonding for such a case would be  $\sigma$  rather than  $\pi$ . It is logical to expect that this type of bonding would be considerably less effective than in-plane  $\pi$  bonding involving the metal and ligand  $b_2$  orbitals and would be less effective for the chloride and bromide ligands than for the fluoride ligands.

The results in Table XI appear to be consistent with this analysis. Metal-ligand overlap integrals of 0.01 to 0.10 could easily account for the observed distribution of electron density. Such overlap integrals are certainly reasonable from the quantum mechanical standpoint by analogy with rigorous Hartree-Fock calculations carried out for other complexes.

TABLE XI. Spin Densities in Ligand Orbitals.

Sample	Ligand		$ \rho_{\mathbf{p_y}} _{\mathbf{L}}$	$ a_{\mathbf{p}_{\mathbf{x}}} _{\mathbf{L}}$
[Mooc1 <sub>5</sub> ] <sup>2-</sup>	<sup>35</sup> C1, <sup>37</sup> C1	0.001	0.059	000.0
$[Mo(OCH_3)_2C1_4]^-$	35 <sub>C1,</sub> 37 <sub>C1</sub>	0.001	0.059	000.0
Mo0C1SO <sub>4</sub>	<sup>35</sup> C1, <sup>37</sup> C1	900.0		
[MoOBr <sub>5</sub> ] <sup>2-</sup>	79Br, 81Br		0.049	000.0
[MoOF <sub>5</sub> ] <sup>2-</sup>	$^{19}_{ m F}$	600.0	0.042	0.013
[Mo0(NCS) <sub>5</sub> ] <sup>2-</sup>	14 <sub>N</sub>	0.046		
$[Mo(OCH_3)_2(NCS)_4]^-$	14 <sub>N</sub>	0.047		
$[MoCl_3(NCS)_3]^-$	14 <sub>N</sub>	0.047		
$[Mo(C1)_{5}SPS(OC_{2}H_{5})_{2}]^{-}$	$^{31}\mathrm{p}$	0.133	0.003	0.003
	<sup>35</sup> C1, <sup>37</sup> C1	0.006	0.076	0.000
$[Mo(HSO_4)_5 SPS(OC_2H_5)_2]^-$	$^{31}\mathrm{p}$	0.133	0.003	0.003

TABLE XI, continued.

Sample	Ligand	$\frac{1}{s}\sigma$	$  \mathbf{a}_{\mathbf{b}_{\mathbf{A}}}  _{\mathbf{L}}$	$ \mathbf{b}_{\mathbf{b}_{\mathbf{c}}} ^{\Gamma}$
$[Mo(OC_2H_5)_5SPS(OC_2H_5)_2]^-$	$^{31} m_p$	0.133	0.003	0.003
[Mo[(Bu0) <sub>3</sub> P0] <sub>2</sub> C1 <sub>4</sub> ] <sup>+</sup>	35 <sub>C1</sub> , 37 <sub>C1</sub>	0.002		

of  $\operatorname{cr}_{-5}^{-3}$  tabulated by Barnes and Smith [R. G. Barnes and W. V. Smith, Phys. Rev., 93, 95 (1954).] The above values of  $|
ho_{
m p}|_{
m L}$  were calculated by using the measured values of A and the values and by Bersohn and Shulman [R. Bersohn and R. G. Shulman, J. Chem. Phys., 45, 2298 (1966).].

Rowlands, and D. H. Whiffen, Mol. Phys., 5, 233 (1962).]; by Clementi, et al. [E. Clementi, C. C. J. Rowlands, and D. H. Whiffen, Proc. Chem. Soc., 1962, 252]; and by Freeman and Watson [A. J. Freeman The above values of  $|\rho_{\rm S}|_{\rm L}$  were calculated by using the observed values of A<sub>S</sub> and the atomic Roothaan, and M. Yoshimine, Phys. Rev., 127, 1618 (1962).]; by Cook, et al. [R. J. Cook, J. R. values of  $\psi_{ns}^2(0)$  tabulated by Chantry, et al. [G. W. Chantry, A. Horsfield, J. R. Morton, J. R. and R. E. Watson, Phys. Rev., 123, 521 (1961).]. B. Discussion of the Complex Superhyperfine Structure Observed in Frozen Glasses.

Measurement of the spectra of single crystals and of polydrystalline powders has greatly facilitated the interpretation of the frozen glass spectra of  $[MoOBr_5]^{2-}$ . A discussion of the more complex frozen glass spectra of  $[MoOF_5]^{2-}$  follows.

Upon close examination it may be noted that the major peaks of the frozen glass spectra (indicated by arrows in Figure 3) are separated by 50 to 55 gauss. Neither the molybdenum perpendicular hyperfine lines nor the  $A_y(L)$  components of the fluorine superhyperfine interaction have the correct intensity ratio to account separately for the observed structure. The studies on crystals and polycrystalline samples of  $K_2[MoOF_5]$  indicate that  $A_{\perp}(^{95}Mo,^{97}Mo)$  and  $A_y(^{19}F)$  are of the same order of magnitude. Hence the overlap of fluorine superhyperfine components from the central molybdenum line and from the molybdenum perpendicular hyperfine components may account for the unusual intensity ratios observed.

II. Mo(V) Complexes with Ligands Containing Phosphorus.

Phosphorus superhyperfine interaction will be discussed first. The spin densities in the s and p orbitals of phosphorus are given in Table XI. The large paramagnetic densities in the phosphorus s orbital indicate that the bonding of the DDPA ligand to molybdenum is through phosphorus, although the possibility of Mo-S=PC bonding cannot definitely be ruled out. The isotropic nature of the superhyperfine interaction also indicated that the bonding is through phosphorus, which implies that the bonding is  $\sigma$  in nature. Since the ground state  $b_2(d_{\chi y})$  orbital of molybdenum has the wrong symmetry for this

type of bonding, configurational interaction involving promotion of an electron to the first excited  $a_1$  orbital must be invoked.

The small electron density in the phosphorus p orbitals also requires configurational interaction for its explanation. In this case metal and ligand e orbitals are involved.

The strong, anisotropic chlorine superhyperfine interaction observed in the  $[\text{MoCl}_5\text{SPS}(\text{OC}_2\text{H}_5)_2]^-$  complex indicates very strong in-plane  $\pi$  bonding involving the molybdenum  $b_2(d_{xy})$  orbital. The greater strength of this interaction in phosphate complexes than in oxopentachloromolybdate complexes probably arises from the reduction of the amount of in-plane  $\pi$  bonding to the equatorial ligands by the strongly covalent molybdenum-oxygen bond.

As is evident from an inspection of Table VI, the Zeeman and hyperfine tensors indicate that the complexes studied fall into two categories. The large differences in the magnitudes of g and A tensors for the complexes of Mo(V) with DDPA as compared to the magnitudes of g and A tensors for the complexes with other phosphorus-containing ligands are interpreted as further indication that a molybdenum-phosphorus bond lies along the highest axis of symmetry in the complex containing DDPA while in the other complexes, a molybdenum-oxygen bond lies along the highest axis of symmetry. It is to be remembered that in terms of molecular orbital theory, g values approaching the free electron value of 2.0023 and increasing metal hyperfine coupling constants indicate increasing covalency in metal-ligand bonding. Since the Zeeman and metal hyperfine interaction tensors have been observed in this investigation to be determined primarily by the nature of the equatorial ligand, the replacement of the stronger molybdenum-oxygen bond by the molybdenum-phosphorus  $\sigma$  bond has been interpreted to result in more effective in-plane  $\pi$  bonding of

molybdenum to the equatorial ligands. This conclusion drawn from a consideration of Zeeman and hyperfine interaction tensors is in agreement with the observation of increased chlorine superhyperfine interaction in the complex containing DDPA.

## III. Mo(V) Complexes with Ligands Containing Nitrogen.

The observed nitrogen splittings in the thiocyanate complexes of Mo(V) would tend to indicate that the bonding involves a Mo-N bond rather than a Mo-S bond. It may be argued that sufficient electron density could carry through the SCN system to the nitrogen as a result of the strongly covalent nature of all the bonds involved in this ligand (i.e., the multi-centered nature of the molecular orbitals). However it is doubtful that this amount of electron density could travel through three bonds, even though they are strongly covalent. It may be noted that  $^{13}\mathrm{C}$  enrichment would be one clear-cut means of resolving this problem, since, if -SCN bonding is involved, an appreciable electron density at the  $^{13}\mathrm{C}$  nuclei would be expected. An attempt was made to observe such interaction by examining the spectra at high gain. No  $^{13}\mathrm{C}$  lines were detected. However, until the resolution of this problem is accomplished, no detailed interpretation of the bonding can be made other than to note that in-plane  $\pi$  bonding involving the  $b_2(d_{xy})$  orbital of molybdenum is probably involved.

# IV. Mo(V) Complexes with Ligands Containing Sulfur.

The anisotropic nature of the chlorine superhyperfine interaction (as indicated by the strong  $m_{\tilde{I}}$  dependence of the linewidths in the EPR spectrum of MoOClSO<sub>4</sub>) indicated that strong in-plane  $\pi$  bonding involving the b<sub>2</sub> orbital of molybdenum is probably present, although the location of the chlorine in the coordination sphere remains uncertain.

#### V. Zeeman and Metal Hyperfine Interactions.

As can be seen from consideration of Table VI, the large variation in the values of the Zeeman and metal hyperfine interaction tensors with changes in equatorial halide ligand do not apparently arise from changes in metal--ligand bonding. Therefore, the conclusion may be drawn that the variations most reasonably arise from changes in the exchange polarization of the ground state d,, and inner s orbitals of molybdenum. The theory of exchange polarization applicable to molybdenum d<sup>1</sup> complexes has recently been extensively reviewed. 3,100,101,103 The exchange polarization parameters have been calculated by using the methods of both McGarvey and Low. 101 The results of this calculation are tabulated in Table XII. The results imply that the most recent spin-polarized Hartree-Fock calculations of Freeman, et al. 100 give rather good agreement with experiment. In particular, the results of this investigation indicate that the calculated value for the core polarization is only about 10% to 20% smaller than the value (approximately -400 to -500 kG) which was estimated from experimental data. When the limitations of the calculations are taken into account, such agreement is rather encouraging.

### VI. Analysis of the Electron Paramagnetic Resonance Linewidth.

The analysis of the EPR linewidths leaves little doubt that the anisotropic and spin-rotational mechanisms of Kivelson  $^{15,16}$  are the dominant relaxation mechanisms in Mo(V) complexes in dilute solutions in non-coordinating solvents (acetone, DMF, chloroform, carbon tetrachloride, benzene, acetonitrile, etc.). Other important mechanisms include electron exchange in solutions in which the concentrations of the paramagnetic species exceeded 5 x  $10^{-2}$ M and ligand exchange in certain solvents which engage in rapid exchange with the ligands (methanol, ethanol, hydrochloric acid, hydrobromic acid, etc.).

Exchange Polarization and Distortion Expressions for Molybdates TABLE XII.

TABLE XII. Exchange Polarization and Distortion Expressions for Molybdates.	ation and Di	istortion Exp	ressions fo	r Molybdates.	
Complex	- Ka	-X (au)	- pa	B 2	q <sub>L</sub>
$(NH_4)_2[MoOC1_5]$ in $(NH_4)_2[InC1_5 H_2^0]$	43.6	5.58	48.0	0.873	75.55
$K_2[MoOF_5]$ in diamagnetic host crystals	0.09	7.67	53.9	0.980	-20.42
MoOC1 <sub>3</sub>	53.7	6.87	33.0	009.0	38.30
[MOOF <sub>5</sub> ] <sup>2-</sup>	56.8	7.27	58.9	1.071	-40.16
$[MOOBr_5]^{2-}$	41.0	5.24	48.9	068.0	12.74
[MoOC1 <sub>5</sub> ] <sup>2-</sup>	44.0	5.62	48.4	0.881	48.33
[MOO(NCS) <sub>5</sub> ] <sup>2-</sup>	41.4	5.29	37.7	0.685	84.38
$C_5H_6N[Mo(OCH_3)_2C1_4]$ in $NH_4SCN/CH_3OH$	41.4	5.29	37.7	0.685	84.38
MoOC1SO <sub>4</sub>	45.1	5.77	41.5	0.755	-117.6
$Mo_2O_3(SO_4)_2$	51.4	6.58	38.4	669.0	-217.7
C <sub>S</sub> H <sub>6</sub> N[Mo(OCH <sub>3</sub> ) <sub>2</sub> C1 <sub>4</sub> ] in H <sub>3</sub> PO <sub>4</sub>	50.4	6.45	61.8	1.123	-47.08

TABLE XII, continued.

-pa
-x (an)
-Ka
Complex

8.068

م. ا

$$^{a}_{\rm In\ units\ of\ cm^{-1}\ x\ 10^{-4}}$$

<sup>b</sup>Crystal field symmetry parameter, defined as

$$\Gamma = \{ [(A - \langle a \rangle)/\langle a \rangle] - [(\langle a \rangle - B)/\langle a \rangle] \} / \{ [(g_{||} - \langle g \rangle)/\langle g \rangle] - [(\langle g \rangle - g_{||})/\langle g \rangle] \}$$

in J. W. Culvahouse, W. P. Unruh, and D. K. Brice, Phys. Rev., 129, 2430 (1963).

TABLE XII, continued.

Complex	e n	۹ <sub>٦</sub>	(8 <sup>2</sup> ) <sup>c</sup>	(8 <sup>2</sup> ) <sup>d</sup>
Mo(V) in K <sub>2</sub> SnC1 <sub>6</sub>	0.0735	0.0315	0.8579	0.9405
$(NH_4)_2[MoOCl_5]$ in $(NH_4)_2[InCl_5]$ H <sub>2</sub> 0]	0.0863	0.0308	0.7805	0.8859
$K_2[MoOF_5]$ in diamagnetic host crystals	0.1563	0.0415	0.7873	0.9971
Mo0C1 <sub>3</sub>	0.1089	0.0308	1.4015	1.5883
[MoOF <sub>5</sub> ] <sup>2-</sup>	0.1563	0.0415	0.7916	1.0017
$[MoOBr_5]^{2-}$		0.0011		0.9975
[MoOC1 <sub>5</sub> ] <sup>2-</sup>	0.0784	0.0327	0.8039	0.8915
[MoO(NCS) <sub>5</sub> ] <sup>2-</sup>	0.1157	0.0288	0.8734	1.0428
$C_5H_6N[Mo(0CH_3)_2C1_4]$ in $NH_4SCN/CH_3OH$	0.1157	0.0288	0.8734	1.0428
MoOC1SO <sub>4</sub>	0.1198	0.0308	0.8082	0.9768
$Mo_2O_3(SO_4)_2$	0.1252	0.0366	1.0632	1.2468

TABLE XII, continued.

Complex	e n	م ا	$(8^2)^{c}$	$(\beta^2)^{d}$	
$C_{S}H_{6}N[Mo(OCH_{3})_{2}C1_{4}]$ in $H_{3}PO_{4}$	0.1443	0.0332	0.5581	0.7476	
$C_{S}H_{6}N[Mo(0CH_{3})_{2}C1_{4}]$ in $H_{2}S0_{4}$	0.0443	0.0269	4.5316	4.6337	
Complex	-pf	- p8	ud-	-p <sup>i</sup>	-Pj
		Cm	$cm^{-1} \times 10^{-4}$		
$Mo(V)$ in $K_2SnC1_6^e$	51.41	49.79	51.41	49.79	67.78
$(NH_4)_2[MoOC1_5]$ in $(NH_4)_2[InC1_5 \cdot H_20]$	52.47	50.36	52.47	50.36	67.78
${\rm K_2[MoOF_5]}$ in diamagnetic host crystals	67.19	62.26	67.19	62.26	67.78
MoOC1 <sub>3</sub>	37.12	34.84	37.12	34.84	67.78
[MOOF <sub>5</sub> ] <sup>2-</sup>	66.94	62.02	66.94	62.02	67.78
$[MOOBr_5]^{2-}$		42.04		42.04	67.78
[MoOC1 <sub>5</sub> ] <sup>2-</sup>	52.07	50.32	52.07	50.32	67.78

TABLE XII, continued.

Complex	-pf	-pg	-ph	-pi	-pj
		_ wo	cm <sup>-1</sup> x 10 <sup>-4</sup>		
[Mo0(NCS) <sub>5</sub> ] <sup>2-</sup>	44.54	41.81	44.54	41.81	67.78
$C_5H_6^N[Mo(OCH_3)_2C1_4]$ in $NH_4SCN/CH_3OH$	44.54	41.81	44.54	41.81	67.78
MoOC1SO <sub>4</sub>	49.08	46.06	49.08	46.06	67.78
$Mo_2O_3(SO_4)_2$	46.25	43.29	46.25	43.29	67.78
C <sub>5</sub> H <sub>6</sub> N[Mo(OCH <sub>3</sub> ) <sub>2</sub> C1 <sub>4</sub> ] in H <sub>3</sub> P0 <sub>4</sub>	74.10	69.03	74.10	69.03	67.78
C <sub>5</sub> H <sub>6</sub> N[Mo(OCH <sub>3</sub> ) <sub>2</sub> C1 <sub>4</sub> ] in H <sub>2</sub> SO <sub>4</sub>	8.406	8.252	8.406	8.252	67.78

aCalculated from Eq. (1), given below.

bCalculated from Eq. (2).

Calculated from Eqs. (1) and (3).

dCalculated from Eqs. (2) and (4).

eData from W. Low, Physics Letters, 24A, 46 (1967).

fcalculated from Eqs. (1), (3), and (4).

(5)

(3)

TABLE XII, continued.

 $g_{\text{Calculated from Eqs. (2), (3), and (4)}$ .

 $^{\rm h}$ Calculated from Eqs. (1), (3), and (5).

icalculated from Eqs. (2), (3), and (5).

JCalculated from Eq. (6).

 $\Xi$  $g_{\parallel\parallel}$  = 2.0023 - (21/4)u<sup>2</sup> + higher order terms connecting the  $\Gamma_{3}$  to the  $\Gamma_{5}$  terms

 $B^{2} = A(\frac{2}{7} - \frac{11u}{7} + \frac{15u^{2}}{28}) - B(-\frac{4}{7} - \frac{6u}{7} - \frac{15u^{2}}{14}) + \cdots$   $A(1 - \frac{7u^{2}}{8}) + B(1 - \frac{7u^{2}}{4}) + \cdots$  $g_1 = 2.0023 - 2u - (3/4)u^2 + \dots$ 

 $A = P[-(4/7) - (6/7)u - (15/14)u^{2} - \beta^{2}\{1 - (7/4)u^{2}\} . . .]$ 

4

(2)

9

(2)

 $B = P[(2/7) - (11/7)u + (15/28)u^2 - \beta^2 \{1 - (7/8)u^2\} ...]$ 

 $P = 2.0023 \gamma_N \beta_{\theta} \beta_N \langle r^{-3} \rangle$ 

 $n = \lambda/\delta$ 

where

6 = tetragonal field splitting parameter

 $\lambda$  = spin orbit coupling constant

 $\beta^2$  = a measure of unpaired spin density

As has been pointed out by Fraenkel,  $^{104,105}$  when both hyperfine and superhyperfine structure are determined by anisotropic tumbling, one may use an analysis of the nuclear spin dependence of the linewidths to determine the sign of the hyperfine and superhyperfine coupling constants. Such was the case for  $[\text{MoOF}_5]^{2-}$ ,  $[\text{MoO(NCS)}_5]^{2-}$ ,  $[\text{Mo(OCH}_3)_2(\text{NCS)}_4]^{-}$ , and  $[\text{MoOClSO}_4]^{2-}$  complexes and the signs of the fluorine, chlorine, nitrogen, and molybdenum hyperfine interactions were determined.

The sign of the isotropic and anisotropic parts of the molybdenum hyperfine interaction were found to be positive. The isotropic and anisotropic parts of the ligand superhyperfine interactions for the ligands giving the superhyperfine structure were found to be opposite in sign with the isotropic parts positive and anisotropic parts negative.

The analysis of electron paramagnetic resonance linewidths has demonstrated that the search for ligand hyperfine interaction can be conducted systematically by following a few simple rules. The key to the resolution of ligand hyperfine interaction lies in obtaining sufficiently narrow EPR linewidths, <u>i.e.</u>, sufficiently long electronic relaxation times. Since chemical exchange broadens lines, measurements should be made in non-coordinating solvents.

Concentration of the paramagnetic ion should be kept sufficiently low that the lines are not broadened by electron-electron dipolar interaction or spin exchange but sufficiently high so that large modulational amplitudes and excessive microwave power are not required to obtain detectable signals, conditions usually met for about 0.01M paramagnetic ion.

Since the anisotropic and spin rotational mechanisms have different dependences upon temperature and viscosity, one should perform a careful temperature study. These machanisms result in the linewidth reaching a

minimum value over a very small temperature range (10° to 30°). Correspondingly, in this investigation detection of ligand hyperfine interaction in solution over only a small range of temperatures was achieved.

In single crystals linewidths are theoretically expected to decrease with decreasing temperature so that a general rule is the lower the temperature, the better the resolution of ligand superhyperfine lines.

VI. Analysis of Electron Spin-Lattice Relaxation Results.

Since, in all mechanisms proposed to date, the electron spin-lattice relaxation times depend upon the magnitude of the splitting of the  $b_2(d_{xy})$  and  $e(d_{xz}, d_{yz})$  energy levels, it may be concluded that the long relaxation times observed indicate a rather large magnitude for this splitting. The long times indicate that there are no low-lying electronic, rotational, or vibrational excited states strongly coupled to the ground state.

Sufficient information is not available at this time to determine the cause of the anisotropy of the observed relaxation times.

VII. Analysis of the Nuclear Relaxation Results.

A. 
$$[MoOC1_5]^2$$

# Concentration of Paramagnetic Ions less than 0.01M.

For this case, the nuclear spin-lattice relaxation times for both hydrogen isotopes are inversely proportional to the concentration of Mo(V) with the quantities  $N_S^T_{1H}$  and  $N_S^T_{1D}$  having the values 5.2 x  $10^{-3}$  msec and  $10^{-1}$  msec, respectively in a field of 6730 gauss. The nuclear spin-spin relaxation times measured by the wide line NMR technique were also inversely proportional to Mo(V) concentration. However, the nuclear spin-spin

relaxation times measured by the normal  $90^{\circ}-180^{\circ}-90^{\circ}$  spin echo pulse technique did not obey this relationship. This discrepancy arises as a result of molecular diffusion in the nuclear spin echo technique. Molecular diffusion as well as relaxation processes can cause the precessing spins to lose transverse phase memory; hence, if accurate measurements of  $T_{2N}$  are to be made by transient pulse techniques, the problem of molecular diffusion must be overcome. When this was done by use of the "picket" technique, 98 good agreement between nuclear spin echo and wide line NMR results were obtained.

The observation that the relationships  $N_S^T_{1N}$ ,  $N_S^T_{2N}$  equal constant values for any given complex indicates that electron-electron spin exchange is negligible in solutions less than 0.01M in paramagnetic Mo(V). Thus the general equations derived in the Theoretical section reduce to

$$T_{1}^{-1} = (4/30)S(S+1)\gamma_{I}^{2}g^{2}\beta^{2}p(\mathbf{r}^{-6})[3\tau_{c} + 7\tau_{c}/(1 + \omega_{s}^{2}\tau_{c}^{2})]$$

$$+ (2/3)S(S+1)A^{2}p(\tilde{h}^{-2})[\tau_{e}/(1 + \omega_{s}^{2}\tau_{e}^{2})]$$
(41)

$$T_{2}^{-1} = (4/60)S(S+1)\gamma_{I}^{2}g^{2}\beta^{2}p(r^{-6})[7\tau_{c} + 13\tau_{c}/(1 + \omega_{s}^{2}\tau_{c}^{2})]$$

$$+ (1/3)S(S+1)A^{2}p(\tilde{h}^{-2})[\tau_{e} + \tau_{e}/(1 + \omega_{s}^{2}\tau_{e}^{2})]$$
(42)

where  $\tau_c$  is the correlation time for the dipolar interaction and  $\tau_e$  is the correlation time for the exchange interaction. It is to be noted that

$$1/\tau_{c} = 1/\tau_{r} + 1/\tau_{s}$$
 (43)

and

$$1/\tau_{e} = 1/\tau_{h} + 1/\tau_{s} \tag{44}$$

where  $\tau_r$  is the correlation time for the "tumbling" of the paramagnetic complex and is the same  $\tau_r$  used in the anisotropic and spin rotational mechanisms of Kivelson, 15,16  $\tau_s$  is the electron relaxation time ( $\tau_s = T_{2e} = T_{1e}$  in solution),

and  $\boldsymbol{\tau}_h$  is the lifetime of the resonant nuclei in the complex. Note that  $\boldsymbol{p}$  is given by

$$p = N_{\varsigma} \cdot n/m$$

where  $N_S$  is the concentration of paramagnetic ions, m is the concentration of resonant nuclei in the solution and n is the number of sites occupied by the resonant nuclei in the paramagnetic complex. The other symbols are defined by Gutowsky, et al. 58

To interpret the data, one must decide whether the measured times are determined by magnetic interaction or by the lifetime of the hydrogen and deuterium nuclei in the first coordination shpere of the paramagnetic complex. In other words, one must determine which of the three correlation times  $\tau_{\mathbf{r}}$ ,  $\tau_{\mathbf{s}}$ , or  $\tau_{\mathbf{h}}$  is the shortest. This problem can be resolved by a comparative study of the relaxation of both isotopes of hydrogen. The ratios of the magnetic relaxation times of protons and deuterons in [MoOCl<sub>5</sub>]<sup>2-</sup> solutions were

$$N_S T_{1D} / N_S T_{1H} = 38.5$$
 and  $N_S T_{2D} / N_S T_{2H} = 39$ .

These values correspond, within experimental error, to the theoretical  $\gamma_H^2/\gamma_D^2$  = 42.5 and imply that the nuclear relaxation is determined by the modulation of electron-nuclear dipolar interaction.

If the relaxation times are expressed as

$$(T_{N1,2})^{-1} = (T_{N1,2})_a^{-1} + p\{(T_{N1,2})_b + \tau_h\}^{-1}$$

where  $(T_{N1,2})_b$  and  $(T_{N1,2})_a$  are the relaxation times of the resonant nuclei in the first coordination shell of the paramagnetic ion and outside this shell respectively, the ratio of spin-lattice to spin-spin relaxation times indicating that  $(T_{N1,2})_b >> \tau_h$  and the upper limit for  $\tau_h$  is less than 1.3 x  $10^{-4}$  sec.

The nearness of the ratios of  $N_S^T_{1D}/N_S^T_{1H}$  and  $N_S^T_{2D}/N_S^T_{2H}$  to 42.5 indicates that the relaxation times given in Figure 20 are represented by the equations

$$(T_1^{-1}) = (4/30)S(S+1)\gamma_1^2 g^2 \beta^2 p(r^{-6}) \tau_c [3 + 7(1 + \omega_S^2 \tau_c^2)^{-1}]$$
 (45)

and

$$(T_2^{-1}) = (4/60)S(S+1)\gamma_I^2 g^2 \beta^2 p(r^{-6}) \tau_c [7 + 13(1 + \omega_s^2 \tau_c^2)^{-1}]$$

$$+ (1/3)S(S+1)pA^2 (\hbar^{-2}) \tau_e [1 + (1 + \omega_s^2 \tau_e^2)^{-1}]$$
(46)

and that the first term in the expression for  $(T_2^{-1})$  dominates.

Next, the correlation time  $\tau_c$  is found by comparing the relaxation rates of either protons or deuterons at several frequencies. For example, if the proton relaxation times are examined at frequencies of 4.4 and 28.7 Mc, the roots of the resultant quadratic equation give  $\tau_{c1} = 6.8 \times 10^{-11}$  sec and  $\tau_{c2} = 1.2 \times 10^{-11}$  sec at 300°K. The choice between these values can be made by measuring  $T_{1H}$  or  $T_{2H}$  for some third value of the field  $H_0$  (or radiofrequency field frequency). Results indicate that  $\tau_c = 1.2 \times 10^{-11}$  sec is the correct value. In addition, on heating a solution,  $T_{1H}$  becomes longer, the rate of the rise depending upon whether or not  $\omega_{s}\tau_{c}$  is comparable to unity. Experiments which compared the influence of heating on  $T_{1H}$  for the two frequencies 4.4 and 28.7 Mc/sec showed that, of the two values found for the correlation time, the relevant one is  $\tau_{c} = 1.2 \times 10^{-11}$  sec.

It is interesting to compare this value of  $\tau_c$ ' with the value of  $\tau_c$  calculated from electron spin relaxation studies (see Table XIII). Similar comparisons have been made by Lewis, et al.  $^{106}$  who have also found good agreement between correlation times calculated by electron and nuclear resonance methods.

TABLE XIII. Values of  $\boldsymbol{\tau}_{\boldsymbol{C}}$  Calculated from Electron and Nuclear Relaxation Studies.

Complex	Temp.	τ <mark>c</mark>	$\frac{\tau_c}{c}$
[MoOC1 <sub>5</sub> ] <sup>2-</sup>	300°K	$2.0 \times 10^{-11}$	1.2 x 10 <sup>-11</sup>
[Mo(OCH <sub>3</sub> ) <sub>2</sub> C1 <sub>4</sub> ]	300°K	5.0 x 10 <sup>-11</sup>	5.0 x 10 <sup>-11</sup>
[MoOF <sub>5</sub> ] <sup>2-</sup>	273°K	$2.0 \times 10^{-9}$	$1.8 \times 10^{-9}$

Units of  $\tau_c$  are sec.

 $<sup>^{\</sup>rm a}$ Calculated from nuclear relaxation results.

<sup>&</sup>lt;sup>b</sup>Calculated from electronic relaxation results.

By setting  $\tau_c = 1.2 \times 10^{-11}$  sec and  $r = 2.7 \text{ Å}^{48,60,61}$  in the above equations, it is found that p = 0.045; <u>i.e.</u>, n, the number of protons or deuterons in the innermost shell of the paramagnetic complex is 4.3, or to within experimental error, 4. This means that in approximately 12N HCl the paramagnetic molybdenum species is either  $[\text{MoOCl}_5(\text{H}_2\text{O})_2]^{2-}$  or  $[\text{MoO(HCl)}_5]^{5+}$ . This latter species may be visualized as follows,

It is impossible to differentiate conclusively between these two possibilities at this time. The best method of testing the possibilities would be to use  $H_2^{17}0$  or  $D_2^{17}0$  instead of water containing a natural abundance of  $^{16}0$ . Several such studies of this type have been performed on solutions of Mn<sup>2+</sup> and Cu<sup>2+</sup> complexes.  $^{62,107}$ 

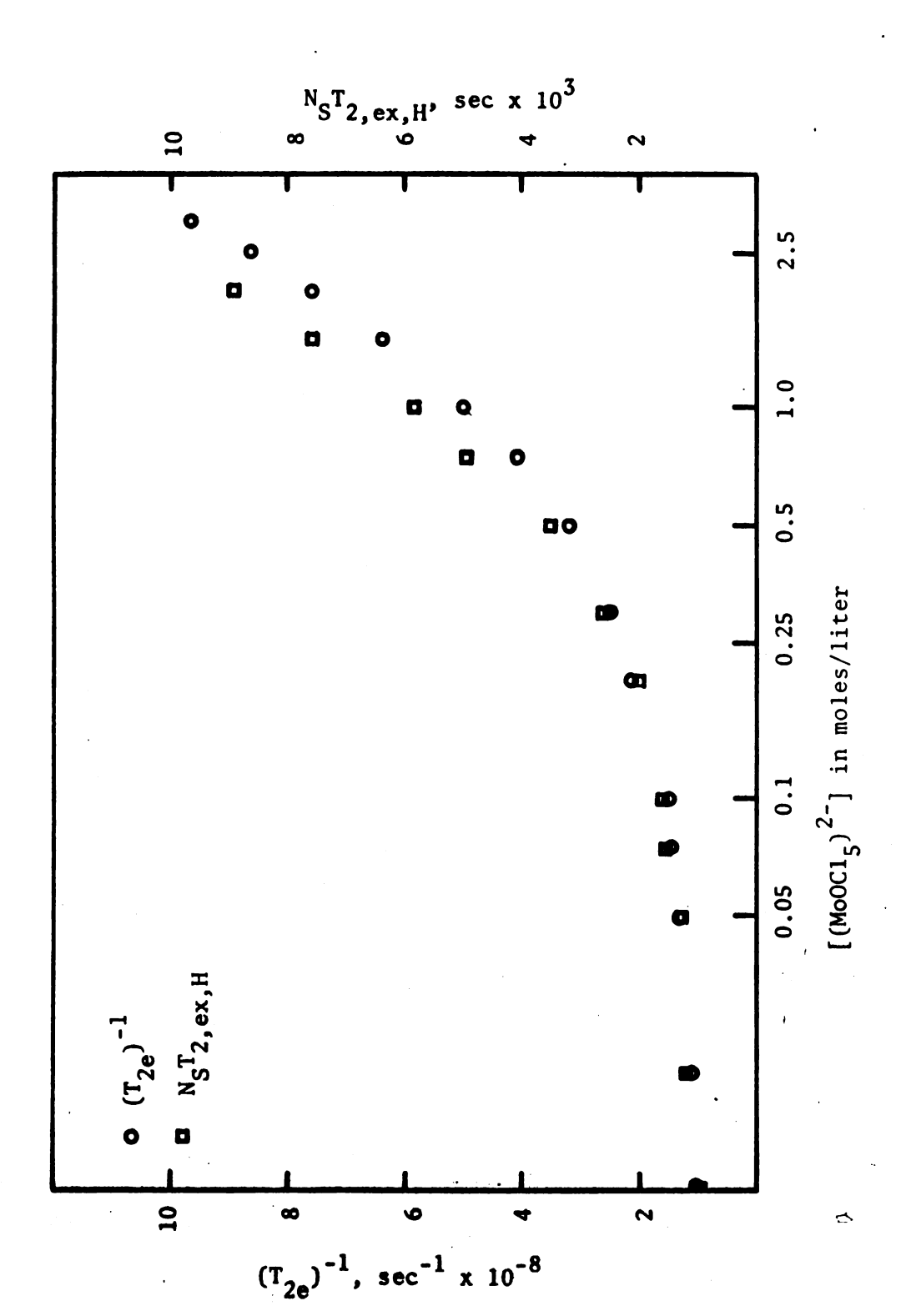
# Concentration of Paramagnetic Ions Greater than 0.01M.

Figure 21 is a plot of  $N_ST_{ex,H}$ , the exchange contribution to the transverse relaxation, and the electron spin-spin relaxation time, in acidified aqueous solutions (about 12M) versus the Mo(V) concentration. The exchange contribution was calculated from the rigorous expression given in the Theoretical section and the expressions (41) and (42) and also from the values of  $T_{1H}$  and  $T_{2H}$  at 28.7 Mc/sec. As the solution is diluted  $T_{2e}^{-1}$  decreases and reaches a limit of 1 x 10<sup>8</sup> sec<sup>-1</sup>. The value of  $N_ST_{2,ex,H}$  also decreases with increasing dilution, and causes  $N_ST_{2N}$  to be non-constant. The similar behavior of  $N_ST_{2,ex,H}$  and  $T_{2e}$  leaves no doubt that the electron relaxation time,  $\tau_s$ , appears as the correlation

Figure 21. Electron Spin-Spin Relaxation Time,  $T_{2e}$ , and Exchange Contribution to the Transverse Proton Relaxation  $N_ST_{2,ex,H}$  as a Function of the Mo(V) Concentration.

Circles indicate  $T_{2e}^{-1}$ .

Squares indicate  $N_S^T_{2,ex,H}$ .



time for exchange interaction between ions and hydrogen nuclei in acid solution. Assuming that the EPR lines are of Lorentzian form, the limiting value was found to be  $\tau_s = T_{2e} = 10^{-8}$  sec. Next the exchange interaction constants for protons and deuterons are calculated to be 3.5 x  $10^5$  cps and 5.0 x  $10^4$  cps respectively. This is in excellent agreement with the measured NMR shifts (see Table IX). Upon comparing  $A_H$  with  $A_D$  it is found that the density of unpaired electrons of the MoO $^{3+}$  ion for protons  $|\psi(0)|_H^2$  is somewhat higher than for deuterons:  $|\psi(0)|_H^2 \approx 1.06 |\psi(0)|_D^2$ .

Since  $\tau_e = \tau_s$ , the lower limit of the residence time of a hydrogen nucleus in the paramagnetic complex is  $10^{-8}$  sec.

## Relaxation Times as a Function of Acid Concentration.

It is well-known that the paramagnetism of Mo(V) ions in aqueous solution depends upon the acid concentration.  $^{2,4,5,6,7,23}$  It is interesting to observe how the pH affects the relaxation rates of protons and deuterons. Such studies were performed, the results being shown in Figure 21. All solutions used in these experiments contained 0.2M Mo(V). The pH was altered by varying the concentration of HCl gas in  $D_2^0$ . It was found that the longitudinal relaxation times of protons and deuterons remained constant between 12N and 5N HCl (and DCl). With acid concentrations less than 5N, the longitudinal relaxation time rose sharply due to the decreased concentration of paramagnetic ions: Mo(V) either is oxidized to Mo(VI) or it forms a diamagnetic dimer. The transverse relaxation times behave quite differently. As the acidity decreases they decrease, pass through a minimum, and then increase rapidly. This increase begins at the same concentration as for the nuclear  $T_{1N}$  times, and is also caused by the decreased concentration of paramagnetic ions. To draw any conclusions about the cause of

the decrease in  $T_{2N}$ , one needs to compare the effects of pH on the EPR linewidth and on the exchange contribution to  $T_{2N}$ . This comparison is made in Figure 21 for protons. There is no correlation of any kind between variations of  $T_{2e}^{-1}$  and  $T_{2,ex,H}$ . The relaxation times of deuterons are determined by quadrupolar relaxation; thus the construction of a similar graph for  $T_{2,ex,D}$  was not possible. On comparing the minimum values of  $T_{2H}$  and  $T_{2D}$  (the latter is 27 msec), it was determined that  $(T_{2D}/T_{2H})$  = 42. Since this figure is close to the ratio of the squares of the magnetogyric ratios,  $(\gamma_H/\gamma_D)^2$  = 42.5, one can infer at this point (5N HC1) that neutralization of the exchange interaction between a paramagnetic ion and a hydrogen nucleus is not due to the loss of a hydrogen nucleus from the complex.

It must be noted that the increase in  $T_{2H}$  is not caused only by the increase in concentration of hydrochloric acid. It also occurs when LiCl is added to a solution containing 6N HCl. For example, addition of six moles of LiCl also increases  $T_{2H}$  by a factor of 12. Thus it is the change in  $Cl^{-}$  concentration rather than of  $H^{+}$  concentration which affects the transverse relaxation time. Changes in  $T_{2N}$  can also be caused by formation of other monomeric complexes of Mo(V) in the solution. In these complexes, the electron transverse relaxation time,  $T_{2e}$ , remains constant because it is largely determined by the Mo-O bond. Reduction in the number of chlorine atoms in the complex probably leads to an increase in n, the number of resonant nuclei in the first coordination sphere, and thus the relaxation rate  $T_{2H}^{-1}$  (since there are two protons in  $H_2O$  but only one in HCl).

B.  $[MoOF_5]^{2}$ 

The interpretation of the relaxation times in solutions containing the  $[MoOF_5]^{2-}$  anion is essentially the same as for the  $[MoOCl_5]^{2-}$  complex.

For protons and deuterons in solutions reasonably dilute in paramagnetic ions the longitudinal relaxation times  $T_{1H}$  and  $T_{1D}$  decrease with increasing temperature and do not depend on the acidity of the medium, <u>i.e.</u>, on the rate of chemical exchange of protons or deuterons. Moreover  $N_S T_{1D}/N_S T_{1H} = 39$ . These results correspond to the conditions under which  $T_1^{-1}$  is determined by electron-nuclear dipolar interaction modulated by the Brownian rotation of the complex. The quantity  $N_S T_1$  was found to be independent of the cation for solutions of the complexes  $(NH_4)_2[MoOF_5]$ ,  $K_2[MoOF_5]$ ,  $Zn[MoOF_5]$  and  $Cu[MoOF_5]$ .  $N_S T_1$  was found equal to 2 x  $10^{-5}$  sec mole/liter.

The transverse relaxation times for protons and deuterons (after correction of the effect of quadrupolar interaction) were observed to decrease with increasing temperature. In general, the transverse relaxation times were found to obey Eq. (46) for solutions dilute in  $[MoOF_5]^{2-}$ .

The ratio of  $T_{1N}/T_{2N}$  for protons and deuterons varies from 2.42 at 273°K to 3.24 at 335°K. When the solution pH is increased, the ratio  $T_{1N}/T_{2N}$  also increases somewhat.

The rates of relaxation for fluorine nuclei do not depend upon the pH of the solution and increase six-fold as the temperature is raised from 273°K to 335°K. However, the ratio  $T_{1F}/T_{2F}$  remains constant and is equal to 2.67. For solutions of the complexes (NH<sub>4</sub>)<sub>2</sub>[MoOF<sub>5</sub>], K<sub>2</sub>[MoOF<sub>5</sub>], and Zn[MoOF<sub>5</sub>] the ratio  $N_ST_{2H}/N_ST_{2F}=1.2$ , which corresponds within experimental error to the value of  $\gamma_F^2/\gamma_H^2$ .

These results indicate that the nuclear relaxation times are determined by electron-nuclear dipolar interaction and that the lifetimes of hydrogen nuclei (protons and deuterons) and fluorine nuclei in the first coordination sphere are fairly long (>  $10^{-5}$ sec).

For solutions of  $\text{Cu[MoOF}_5]$ , the ratio of  $\text{N}_S\text{T}_{2H}/\text{N}_S\text{T}_{2F}$  equals 200, due to the relaxation of the F ions in the first coordination sphere of Cu(II). From the data for solutions of this complex the lifetime in the first coordination sphere of Cu(II) is calculated to be  $10^{-7}$  sec. For concentrated solutions of  $[\text{MoOF}_5]^{2-}$  in aqueous hydrofluoric acid the nuclear relaxation time  $\text{T}_{2N}^{-1}$  was found to be determined by electron exchange.

An evaluation of the relaxation times yielded values of the correlation times and electron-nuclear coupling constants in good agreement with EPR and NMR frequency shift data. Further calculation yielded a value for n, the number of resonant nuclei in the first coordination sphere, of approximately four. Thus the  $[\text{MoOF}_5]^{2-}$  complex may be formulated as  $(\text{MoO}(\text{HF})_5]^{5+}$  or  $[\text{MoOF}_5(\text{H}_2\text{O})_2]^{2-}$ .

C.  $[Mo(OCH_3)_2Cl_4]$  Complex.

The relaxation times for dilute solutions of the complexes  $C_5H_6N[Mo(OCH_3)_2Cl_4]$ ,  $[(CH_3)_4N][Mo(OCH_3)_2Cl_4]$ , and  $C_9H_8N[Mo(OCH_3)_2Cl_4]$  in methanol can be interpreted by using Eqs. 45 and 46. The nature of the cation had no effect upon the observed relaxation rates. An analysis of the experimental data yield values for the rotational correlation time in good agreement with values obtained from EPR linewidth measurements.

Calculation yielded a value for n of approximately 6, which is in good agreement with the formula  $[Mo(OCH_3)_2Cl_4]$ . Comparison of nuclear and electronic relaxation results indicated that for solutions above 0.1M in  $[Mo(OCH_3)_2Cl_4]$  the relaxation times are determined by electron exchange.

#### REFERENCES

- 1. K. DeArmond, B. B. Garrett, and H. S. Gutowsky, J. Chem. Phys., 42, 1019 (1965).
- 2. C. R. Hare, I. Bernal, and H. B. Gray, Inorg. Chem., 1, 831 (1962).
- 3. B. R. McGarvey, J. Phys. Chem., 71, 51 (1967).
- 4. R. D. Dowsing and J. F. Gibson, J. Chem. Soc., 1967, 655.
- 5. G. P. Haight, Jr., J. Inorg. Nucl. Chem., 3, 1612 (1964).
- 6. J. F. Allen and H. M. Neumann, Inorg. Chem., 3, 1612 (1964).
- 7. E. Wendling, Bull. Soc. Chim. France, 1966, 413.
- 8. D. I. Ryabchikov, I. N. Marov, Yu. N. Dubrov, V. K. Belyaeva, and A. N. Ermakov, Dokl. Akad. Nauk SSSR, 169, 1107 (1966).
- 9. D. I. Ryabchikov, I. N. Marov, Yu. N. Dubrov, V. K. Belyaeva, and A. N. Ermakov, Dokl. Akad. Nauk SSSR, 165, 842 (1965).
- 10. H. Kon and N. E. Sharpless, J. Phys. Chem., 70, 105 (1966).
- 11. D. I. Ryabchikov, I. N. Marov, Yu. N. Dubrov, V. K. Belyaeva, and A. N. Ermakov, Dokl. Akad. Nauk SSSR, 167, 629 (1966).
- 12. J. T. C. Van Kemenade, J. L. Verbeek and P. F. Cornaz, Rec. Trav. Chim., 85, 629 (1966).
- 13. H. Funk, F. Schmeil, and H. Scholz, Z. Anorg. Allgem. Chem., 310, 86 (1961).
- 14. D. A. McClung, L. R. Dalton, and C. H. Brubaker, Jr., Inorg. Chem., <u>5</u>, 1985 (1966).
- 15. R. Wilson and D. Kivelson, J. Chem. Phys., 44, 154 (1966).
- 16. P. Atkins and D. Kivelson, J. Chem. Phys., 44, 169 (1966).
- 17. R. Wilson and D. Kivelson, J. Chem. Phys., 44, 4440 (1966); 44, 4445 (1966).
- 18. R. G. James and W. Wardlaw, J. Chem. Soc., 1927, 2145.
- 19. F. G. Angell, R. G. James, and W. Wardlaw, J. Chem. Soc., 1929, 2578.
- E. A. Allen, B. J. Brisdon, D. A. Edwards, G. W. A. Fowles, and R. G. Williams, J. Chem. Soc., 1963, 4649.

- 21. M. M. Abraham, J. P. Abriata, M. E. Foglio, and E. Pasquini, J. Chem. Phys., 45, 2069 (1966).
- 22. N. S. Garif'yanov and V. N. Fedotov, Zh. Strukturn. Khim., 3, 711 (1962).
- 23. L. Sacconi and R. Cini, J. Am. Chem. Soc., 76, 4239 (1954).
- 24. R. A. D. Wentworth and T. S. Piper, J. Chem. Phys., 41, 3884 (1964).
- 25. D. I. Ryabchikov, I. N. Marov, Yu. N. Dubrov, V. K. Belyaeva, and A. N. Ermakov, Dokl. Akad. Nauk SSSR, 166, 623 (1966).
- L. R. Dalton, J. D. Rynbrandt, E. M. Hansen, and J. L. Dye, J. Chem. Phys., 44, 3969 (1966).
- 27. L. S. Singer and J. Kommandeur, J. Chem. Phys., 34, 133 (1961).
- 28. L. S. Singer, "A Review of Electron Spin Resonance in Carbonaceous Materials" in Proceedings of the Fifth Conference on Carbon, vol. 2, (New York, The MacMillan Company, 1963).
- 29. N. S. Garif'yanov, B. M. Kozyrev, and V. N. Fedotov, Dokl. Akad Nauk SSSR, 156, 641 (1964).
- 30. N. S. Garif'yanov, B. M. Kozyrev, and V. N. Fedotov, Teortich. i éksp. khim., 1, 118 (1965).
- 31. Low, W., Paramagnetic Resonance, vol. I and II, (New York, Academic Press, 1963).
- 32. Low, William, <u>Paramagnetic Resonance in Solids</u>, (New York, Academic Press, 1960)
- 33. Pople, J. A., Schneider, W. G., and Bernstein, H. J., <u>High-Resolution Nuclear Magnetic Resonance</u>, (New York, McGraw-Hill Book Company, Inc., 1959).
- 34. Williams, Dudley, "Molecular Physics", Methods of Experimental Physics, L. Marton, Ed., vol. 3, (New York, Academic Press, 1962).
- Abragam, A., The Principles of Nuclear Magnetism (London, Oxford University Press, 1961).
- 36. Al'tshuler, S. A., and Kozyrev, B. M., <u>Electron Paramagnetic Resonance</u>, (New York, Academic Press, 1964).
- 37. Slichter, Charles P., <u>Principles of Magnetic Resonance</u>, (New York, Harper and Row Publishers, 1963).

- 38. Pake, G. E., Paramagnetic Resonance, (New York, W. A. Benjamin, Inc., 1962).
- 39. Carrington, A., and McLachlan, A. D., <u>Introduction to Magnetic Resonance</u>, (London, Harper and Row, Publishers, 1967).
- 40. Alexsandrov, I. V., The Theory of Nuclear Magnetic Resonance, (New York, Academic Press, 1966).
- 41. G. Breit and I. I. Rabi, Phys. Rev., 38, 2082 (1931).
- 42. J. E. Nafe and E. B. Nelson, Phys. Rev., 73, 718 (1948).
- 43. H. M. McConnell and J. Strathdee, Mol. Phys., 2, 129 (1959).
- 44. E. Fermi and E. Segre, Z. Physik, 82, 729 (1933).
- 45. R. Lefebvre and J. Maruani, J. Chem. Phys., 42, 1480 (1965).
- 46. F. Bloch, Phys. Rev., 102, 104 (1956).
- 47. A. G. Redfield, IBM Journal, 1, 19 (1957).
- 48. N. Bloembergen, E. M. Purcell, and R. V. Pound, Phys. Rev., 73, 678 (1948).
- 49. P. W. Anderson and P. R. Weiss, Rev. Mod. Phys., 25, 269 (1953).
- 50. P. W. Anderson, J. Phys. Soc. Japan, 9, 316 (1954).
- 51. N. Bloembergen, <u>Nuclear Magnetic Relaxation</u> (New York, W. A. Benjamin, Inc., 1961)
- 52. A. A. Manenkov and R. Orbach, <u>Spin-Lattice Relaxation in Ionic Solids</u>, (New York, Harper and Row Publishers, 1966).
- 53. N. Bloembergen and W. C. Dieckinson, Phys. Rev., 79, 179 (1950).
- 54. I. Solomon, Phys. Rev., 99, 559 (1965).
- 55. N. Bloembergen, J. Chem. Phys., 27, 572 (1957).
- 56. N. Bloembergen, J. Chem. Phys., 27, 595 (1957).
- 57. I. Solomon and N. Bloembergen, J. Chem. Phys., 25, 261 (1956).
- 58. R. A. Bernheim, T. H. Brown, H. S. Gutowsky, and D. E. Woessner, J. Chem. Phys., 30, 950 (1959).
- 59. A. L. Bloom, J. Chem. Phys., 25, 793 (1956).

- 60. R. S. Codrington and N. Bloembergen, J. Chem. Phys., 29, 600 (1958).
- 61. J. King and N. Davidson, J. Chem. Phys., 29, 787 (1958).
- 62. L. O. Morgan and A. W. Nolle, J. Chem. Phys., 25, 793 (1956); 31, 365 (1959).
- 63. N. Bloembergen and L. O. Morgan, J. Chem. Phys., 34, 842 (1961).
- 64. T. J. Swift and R. E. Connick, J. Chem. Phys., 37, 307 (1962).
- 65. R. Kubo and K. Tomita, J. Phys. Soc. Japan, 9, 888 (1956).
- 66. K. Tomita, Progr. Theort. Phys. (Kyoto), 19, 541 (1958).
- 67. The shift  $\delta$  must be measured from the frequency  $\omega_{\text{T}}$  +  $\Delta$ , where  $\Delta$  is a line shift of the Knight type which is proportional to the magnetization of the system in the field H<sub>\(\Delta\)</sub>.
- 68. R. L. Conger and P. W. Selwood, J. Chem. Phys., 20, 383 (1952).
- 69. D. E. Woessner, J. Chem. Phys., 36, 1 (1962); 42, 1855 (1965).
- 70. H. M. McConnell, J. Chem. Phys., 25, 709 (1956).
- 71. D. Kivelson, J. Chem. Phys., <u>33</u>, 1094 (1960).
- 72. J. H. Freed and G. K. Fraenkel, J. Chem. Phys., 39, 326 (1963).
- 73. J. L. Dye and L. R. Dalton, J. Phys. Chem., 71, 184 (1967).
- 74. P. S. Hubbard, J. Chem. Phys., 42, 3546 (1965).
- 75. P. A. M. Dirac, <u>The Principles of Quantum Mechanics</u>, (New York, Oxford University Press, 1935).
- 76. J. H. Van Vleck, Phys. Rev., <u>74</u>, 1168 (1948).
- 77. M. H. L. Pryce and K. W. H. Stevens, Proc. Phys. Soc., A63, 36 (1950).
- 78. P. W. Anderson and M. T. Weiss, Revs. Modern Phys., 25, 269 (1953).
- 79. J. H. Van Vleck, Phys. Rev., 57, 426 (1940).
- 80. R. Orbach, Proc. Phys. Soc. (London), A77, 821, (1961).
- 81. D. Kivelson, J. Chem. Phys., 45, 1324 (1966).
- I. V. Aleksandrov, Teoretich. i eksp. khim., 1, 211 (1965).
- 83. I. V. Aleksandrov and A. V. Kessesikh, Teoretich. i eksp. khim., 1, 221 (1905).

- 84. P. W. Atkins, Mol. Phys., 12, 201 (1967).
- 85. P. W. Atkins and M. T. Crofts, Mol. Phys., 12, 211 (1967).
- 86. L. Dalton, J. Cowen, and A. Kwiram, Phys. Rev., to be published.
- 87. A. I. Busev, Analytical Chemistry of Molybdenum (Daniel Davey and Co., New York, 1964).
- 88. C. W. Balke and E. F. Smith, J. Am. Chem. Soc., 30, 1662 (1908).
- 89. P. Pascal, Nouveau Traité de Chimie Minérale, (Masson et Cie., Paris, 1963).
- 90. W. G. Palmer, Experimental Inorganic Chemistry (New York, Cambridge University Press, 1964). p. 281
- 91. W. P. Griffith, J. Lewis, and G. N. Wilkinson, J. Chem. Soc., 1959, 872.
- 92. L. R. Dalton, M. S. Thesis, Michigan State University, East Lansing, Mich,, 1966.
- 93. H. A. Kuska, PhD. Thesis. Michigan State University, East Lansing, Mich., 1965.
- 94. N. Bloembergen, S. Shapiro, P. S. Pershan, and J. O. Artman, Phys. Rev., 114, 445 (1959).
- 95. P. S. Pershan, Phys. Rev., 117, 109 (1960).
- 96. U. Kh. Kopvillem, Soviet Physics--Solid State, 3, 865 (1960).
- 97. A. A. Manenkov and A. M. Prokhorov, Soviet Physics--JETP, 15, 54 (1962).
- 98. H. Y. Carr and E. M. Purcell, Phys. Rev., 94, 630 (1954).
- 99. J. D. Rynbrandt, M. S. Thesis, Michigan State University, East Lansing, Mich., 1966.
- 100. A. J. Freeman, B. Bagus, and R. E. Watson, Colloques Internationaux de C.N.R.S., Hyperfine Structure of Atoms and Molecules, No. 164, Paris, 1966.
- 101. L. Low, Phys. Letters, 24A, 46 (1967).
- 102. J. W. Culvahouse, W. P. Unruh, and D. K. Brice, Phys. Rev., 129, 2430 (1963).
- 103. At this time only superhyperfine interaction involving the four equatorial ligands is considered since ENDOR measurements have shown that the superhyperfine interaction arising from interaction of the paramagnetic electron with the axial halide ligand is less than 1 gauss.

- 103. A. J. Freeman and R. E. Watson, Magnetism, Vol. IIA, eds. H. Suhl and G. Rado, (Academic Press, Inc., New York, 1965).
- 104. G. K. Fraenkel, J. Phys. Chem., 71, 139 (1967).
- 105. J. H. Freed and G. K. Fraenkel, J. Chem. Phys., 40, 1815 (1964).
- 106. W. B. Lewis, M. Alei, Jr., and L. O. Morgan, J. Chem. Phys., 45, 4003 (1966).
- 107. R. E. Connick and E. D. Stover, J. Phys. Chem., 65, 2075 (1962).

